

**University of Naples “Federico II”
School of Polytechnic and Basic Sciences**

Department of Structures
for Engineering and Architecture

**Ph.D. Programme in Structural, Geotechnical and
Seismic Engineering**

XXIX Cycle



MARIA GRAZIA SIMONELLI

Ph.D. Thesis

**PLASTIC BUCKLING OF THIN AND
MODERATELY THIN PLATES AND
SHELLS: CLASSIC PROBLEMS AND
NEW PERSPECTIVES**

TUTOR: PROF. ING. FEDERICO GUARRACINO

2017

To my family and Eric

Acknowledgments

First of all, I would like to express my sincere gratitude to Prof. Federico Guarracino who followed and supported me during the whole Ph.D. programme and offered me the opportunity to work in an outstanding academic department. His guidance has given me the chance to develop a more rigorous and critic approach to scientific research and has encouraged me to have more self-confidence about my personal.

I am grateful to Prof. Luciano Rosati for his patience and understanding. His suggestions and practical indications have always incited me to expand my knowledge in the broad field of research. A special thank goes also to Prof. Paolo Budetta for supporting me in experimental research and for having shared his knowledge and time with me.

A particular acknowledgment is due to two persons who have appreciated me. First, I would like to express my gratitude to Aldo Giordano for trusting me since I was a student. He has understood my passion and determination in the field and, despite the lack of time, he has always taught me more than I could dare to ask. Also, I wish to thank Francesco Marmo for making me believe in the quality of research, giving me the motivation and the confidence to go ahead and sharing with me his knowledge.

I would like to express my sincere and devoted gratitude to Prof. Carlalberto Anselmi for the initial inspiration. He has motivated me with his profound passion for scientific studies, giving me the methodology and the fundamental knowledges which have made possible my achievements.

A warm acknowledgment is due to my Ph.D. colleagues, Stefania Fabozzi, Fabiana De Serio and Antonino Iannuzzo for their example of perseverance. They have shown me in a friendly manner how to face everyday difficulties in academic life. In particular, special thanks go to my roommate Francesca Linda Perelli for the light-hearted atmosphere and for sharing the passion for mathematics and physics.

I would like to thank all the students of the courses of “Analisi Limite delle Strutture” and “Scienza delle Costruzioni” taught by Prof. Federico Guarracino for motivating me to face difficulties, for trusting my advice and my knowledge and for having enriched me with their opinions and doubts about structural engineering problems.

I am particularly grateful to my friend Maria Romano for supporting me all the time with her wise suggestions, in many circumstance she has helped me to improve myself and never give up. Special thanks to Le Socie which encouraged me like sisters: their support has been always felt. They continue to inspire me day by day and make me give my best in both professional and personal aspects of my life.

Last but not least, I would like to thank my mother and my father for giving me the most important natures: the determination, the spirit of sacrifice and the willpower to go ahead. They have always strongly supported me in any decision. I would also like to thank my brother and Lilla for their patience and loving support and Eric for the love and the understanding: he is the reason why I go successfully ahead in my life and to him I wish to dedicate this important achievement.

Naples, March 2017

Maria Grazia Simonelli

Index

Acknowledgments	1
List of figures	5
List of tables	9
Introduction	11
1. The theory of plasticity	17
1.1. Flow and deformation theories of plasticity	19
1.2. Constitutive laws and analytical relations in the flow theory of plasticity	21
1.3. Constitutive laws and analytical relations in the deformation theory of plasticity	35
1.4. Other plasticity approaches	39
1.5. Experimental stress-strain curves	41
1.6. Uniaxial behaviour	47
2. The “plastic buckling paradox”	51
2.1. The concept of buckling	53
2.2. Bifurcation buckling.....	55
2.3. Elastic buckling.....	57
2.4. Plastic buckling	60
2.5. The “plastic buckling paradox”	65
2.6. Open issues in the investigation of the plastic buckling paradox.....	76
3. Plastic buckling of a cruciform column	79
3.1. Historical background	81
3.2. Torsional buckling: canonic results	84
3.3. A procedure for the evaluation of the critical load according to the flow theory of plasticity	88
3.4. Discussion of the results.....	96

4. Plastic buckling of cylindrical shells	113
4.1. Historical background.....	115
4.2. Buckling of cylindrical shells: an overview	117
4.3. Estimation of buckling strength in case of non-proportional loading	123
4.4. Discussion of the results	131
4.5. The role of the mode switching	137
5. Conclusions	149
References	153
References for Section 1.	153
References for Section 2.	153
References for Section 3.	155
References for Section 4.	158
Appendixes	163
Appendix 1. Plastic work in Prandtl-Reuss material	163
Appendix 2. Description of Ramberg-Osgood stress-strain curve	166

List of figures

Figure 1 - Geometric illustration of associated flow rule	23
Figure 2 - Flat and corner plasticity (Chen and Han, 1988)	25
Figure 3 – Differences in plastic flow between von Mises and Tresca yield surfaces.	26
Figure 4 - Hardening and softening in rate-independent plasticity: motion of yield surface in stress space	31
Figure 5 – The concept of slip in single crystal (schematic).(Batdorf and Budiansky, 1949).....	40
Figure 6 – A loading surface with a corner in stress space.....	40
Figure 7 – Determination of K and n in the Ramberg-Osgood stress-strain curve. (Jones, 2009).....	43
Figure 8 - Ramberg-Osgood stress-strain curves for various strain hardening values.(Jones, 2009).....	44
Figure 9 - Overlap of Ramberg-Osgood and Nadai stress-strain curves for an aluminium alloy.	46
Figure 10: Tangent, E_t , and secant, E_s , moduli in a simple tension test.....	48
Figure 11: Unloading in the J_2 flow theory of plasticity.....	49
Figure 12: Bifurcation buckling.	53
Figure 13: Nonlinear collapse.	54
Figure 14: Stable symmetric buckling and influence of imperfections.	56
Figure 15: Unstable symmetric buckling and influence of imperfections.....	56
Figure 16: Asymmetric buckling and influence of imperfections.	57
Figure 17: Critical load for a simply supported and uniformly compressed rod.	58
Figure 18: Plate subjected to in-plane compressive loading. (Singer, Arbocz and Weller, 1998).....	59
Figure 19: Plastic buckling of a cylindrical shell subjected to axial compression.	61
Figure 20: Euler’s curve of instability.....	62
Figure 21: Shanley approach to inelastic column buckling.....	64

Figure 22: Onat and Drucker model (1953). a) simplified geometrical model. b) simplified material model.....	67
Figure 23: Hutchinson and Budiansky numerical results for critical load as a function of imperfection amplitude (1976).....	68
Figure 24: Modes of buckling of Lee's tests (1962).....	68
Figure 25: Batterman hinge model for cylindrical shells (1965).	69
Figure 26: Numerical and experimental results fo. specimens (Set A). (Giezen, Babcock and Singer, 1991)	72
Figure 27: Theoretical and experimental results for $L/D = 1$ cylinders. (Blachut, Galletly and James, 1996)	73
Figure 28: Axisymmetric mode of wrinkling observed by Bardi and Kyriakides (2006).....	74
Figure 29: Results of axially compressed imperfect cylinders. (Shamass, Alfano and Guarracino, 2014).....	75
Figure 30: Torsional buckling of a cruciform column.	84
Figure 31: Cross section of a cruciform column.....	85
Figure 32: Strain increment for a perfect column according to the flow theory of plasticity.....	87
Figure 33: Strain increment for an imperfect $(\bar{\sigma})$ vs a perfect $(\bar{\sigma})$ column according to the flow theory of plasticity.	89
Figure 34: Twisted configuration of an imperfect cruciform column.	90
Figure 35: Iterative procedure for the evaluation of the critical twisting load of an imperfect cruciform column according to the deformation theory of plasticity.	94
Figure 36: Iterative procedure for the evaluation of the critical twisting load of an imperfect cruciform column according to the flow theory of plasticity.	95
Figure 37: Plots of the Ramberg-Osgood curves for the considered aluminium alloys.....	98
Figure 38: Non-dimensional plots of the Ramberg-Osgood curves for the considered aluminium alloys.....	98
Figure 39: FE model of a cruciform column.	100
Figure 40: Plots of different shear moduli versus the compressive stress, σ for an imperfection amplitude $\delta = 1/10h$	102

Figure 41: Plots of different shear moduli versus the compressive stress, σ for an imperfection amplitude $\delta = 1/10h$	103
Figure 42: Plots of different shear moduli versus the compressive stress, σ for an imperfection amplitude $\delta = 1/10h$	104
Figure 43: Plots of different shear moduli versus the compressive stress, σ for an imperfection amplitude $\delta = 1/100h$	105
Figure 44: Plots of different shear moduli versus the compressive stress, σ for an imperfection amplitude $\delta = 1/100h$	106
Figure 45: Plots of different shear moduli versus the compressive stress, σ for an imperfection amplitude $\delta = 1/100h$	106
Figure 46: Axial load versus torsional rotation in ABAQUS, imperfection amplitude: $\delta = 1/10h$	107
Figure 47: Axial load versus torsional rotation in ABAQUS, imperfection amplitude: $\delta = 1/10h$	108
Figure 48: Axial load versus torsional rotation in ABAQUS, imperfection amplitude: $\delta = 1/10h$	108
Figure 49: Axial load versus torsional rotation in ABAQUS, imperfection amplitude: $\delta = 1/100h$	109
Figure 50: Axial load versus torsional rotation in ABAQUS, imperfection amplitude: $\delta = 1/100h$	109
Figure 51: Axial load versus torsional rotation in ABAQUS, imperfection amplitude: $\delta = 1/100h$	110
Figure 52: Load-deflection curves showing limit and bifurcation points. (Bushnell, 1984)	116
Figure 53: Cylindrical shell displacements and forces. (Yoo and Lee, 2011)	118
Figure 54: Cylindrical shells under simple loading conditions: a) axial compression;	120
Figure 55: Equilibrium paths of axially compressed cylinder. (Yoo and Lee, 2011)	121
Figure 56: Buckling of a cylindrical shell subjected to a non-proportional loading.	124
Figure 57: Ramberg-Osgood stress-strain curves of the considered aluminium alloys	127

Figure 58: Dimensions and coordinate system of a cylindrical shell.	128
Figure 59: Experimental setting by Giezen et al. (Giezen, Babcock and Singer, 1991)	129
Figure 60: FE model of cylindrical shells.	130
Figure 61: Load arc length paths for specimen S1.	134
Figure 62: Lateral pressure-arc length paths for specimen S2.	135
Figure 63: Lateral pressure-arc length paths for specimen S3.	135
Figure 64: Lateral pressure-arc length paths for specimen S4.	136
Figure 65: Representation of first two circumferential modes for specimens S1-S3.	138
Figure 66: Representation of circumferential modes for specimens S1-S3. ...	139
Figure 67: Representation of circumferential modes for specimen S4.	140
Figure 68: Representation of circumferential modes for specimen S2.	140
Figure 69: Lateral pressure-arc length paths for specimen S1.	142
Figure 70: Lateral pressure-arc length paths for specimen S2.	142
Figure 71: Lateral pressure-arc length paths for specimen S3.	143
Figure 72: Lateral pressure-arc length paths for specimen S4.	143

List of tables

Table 1 – Difference between flow and deformation theories of plasticity and the plastic buckling paradox.....	66
Table 2 - Ramberg-Osgood parameters for the considered aluminium alloys...97	
Table 3 - Characteristics of the analysed specimens.	99
Table 4 - Critical stress for a perfect specimen according to Eqs. (72), flow, and (78), deformation theory of plasticity vs ABAQUS elastic results.	100
Table 5 - Results obtained from the procedure proposed in this paper for an imperfection equal to 1/10 of the flange thickness, h , versus FE and experimental ones.....	101
Table 6 - Results obtained from the procedure proposed in this paper for an imperfection equal to 1/100 of the flange thickness, $\delta = 1/100 h$, versus FE and experimental ones.	105
Table 7 - Percent differences between the analytical solutions for the two different values of the imperfection amplitude, $\delta = 1/10h$ and $\delta = 1/100h$	110
Table 8 - Ramberg-Osgood parameters for the considered aluminium alloys.	126
Table 9 - Characteristics of the analysed specimens.	127
Table 10 – Applied axial loads, $\bar{\sigma}$	129
Table 11 – Calculated limit values of the lateral pressure.	132
Table 12 – Influence of the initial imperfection shape and amplitude on the buckling loads.	133
Table 13 – Calculated limit values of the lateral pressure for low imperfection amplitudes.....	134
Table 14 – Elastic buckling modes.	139
Table 15 – Results of non-linear buckling analysis for specimen S2.	141
Table 16 – Results of non-linear buckling analysis for specimen S2.	144
Table 17 – Results of non-linear buckling analysis for specimen S3.	145
Table 18 – Results of non-linear buckling analysis for specimen S3.	146

Introduction

Elastic-plastic instability of structures is a widespread field which involves a broad category of civil and mechanical engineering problems and allows to investigate a rather large variety of structural problems including: the physical and mechanical characterization of materials, the resistance criteria, the modelling of materials respecting to the main theories of plasticity and the phenomena related to material and geometric nonlinearities especially for thin and moderately thin plates and shells.

The concept of buckling involves a sudden lost in strength of a structure due to its lost in shape. In structural engineering, different types of buckling have been shown depending on its appearance in the elastic or plastic range and on the loading path followed. The aim of this work is to investigate the plastic buckling of plates and shells subjected to different loading conditions with respect to the phenomenon of the “plastic buckling paradox”. In particular, by means of a deep numerical investigation on cylindrical shells with different geometrical and material properties, some limitations about the modern numerical nonlinear analyses conducted by the use of the Finite Elements are highlighted and discussed in detail.

In the study of the elastic-plastic response of structures under certain loading conditions, the first issue to deal with is the knowledge of the material behaviour with the definition of appropriate strain-stress relationships. A well-known way to observe a material behaviour is the uniaxial stress test which produces a simple stress-strain curve, in case of compression or tension only. However, in many cases, particular attention must be pay to the material behaviour under multiaxial states of stress for which defining an appropriate constitutive relation is much more complex. Therefore, it becomes necessary to generalize the stress-strain relationships observed from a simple uniaxial test to more general multiaxial stress states. A large amount of stress-strain curves are considered and represented by use of simplified material models, as the Ramberg-Osgood or Nadai ones.

At the same time, the study of the main theories of plasticity is conducted. Since the beginning of the twentieth century, there have been many developments in the study of elastic-plastic behaviour of structures. Accordingly, a large improvement has been made in the study of the theory of plasticity, leading to identify different models for engineering materials based on whether path-dependence is accounted for or not. The plasticity models proposed for metals can be divided into two main groups: the deformation (Hencky-Nadai) and the flow (Lévy-Mises) theories of plasticity. In both of these theories the plastic deformation does not allow volume changes because it is ruled by the second invariant of the stress deviator and, in this respect, the flow and the deformation theories are both called J_2 theories of plasticity. The flow theory of plasticity assumes that an infinitesimal increment of strain is determined by the current stress and its increment, that is a path-dependent relationship in which the current strain depends not only on the value of the current total stress but also on how the actual stress value has been reached while the deformation theory of plasticity is based on the assumption that, for continued loading, the state of strain is uniquely determined by the state of stress and, therefore, it is essentially a special path-independent nonlinear constitutive law. Details on the theories of plasticity and on the constitutive relations are described and discussed in Section 1.

Notwithstanding the fact that the deformation theory lacks of physical rigour with respect to the flow theory of plasticity, in many engineering problems involving the inelastic buckling of structures, the deformation theory seems to be more in agreement with the experimental results. This phenomenon is commonly known as the “plastic buckling paradox” and shows that the J_2 flow theory of plasticity brings to a significantly overestimation of the critical load while the J_2 deformation theory of plasticity seems to obtain more accurate results with respect to the experimental data. This paradox has existed for many years and has involved a multitude of controversies, many of them are still to be resolved.

In order to deeply examine the roots of the plastic buckling paradox, several plastic buckling problems for plates and shells are investigated. An important observation is made on the nonlinear character of the plastic buckling from both geometrical and material points of view. From the material point of view, the

nonlinearity depends on the nonlinearity of the stress-strain relationship of the material while from the geometrical one, it depends on the geometrical configurations of the structural element before and during the loading process, i.e. on account of some initial imperfections or of second order effects when large deformations appear. Including nonlinearities in the buckling analysis makes the investigation of the equilibrium paths more elaborate. The effects of nonlinearities are decisive in the prediction of the critical load and also in the definition of the post-buckling behaviour. Details on the plastic buckling phenomenon and several examples about the influence of the nonlinearities are illustrated and discussed in Section 2.

Focusing the attention on the fundamentals of the problem, in Section 3 the case of axially compressed cruciform column showing a torsional buckling is thoroughly analysed. As back as 1953, Onat and Drucker found the plastic buckling paradox: the critical compressive stress predicted by the deformation theory was in a better agreement with the experimental results than that predicted by the flow theory. The reasons for this discrepancy were found in the high value of the shear modulus in the flow theory formula. The solution was investigated by conducting an approximate analysis in which small initial imperfections were taken into account. In this manner, assuming that there existed a very small imperfection in the column, the critical load predicted by the flow theory was found to be reduced significantly, getting itself close to that predicted by the deformation theory.

Nevertheless, in other investigations concerning the plastic buckling of the cruciform column it was seen that, depending on the strain hardening of the material, the initial imperfections have to be too much higher and thus no more compatible with those experimentally measured (Gerard and Becker, 1957, Hutchinson and Budiansky, 1976). In this respect, in Section 3 a careful analysis is conducted in order to resolve the discrepancies in the flow theory of plasticity due to the shear modulus and also considering the imperfection sensitivity on account of different strain-hardening materials. A new approach for the evaluation of the critical load according to the flow theory of plasticity is presented in detail.

In such a manner, a very good agreement between the results from the flow theory of plasticity and other analytical and experimental results can be obtained also for metals with significant strain-hardening without the necessity of accounting large initial imperfections.

In the light of the results achieved with the simple case of the cruciform column, the investigation in the plastic buckling is extended in Section 4 to more complex structures such as cylindrical shells of moderate thickness. There are different loading conditions under which the cylindrical shells show the paradox and often it is not possible to obtain reasonable results either by the use of the flow and the deformation theories of plasticity. Indeed, in the case of nonproportional loading, as for instance in the condition of combined axial tension and external pressure investigated by Giezen and Blachut, both the two theories fail to predict the critical load. However, with the contemporary diffusion of powerful computational instruments able to conduct incremental analyses in the plastic range by the use of the Finite Elements, the discrepancy between flow and deformation theories has been reduced and many problems have been resolved. But a doubt still remains: can a modern incremental analysis naturally avoid the plastic buckling paradox? Is that sufficient?

In Section 4, by examining in depth the case of nonproportional loading it is shown that, contrary to what observed in several studies present in literature, is not much the amount of the initial imperfection to govern the problem as its shape. Indeed, by conducting several numerical analyses, it may be shown that in some cases an opposite phenomenon occurs, i.e. the deformation theory fails in the prediction of the critical load on account of low initial imperfections. This may be thus called the “inverse buckling paradox”, given that it is the deformation theory to overestimate the critical load while the flow theory results more in accordance with the experimental data. Numerical calculations on cylindrical specimens with different geometry and material have been conducted and finally some limitations of the modern numerical non-linear Finite Element analyses have been discussed.

The use of the deformation theory of plasticity in the investigation of the inelastic buckling of plates and shells is still recommended for practical applications. In years, many researchers attempted to revise its formulation including unloading (Peek, 2000) or redefining it as a sequence of linear loadings in the case of nonproportional loading (Jahed et al.,1998).

However, the results of the present dissertation highlight a superior reliability of the flow theory of plasticity in the estimation of the critical load with respect to the commonly used deformation theory, contrarily to what is normally agreed in literature. In fact, by conducting a geometrical and material nonlinear finite element analysis, a very good agreement between numerical and experimental results can be found even in presence of the physically more sound flow theory of plasticity, provided that particular attention is pay to constitutive laws and imperfection amplitudes.

KEYWORDS: • Plasticity • Flow theory • Deformation theory • Stability
• Plastic buckling paradox • Plates • Shells • Non-linear FEA

Section 1.

The theory of plasticity

1.1. Flow and deformation theories of plasticity

Since the beginning of the twentieth century, there have been several developments in the study of elastoplastic behaviour of structures and, accordingly, enormous progress has been made in the theories of plasticity leading to identify different models for engineering materials based on whether path-dependence is accounted for or not. The plasticity models that have been proposed for metals in the strain hardening range can be divided into two main groups: the deformation (Hencky) and the flow (Lévy-Mises) theories of plasticity. In both of these theories the plastic deformations do not allow volume changes as plastic yielding is ruled by the second invariant of the deviatoric part of the stress tensor and, in this respect, they are both called J_2 theories of plasticity.

Deformation theory was proposed by Hencky in 1924 and subsequently developed around 1945 by the Russian school of Nadai and Ilyushin. This theory of plasticity is essentially based on the assumption of a relationship between stress and strain in global terms, and basically refers to the loading processes that do not involve returns in the elastic path of parts of the structure previously plasticized. Thus, the elastoplastic problem is treated as a kind of nonlinear elastic problem. However, while in the loading path a nonlinear elastic relationship has the ease of considering total strains in a one-to-one correspondence with total stresses also during plastic deformation, on the other hand upon unloading the main plastic deformation characteristic of irreversibility is not accounted for and this implies that the application of the deformation theory is very limited. In fact this approach can be applicable only to problems of proportional or simple loading, that is a loading in which the ratios among the stress components remain constant, so that no reversal or cyclic loading are allowed, given that no stress history effects can be accounted for.

Conversely, in the flow or “incremental” theory of plasticity, strain increments are related to stress increments and there are irreversible plastic deformations because of the energy dissipation and, as a consequence, the stress history effects are accounted for. In this manner, at the end of each loading process that leads the material to plasticity, the total strain increment can be decomposed in the sum of two parts, elastic and plastic, so that in the unloading phase the elastic deformation

is completely reversible while the plastic one is irreversible and given in value by the difference between the total and the elastic part. The incremental approach has proved to be more effective in describing the non-holonomic nature of the elastic-plastic behaviour of metals, i.e. the final strain is dependent not only on the final value of the load but also on the loading path, and it is extensible to generic loading processes, including reversal or cyclic loading.

In conclusion, while the deformation theory of plasticity is based on the assumption that for continued loading the state of strain is uniquely determined by the state of stress and, therefore, it is essentially a special path-independent non-linear constitutive law, the flow theory of plasticity assumes that an infinitesimal increment of strain is determined by the current stress and its increment, that is a path-dependent relationship in which the current strain depends not only on the value of the current total stress but also on how the actual stress value has been reached.

Finally, it is clear that the incremental theory of plasticity is more in agreement with the experimental behaviour of engineering materials than the deformation theory, and hence more widely applicable. However, that generality and applicability collide with a much higher analytical complexity in calculations. Notwithstanding the fact that there is a general agreement that the deformation theory of plasticity lacks of physical rigour in comparison to the flow theory, the use of deformation theory is thus practically motivated by the capacity to solve certain problems without the mathematical complications of the flow theory and moreover, in the case of plastic buckling problems of elements under multiaxial stress, the use of deformation theory has been repeatedly reported to predict buckling loads that are in better agreement with the experimental results.

1.2. Constitutive laws and analytical relations in the flow theory of plasticity

The study of the elastic-plastic response of structures under certain load conditions is a rather complex problem that requires a deep knowledge of the material behaviour under applied loads and, as well, its translation in mathematical terms with an appropriate stress-strain law. A customary way to observe a material behaviour is the uniaxial stress test which leads to a simple stress-strain curve, in case of compression or tension stress state only. However, in order to predict the behaviour of the material under any general combined stress state, it is necessary to understand how to generalize the simple stress-strain relationships observed from an uniaxial test into a more general multiaxial stress states. One-dimensional curves of the constitutive relation that are in accordance with the principal elastic-plastic behaviours highlighted by laboratory experiments show a first elastic linear part and then, above the point of yielding, a nonlinear plastic part. The elastic limit in uniaxial case is well identified by the yielding stress σ_y only, above which the material is considered in plastic range. For a material under all possible combinations of stresses a yield function in terms of stress tensor in the indicial form can be defined as:

$$f(\sigma_{ij}) = F(\sigma_{ij}) - k = 0 \quad (1)$$

This relationship, in the stress space $(\sigma_I, \sigma_{II}, \sigma_{III})$, provides the geometrical representation of a yield surface. The term $F(\sigma_{ij})$ is function of the stresses and k is a parameter which expresses the limit properties of the material in multiaxial states of stress and it may be obtained particularizing the results from the uniaxial case with known experimental results or by more sophisticated triaxial tests. The $f(\sigma_{ij})$ yield function is assumed differentiable so the tangent hyperplane exists at every point belonging to the surface. Considering, in the first instance, an elastic-perfectly plastic material, plastic deformation occurs as soon as the stress vector reaches the yield surface. Continuing the loading above the yielding, for the perfectly plastic equilibrium the increment of stress $d\sigma_{ij}$ has to remain tangent to the yield surface and the plastic flow continues showing a plastic strain increment

vector $d\varepsilon_{ij}^p$ normal to the yield surface. In unloading process, the stress state returns inside the yield surface and the irreversible plastic deformation remains constant and all the increments in deformation are purely elastic.

During the loading process the condition of plastic flow is:

$$f(\sigma_{ij})=0 \text{ and } df = \frac{\partial f}{\partial \sigma_{ij}} d\sigma_{ij} = 0 \quad (2)$$

while during the unloading process the condition of elastic return is:

$$f(\sigma_{ij})=0 \text{ and } df = \frac{\partial f}{\partial \sigma_{ij}} d\sigma_{ij} < 0 \quad (3)$$

At any loading step, in the flow theory an infinitesimal increment of strain is determined by the current stress and its increment and, recalling that the total strain increment $d\varepsilon_{ij}$ satisfies the additive decomposition property, it can be written as the sum of the elastic and plastic strain increments:

$$d\varepsilon_{ij} = d\varepsilon_{ij}^e + d\varepsilon_{ij}^p \quad (4)$$

In this manner, the elastic strain increment may be directly derived by differentiating the elastic potential function $\varphi = \varphi(\varepsilon_{ij}^e)$ with respect to stresses σ_{ij} , recalling that in the elastic path:

$$d\varphi = \frac{\partial \varphi}{\partial \varepsilon_{ij}^e} d\varepsilon_{ij}^e \text{ and } \sigma_{ij} = \frac{\partial \varphi}{\partial \varepsilon_{ij}^e} \quad (5)$$

Similarly, for the plastic strain increment, in 1928 von Mises proposed the concept of the plastic potential function $g(\sigma_{ij})$, which frequently assumes the form of $g(\sigma_{ij})=J_2$, where J_2 is the second invariant of the stress deviator. Therefore the plastic strain increment can be expressed by the equation:

$$d\varepsilon_{ij}^p = d\lambda \frac{\partial g}{\partial \sigma_{ij}} \quad (6)$$

where $d\lambda$ is a positive scalar function which is nonzero only at yielding, that is when plastic deformation occurs. Eq.(6) defines the plastic flow rule that postulates an important kinematic assumption for the plastic deformation tensor. It naturally gives the magnitude of the plastic strain tensor components and implies that the plastic flow vector $d\varepsilon_{ij}^p$, geometrically represented by a vector with nine components in strain space $(\varepsilon_I, \varepsilon_{II}, \varepsilon_{III})$ is directed along the normal to the surface of plastic potential $g(\sigma_{ij})$, when plotted as a free vector in stress space $(\sigma_I, \sigma_{II}, \sigma_{III})$.

Another important consequence of this flow law which involves a plastic potential function $g(\sigma_{ij}) = J_2$ dependent only on the stress deviator, is that the volume deformation is purely elastic which is in agreement with experimental evidence. Indeed, it has been generally observed that in metals the largest amount of plastic deformation is due to changes in shape accompanied by very slight, if any, changes in volume. Consequently, the stress deviator does most of the work because of the prevalently distortional nature of plastic deformation. Furthermore, it is worth to underline that plastic deformation is assumed to be rate insensitive. This assumption implies that all plastic processes are considered to be infinitely slow thus the constitutive equations for plastic deformation may be homogeneous in time and the viscous effects may be neglected.

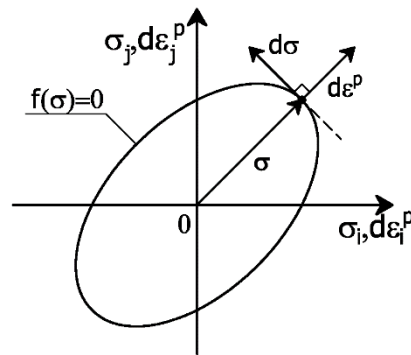


Figure 1 - Geometric illustration of associated flow rule

When using the plastic potential theory, the main problem is how to assume the plastic potential $g(\sigma_{ij})$, given that the effective form of the function $g(\sigma_{ij})$ is undetermined. A simple approach in plasticity theory is to consider that the plastic potential function and the yield function coincide, i.e. $g(\sigma_{ij}) = f(\sigma_{ij})$:

$$d\varepsilon_{ij}^p = d\lambda \frac{\partial f}{\partial \sigma_{ij}} \quad (7)$$

and the direction of the plastic strain increment is thus coincident with the normal to the yield surface at the current stress (see Figure 1), in the coincident stress and strain space $(\sigma_I, \sigma_{II}, \sigma_{III}) \cup (\varepsilon_I, \varepsilon_{II}, \varepsilon_{III})$. This simplified equation is called the “associated flow rule” because the plastic flow is no more related to an any unknown potential function but it is associated with a precisely yield criterion function, chosen on the base of the material behaviour. Conversely, if $g(\sigma_{ij}) \neq f(\sigma_{ij})$ the plastic flow follows a “non-associated flow rule”.

This simplification is very useful in practical applications since, particularly for materials such as metals, it is possible to choose an adequate yielding surface that agrees with either the constitutive law and the experimental evidence. In this respect, the most widely used criterion for metals is the von Mises yield criterion that has a large applicability not only for its adherence to the real behaviour of the material but also for the regular shape of its surface. Indeed, one has to be very careful in the choice of the surface because in some cases phenomena of corner or flat plasticity may occur (see Figure 2).

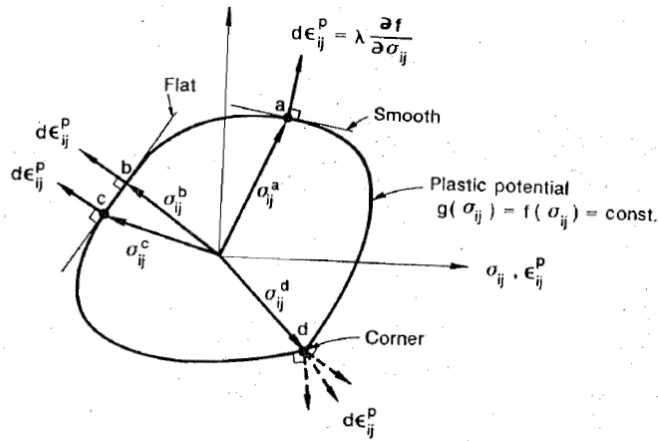


Figure 2 - Flat and corner plasticity (Chen and Han, 1988)

These two phenomena take place on account of the geometry of yielding surface. In fact, on regions of the domain with the same tangent plane the flat plasticity occurs, i.e. the same plastic deformation increment $d\varepsilon_{ij}^p$ corresponds to different stress states while if the surface has some angular points the corner plasticity occurs, i.e. there are different plastic strain increments corresponding to a unique state of stress σ_{ij} .

Both flat and corner plasticity phenomena are particularly evident in Tresca yielding surface, a criterion widely used for metals on account of its more restrictive nature with respect to von Mises' one, but not as effectively applicable in plasticity. In fact, considering a plane representation in $(\sigma_I, \sigma_{II}) \cup (\varepsilon_I, \varepsilon_{II})$ it may be seen that due to the geometry of the Tresca surface on the planes normal to the principal axes σ_I, ε_I and $\sigma_{II}, \varepsilon_{II}$ the flat plasticity occurs while at the corners of the domain the corner plasticity occurs. This does not happen in the case of von Mises surface because of its elliptic shape. In fact, at any point, there is a unique correspondence between the stress state σ_{ij} and the plastic strain increment $d\varepsilon_{ij}^p$ (see Figure 3).

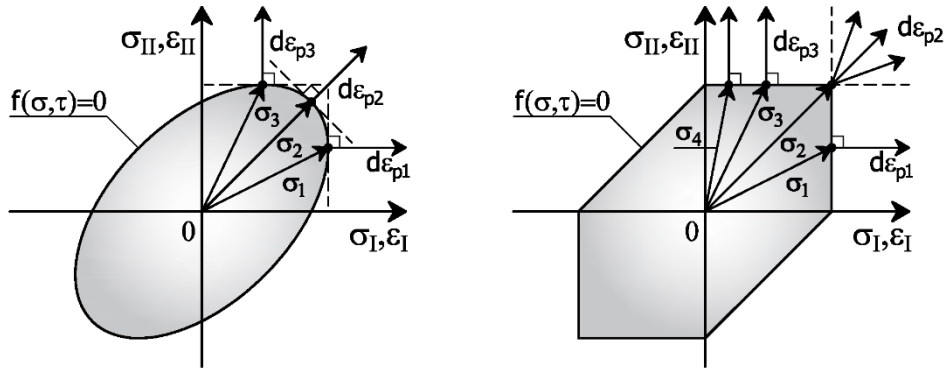


Figure 3 – Differences in plastic flow between von Mises and Tresca yield surfaces.

Due to the irreversible character of the plastic deformation, the increment of plastic work cannot be recovered. This implies that whenever a change of plastic strain occurs the work of the stresses on the increment of plastic strain must be positive and this condition leads to the convexity of the yield surface and to the normality of the plastic flow:

$$dW^p = \sigma_{ij} d\varepsilon_{ij}^p = d\lambda \left(\sigma_{ij} \frac{\partial f}{\partial \sigma_{ij}} \right) \geq 0 \quad (8)$$

where the gradient of the yield function $\frac{\partial f}{\partial \sigma_{ij}} = \nabla f = \mathbf{n}_f$ coincides with the normal to the yield surface. This convexity of the yield surface implies that the scalar product of the stress vector and the normal to the yield surface is non-negative, so that this two vectors must form an angle not larger than $\pi/2$.

Furthermore, it is opportune to underline that also the undetermined factor $d\lambda$ is related to the magnitude of the increment of plastic work dW^p . The scalar multiplier $d\lambda$ must always be positive when plastic flow occurs in order to assure the irreversibility of the plastic deformation and it can be evaluated combining the stress-strain relation with the consistency condition.

In particular, expressing the constitutive relation in terms of stress increments in explicit form:

$$d\sigma_{ij} = C_{ijhk} (d\varepsilon_{hk} - d\varepsilon_{hk}^p) \quad (9)$$

and combining it with the consistency condition which maintains the stress increment vector tangent to the yielding surface, that is the scalar product between the stress increment and the gradient of f is zero, it is:

$$df = 0 \Rightarrow \frac{\partial f}{\partial \sigma_{ij}} d\sigma_{ij} = 0 \quad (10)$$

where the scalar factor $d\lambda$ can be obtained substituting the stress increment of the Eq. (9) in Eq. (10):

$$\frac{\partial f}{\partial \sigma_{ij}} \left(C_{ijhk} d\varepsilon_{hk} - C_{ijhk} d\lambda \frac{\partial f}{\partial \sigma_{hk}} \right) = 0 \quad (11)$$

and finally:

$$d\lambda = \frac{\frac{\partial f}{\partial \sigma_{ij}} C_{ijhk} d\varepsilon_{hk}}{\frac{\partial f}{\partial \sigma_{lm}} C_{lmno} \frac{\partial f}{\partial \sigma_{no}}} \quad (12)$$

where all indices are dummy ones, confirming the scalar character of $d\lambda$. Therefore, given the yield function and defined the strain increments, the scalar multiplier $d\lambda$ can be uniquely determined. In this form, the scalar factor $d\lambda$ may be substituted in the Eq.(13) of the constitutive relation:

$$d\sigma_{ij} = \left(C_{ijhk} - \frac{C_{ijpq} \frac{\partial f}{\partial \sigma_{pq}} C_{rshk} \frac{\partial f}{\partial \sigma_{rs}}}{\frac{\partial f}{\partial \sigma_{lm}} C_{lmno} \frac{\partial f}{\partial \sigma_{no}}} \right) d\varepsilon_{hk} \quad (13)$$

and finally the elastic-plastic tensor of tangent moduli for an elastic-perfectly plastic material can be written as:

$$C_{ijhk}^{EP} = C_{ijhk} - \frac{C_{ijpq} \frac{\partial f}{\partial \sigma_{pq}} C_{rshk} \frac{\partial f}{\partial \sigma_{rs}}}{\frac{\partial f}{\partial \sigma_{lm}} C_{lmno} \frac{\partial f}{\partial \sigma_{no}}} \quad (14)$$

The generical formulation of the associated flow rule can be hence particularized considering the simplest form of the von Mises yield criterion. As previously mentioned, the term $F(\sigma_{ij})$ in Eq.(1) results dependent on the second invariant of the stress deviator and thus substituting the expression $F(J_2) = \sqrt{J_2}$ in Eq.(1), the plastic potential function becomes:

$$f(\sigma_{ij}) = J_2 - k^2 = 0 \quad (15)$$

The flow rule in Eq. (7) as well can be written in the simple form:

$$d\varepsilon_{ij}^p = d\lambda \frac{\partial J_2}{\partial \sigma_{ij}} = d\lambda s_{ij} \quad (16)$$

where s_{ij} is the deviatoric stress tensor and $d\lambda$ is the factor of proportionality with the value:

$$d\lambda \begin{cases} = 0 \\ > 0 \end{cases} \text{ wherever } \begin{cases} f < 0 & \text{or} & f = 0 \\ f = 0 & & \end{cases} \text{ and } \begin{cases} df < 0 \\ df = 0 \end{cases} \quad (17)$$

for an elastic-perfectly plastic material model. The flow rule in Eq. (16) can also be expressed in terms of the components of the strain increments and stresses as:

$$\frac{d\varepsilon_x^p}{s_x} = \frac{d\varepsilon_y^p}{s_y} = \frac{d\varepsilon_z^p}{s_z} = \frac{d\gamma_{yz}^p}{2\tau_{yz}} = \frac{d\gamma_{zx}^p}{2\tau_{zx}} = \frac{d\gamma_{xy}^p}{2\tau_{xy}} = d\lambda \quad (18)$$

These simplified expressions of the stress-strain relations, Eq.(16) or Eq.(18), are known as the Prandtl-Reuss equations after Prandtl who, in 1924, extended the earlier Levy-von Mises equations and Reuss who, in 1930, extended the Prandtl equations to the three-dimensional case and formulated their general form.

As meaningful consequences, it may be noted that a small increment of plastic strain $d\varepsilon_{ij}^p$ depends only on the current state of the stress deviator s_{ij} and not on the total stress increment $d\sigma_{ij}$ which is required to reach that state and to maintain the plastic flow. Also, the principal axes of stress σ_{ij} (or s_{ij}) and the plastic strain increment are coincident by means of the scalar factor $d\lambda$. The Prandtl-Reuss equations confirm that there is no volume change during the plastic flow. In fact, by Eq. (16) it is easy to note that the plastic volumetric deformation results equal to zero:

$$d\varepsilon_{ii}^p = d\lambda s_{ii} = 0 \quad (19)$$

Conclusively, it is possible to specify the previously mentioned relation between the undetermined factor $d\lambda$ and the increment of plastic work dW^p . Recalling that in incremental theory of plasticity the total strain increment $d\varepsilon_{ij}$ is the sum of the elastic and plastic strain increments, as seen in Eq.(4), the elastic strain increment can be deduced from Hooke's law:

$$d\varepsilon_{ij}^e = D_{ijhk} d\sigma_{hk} \quad (20)$$

where D_{ijhk} is the tensor of the elastic moduli, or in other terms:

$$d\varepsilon_{ij}^e = \frac{ds_{ij}}{2G} + \frac{d\sigma_{kk}}{9K} \delta_{ij} \quad (21)$$

and the plastic strain increment can be obtained from the previous flow rule.

Thus, combining Eq.(21) and (16), the complete stress-strain relation for an elastic-perfectly plastic material can be expressed as:

$$d\varepsilon_{ij} = \frac{ds_{ij}}{2G} + \frac{d\sigma_{kk}}{9K} \delta_{ij} + d\lambda s_{ij} \quad (22)$$

in which the unknown term $d\lambda$ is related to the amount of the current increment in the work of plastic deformation dW_p by:

$$d\lambda = \frac{dW^p}{2k^2} \quad (23)$$

which is obtained by simply derivating the rate of plastic work for a Prandtl-Reuss material (see Appendix 1). By recalling the second invariant of the stress deviator, $J_2 = 1/2 s_{ij}s_{ij}$, and that for a flow rule associated with the von Mises yield criterion it is also $J_2 = k^2$, it is:

$$dW_p = \sigma_{ij} d\varepsilon_{ij}^p = 2d\lambda k^2 \quad (24)$$

These formulae hold true for an elastic-perfectly plastic material, as said before. On the other hand, in the case of materials with isotropic hardening, the stress increment allows the yield surface expand homothetically in the stress space for any loading increment. This behaviour of the yield surface in the stress space corresponds to the positive slope of the stress-strain curve in the uniaxial state of stress. Similarly, if the uniaxial stress-strain curve in the plastic range has no slope, the material is elastic-perfectly plastic and the yield surface unchanges during the plastic flow while for an uniaxial stress-strain curve with softening the yield surface above the yielding contracts (see Figure 4).

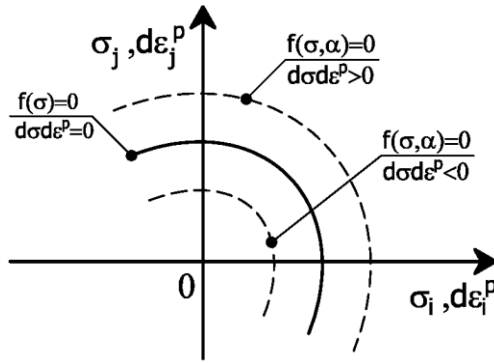


Figure 4 - Hardening and softening in rate-independent plasticity: motion of yield surface in stress space

In the light of this similarity between the uniaxial and the multiaxial behaviours, the conditions of hardening in the stress space related to the motion of the yield surface (expanding, constant and contracting) was generalized from the uniaxial stress-strain curves by Drucker in 1950. In particular, he stated that considering a single stress component σ and the corresponding increment of plastic deformation $d\varepsilon^p$, the conditions of hardening was:

$$\begin{aligned}
 d\sigma d\varepsilon^p &\geq 0 && \text{for positive hardening with expanding surface} \\
 d\sigma d\varepsilon^p &= 0 && \text{for perfect plasticity with constant surface} \\
 d\sigma d\varepsilon^p &\leq 0 && \text{for softening with contracting surface} \quad (25)
 \end{aligned}$$

For isotropic hardening materials, the yield function depends not only on the stress tensor σ_{ij} but also on some hardening parameters which constitute internal variables of the material deduced by experimental evidence.

In particular, if the material plasticity is independent on hydrostatic pressure and depends on only one hardening parameter, the yield function may be expressed by:

$$f(\sigma_{ij}) = F(\sigma_{ij}) - k(\alpha) = 0 \quad (26)$$

where α is the hardening parameter and $k(\alpha)$ is a monotonically increasing function of α . The parameter α characterizes the hardening and it depends on the loading process, in particular on the energy dissipated in the straining process. Until the first yield surface is attained, the hardening parameter is a constant (as seen in the case of elastic-perfectly plastic material with the Eq.(1)) and successively, once plastic deformation occurs, it increases and makes the yield surface expand to a larger one in case of positive hardening material. If the loading process is first reversed and successively reapplied, plasticity is attained on the expanded surface.

In the case of von Mises yield criterion, the term $F(\sigma_{ij})$ is a function of the second invariant of the stress deviator, $F(\sigma_{ij}) = F(J_2) = \sqrt{J_2}$, and the yield function in Eq. (26) results:

$$f(\sigma_{ij}) = J_2 - k^2(\alpha) = 0 \quad (27)$$

where the unknown terms are the hardening parameter α and the hardening function $k(\alpha)$.

In order to obtain the hardening parameter α , two types of assumption are generally made: the strain-hardening or the work-hardening. The choice of one of these hypothesis for the determination of the hardening parameter depends on the constitutive relation characterizing the material and on the yield criterion adopted. The strain-hardening assumption is easier to apply than the work-hardening one and for this reason it is used in most applications. Incidentally, by using the von Mises yield criterion and assuming the constitutive Prandtl-Reuss equations, the strain-hardening and the work-hardening assumptions lead to equivalent results so that the strain-hardening assumption can be chosen to evaluate the hardening

parameter α . For the strain-hardening assumption, the hardening parameter can be determined as a function of the total equivalent plastic strain. In this manner, it is introduced as:

$$\alpha = \varepsilon_{eq}^p = \int d\varepsilon_{eq}^p \quad (28)$$

Under this assumption, an important observation is that the measure of the hardening parameter does not depend upon the strain path but only on the initial and final points of the strain flow in the plastic strain space. The increment of the equivalent plastic strain $d\varepsilon_{eq}^p$ in Eq. (28) can be described as:

$$d\varepsilon_{eq}^p = \frac{2}{\sqrt{3}} \sqrt{\frac{1}{2} d\varepsilon_{ij}^p d\varepsilon_{ij}^p} \quad (29)$$

and likewise the increment of the hardening parameter $d\alpha$ can be obtained by recalling that the normality condition holds by the Eq. (7), and that the increment of plastic deformation follows an associated (von Mises) flow rule:

$$d\alpha = d\varepsilon_{eq}^p = \frac{2}{\sqrt{6}} d\lambda \sqrt{\frac{\partial f}{\partial \sigma_{ij}} \frac{\partial f}{\partial \sigma_{ij}}} \quad (30)$$

where the only unknown term is the scalar multiplier $d\lambda$ which can be calculated in a manner analogous to what has been shown before. Therefore, by virtue of Eq. (30), since the multiplier $d\lambda$ is determined, the increment of the hardening parameter in the loading path can be obtained.

On the other hand, in the Eq. (27) the unknown function $k(\alpha)$ has to be defined and it is sufficient to make reference to the uniaxial state of stress. For uniaxial tension only, the hardening function can be obtained from the uniaxial stress-strain curve in the plastic range and the equation of the yield surface can be simply expressed as:

$$\sigma = k(\varepsilon^p) \quad (31)$$

In such a way, the hardening function depends on the plastic strain $k(\varepsilon^p)$. As in the determination of the hardening parameter α , by replacing the plastic strain ε^p with the equivalent plastic strain ε_{eq}^p and using a von Mises yield surface, the expression for the expanding yield surface due to isotropic strain-hardening is obtained by:

$$J_2 = k^2(\varepsilon_{eq}^p) \quad (32)$$

As previously mentioned, also in the case of isotropic hardening the undetermined factor $d\lambda$ can be found by combining the stress-strain relation with the consistency condition as done for perfect plasticity. In particular, it is:

$$df = 0 \Rightarrow \frac{\partial f}{\partial \sigma_{ij}} d\sigma_{ij} + \frac{dk}{d\varepsilon_{eq}^p} d\varepsilon_{eq}^p = 0 \quad (33)$$

And, by substituting the definition in Eq. (29) for the increment of the equivalent plastic strain, it follows that:

$$\frac{\partial f}{\partial \sigma_{ij}} d\sigma_{ij} + \frac{dk}{d\varepsilon_{eq}^p} \frac{2}{\sqrt{6}} d\lambda \sqrt{\frac{\partial f}{\partial \sigma_{ij}} \frac{\partial f}{\partial \sigma_{ij}}} = 0 \quad (34)$$

Thus, rearranging the terms, the proportionality scalar factor $d\lambda$ can be written as:

$$d\lambda = \frac{\frac{\partial f}{\partial \sigma_{ij}} d\sigma_{ij}}{\frac{dk}{d\varepsilon_{eq}^p} \frac{2}{\sqrt{6}} \sqrt{\frac{\partial f}{\partial \sigma_{ij}} \frac{\partial f}{\partial \sigma_{ij}}}} \quad (35)$$

It may be useful to observe that the terms:

$$\frac{\frac{\partial f}{\partial \sigma_{ij}}}{\sqrt{\frac{\partial f}{\partial \sigma_{ij}} \frac{\partial f}{\partial \sigma_{ij}}}} = \frac{\nabla f}{|\nabla f|} = \hat{n}_f \quad (36)$$

correspond to the unit normal to the yield surface. Thus, by substituting this formula into Eq. (35), the scalar function $d\lambda$ simplifies as:

$$d\lambda = \frac{\sqrt{6}}{2 \frac{dk}{d\varepsilon_{eq}^p}} \hat{n}_f d\sigma_{ij} \quad (37)$$

In this compact form, the term $d\lambda$ can be replaced in the constitutive relation which has a similar expression to the one used for the elastic-perfectly plastic material in Eq.(9). Indeed, the stress-strain relation for isotropic hardening material can be expressed in the form:

$$d\sigma_{ij} = \left(C_{ijhk} - \frac{\sqrt{6}}{2 \frac{dk}{d\varepsilon_{eq}^p}} C_{ijlm} \hat{n}_f C_{nohk} \frac{\partial f}{\partial \sigma_{no}} \right) d\varepsilon_{hk} \quad (38)$$

where the elastic-plastic tensor of tangent moduli for an isotropic hardening material is found as:

$$C_{ijhk}^{EP} = C_{ijhk} - \frac{\sqrt{6}}{2 \frac{dk}{d\varepsilon_{eq}^p}} C_{ijlm} \hat{n}_f C_{nohk} \frac{\partial f}{\partial \sigma_{no}} \quad (39)$$

1.3. Constitutive laws and analytical relations in the deformation theory of plasticity

As said in Section 1.1., the deformation theory of plasticity is essentially a nonlinear stress-strain relationship. Using the additive decomposition property also in this circumstance, the total strain tensor can be expressed by the sum of the elastic and plastic tensors:

$$\varepsilon_{ij} = \varepsilon_{ij}^e + \varepsilon_{ij}^p \quad (40)$$

where the elastic part is governed by Hooke's law and the plastic part is much simple with respect to its counterpart in the flow theory of plasticity. The Hencky-Nadai deformation theory for initially isotropic materials, in fact, proposes that the total plastic strain is merely proportional to the stress deviator, so that:

$$\varepsilon_{ij}^p = \phi s_{ij} \quad (41)$$

where ϕ is a scalar which may be considered a function of the invariant J_2 . The Hencky-Nadai equation (41) is similar to Prandtl-Reuss equation (16) except for the use of the total plastic strain ε_{ij}^p instead of the incremental plastic strain $d\varepsilon_{ij}^p$. The important property of coaxiality between the increment of plastic strain $d\varepsilon_{ij}^p$ and the total deviatoric stress s_{ij} in the incremental theory can be extended to the deformation theory. Thus, coaxiality between the total plastic strain ε_{ij}^p and the total deviatoric stress s_{ij} and consequently also with total stress tensor σ_{ij} , can be stated. This because the principal axes of the stress deviator tensor \mathbf{S} and the total stress tensor $\boldsymbol{\sigma}$ coincide.

The scalar function $\phi(J_2)$ is dependent on material properties which can be determined by experimental uniaxial stress-strain curve and by introducing the definition of effective stress and effective plastic strain. By multiplying Eq. (41) by itself, it is:

$$\varepsilon_{ij}^p \varepsilon_{ij}^p = \phi^2 s_{ij} s_{ij} \quad (42)$$

and introducing the definition of effective stress and effective plastic strain, respectively, it is:

$$\sigma_{ef} = \sqrt{3J_2} = \sqrt{\frac{3}{2} s_{ij} s_{ij}} \quad \text{and} \quad \varepsilon_{ef}^p = \sqrt{\frac{2}{3} \varepsilon_{ij}^p \varepsilon_{ij}^p} \quad (43)$$

In terms of stress, in the uniaxial tension case with $\sigma_I > 0$ and $\sigma_{II} = \sigma_{III} = 0$ the effective stress reduces to the stress σ_I . In terms of strain, given that the first principal plastic strain is $\varepsilon_I^p > 0$ while the other two principal

strains are not zero on account of the plastic incompressibility condition, being them related to the first principal value by $\varepsilon_{II}^p = \varepsilon_{III}^p = -\frac{1}{2}\varepsilon_I^p$, the effective strain reduces again to the uniaxial strain ε_I^p . In this manner, by combining Eqs. (42) and (43) after some manipulations, the proportional function ϕ can be obtained in terms of effective stress and effective plastic strain:

$$\phi = \frac{3\varepsilon_{ef}^p}{2\sigma_{ef}} \quad (44)$$

Substituting the resulting function ϕ in the Hencky-Nadai equation (41), the latter becomes:

$$\varepsilon_{ij}^p = \frac{3\varepsilon_{ef}^p}{2\sigma_{ef}} s_{ij} \quad (45)$$

The dependence of the plastic strain on the effective values of strain and stress implies that a general function of stresses and strains connects the effective stress with the effective plastic strain:

$$\sigma_{ef} = \sigma_{ef}(\varepsilon_{ef}^p) \quad (46)$$

This function is independent from the loading path and can be therefore found from a simple uniaxial tension or compression laboratory test.

In the total strain expression of Eq.(40), the plastic part of the strain tensor can be now replaced by the Eq. (45) so that the total strain tensor can be written as the sum its elastic and plastic parts:

$$\varepsilon_{ij} = \frac{s_{ij}}{2G} + \frac{\sigma_{kk}}{9K} \delta_{ij} + \frac{3\varepsilon_{ef}^p}{2\sigma_{ef}} s_{ij} \quad (47)$$

where K is the elastic bulk modulus $K = E/3(1-2\nu)$. Since the effective stress is a function of effective plastic strain as seen in Eq. (46) and ϕ is a function of these two effective values as seen in Eq.(44), the Hencky-Nadai constitutive

relation can be rewritten in an explicit form in terms of stress and strain components as:

$$\begin{aligned}
\varepsilon_x^p &= \frac{\varepsilon_{ef}^p}{\sigma_{ef}} \left[\sigma_x - \frac{1}{2}(\sigma_y + \sigma_z) \right] & \gamma_{xy}^p &= \frac{3\varepsilon_{ef}^p}{\sigma_{ef}} \tau_{xy} \\
\varepsilon_y^p &= \frac{\varepsilon_{ef}^p}{\sigma_{ef}} \left[\sigma_y - \frac{1}{2}(\sigma_z + \sigma_x) \right] & \text{and} & \gamma_{yz}^p &= \frac{3\varepsilon_{ef}^p}{\sigma_{ef}} \tau_{yz} \\
\varepsilon_z^p &= \frac{\varepsilon_{ef}^p}{\sigma_{ef}} \left[\sigma_z - \frac{1}{2}(\sigma_x + \sigma_y) \right] & & \gamma_{zx}^p &= \frac{3\varepsilon_{ef}^p}{\sigma_{ef}} \tau_{zx}
\end{aligned} \tag{48}$$

The concept of plastic incompressibility implies an important consequence on the expression of the Poisson's ratio which, starting from his elastic value, becomes a function of the stress in the elastic-plastic regime until it reaches a constant value of 0.5 in plastic range. This is valid only for isotropic materials.

As known, the Poisson's ratio is linked with two other material parameters: the secant longitudinal modulus E_s and the secant shear modulus G_s . The relationship between the material parameters ν , E_s and G_s is:

$$\nu = \frac{1}{2} - \left(\frac{1}{2} - \nu_{el} \right) \frac{E_s}{E} \tag{49}$$

$$E_s = \frac{\sigma}{\varepsilon} \tag{50}$$

$$G_s = \frac{E_s}{3 + (2\nu - 1) \frac{E_s}{E}} \tag{51}$$

Therefore, once two of them are given, the third can be directly determined. With the respect to Eq. (47), if the elastic part of the total strain tensor is negligible with respect to the plastic one, the constitutive equation based on the deformation theory can be determined by the plastic tensor only:

$$\varepsilon_{ij} = \frac{3\varepsilon_{ef}^p}{2\sigma_{ef}} s_{ij} \tag{52}$$

Thus, also the previous relation between effective stress and effective plastic strain in Eq. (46) can be extended to encompass the whole effective strain:

$$\sigma_{ef} = \sigma_{ef}(\varepsilon_{ef}) \quad (53)$$

In this manner, the explicit expression of the Hencky-Nadai constitutive relation in Eq. (48) can be rewritten in terms of total strain by introducing the relations between the material parameters ν , E_s and G_s in the plastic range:

$$\begin{aligned} \varepsilon_x &= \frac{1}{E_s} \left[\sigma_x - \nu(\sigma_y + \sigma_z) \right] & \gamma_{xy} &= \frac{\tau_{xy}}{G_s} \\ \varepsilon_y &= \frac{1}{E_s} \left[\sigma_y - \nu(\sigma_z + \sigma_x) \right] \text{ with } \nu = \frac{1}{2} \text{ and } \gamma_{yz} = \frac{\tau_{yz}}{G_s} \text{ with } G_s = \frac{E_s}{3} & & (54) \\ \varepsilon_z &= \frac{1}{E_s} \left[\sigma_z - \nu(\sigma_x + \sigma_y) \right] & \gamma_{zx} &= \frac{\tau_{zx}}{G_s} \end{aligned}$$

1.4. Other plasticity approaches

Notwithstanding the wide adoption of the J_2 flow and deformation plasticity theories in many engineering applications, it has been shown that in particular cases, as for instance in the plastic instability of plates and shells, both the flow and deformation theories present some problems in predicting correct results and more elaborated theories of plasticity have been proposed.

In 1949, Batdorf and Budiansky proposed a theory of plasticity for initially isotropic materials in the strain-hardening range based on the concept of slip. Their theory was essentially based on the physical evidence that for metals plastic deformation occurs on certain slip lines defined by the sliding along parallel planes between small blocks of the metallic crystals (Figure 5). As the applied stress increases beyond a certain limit, the corresponding shear stress increases and metallic crystals begin to slip along the orientation of that shear stress. Plastic deformations are hence caused by slipping along the plane of the maximum shear

stress and the amount of slipping in that direction depends on the history of the corresponding component of shear stress.

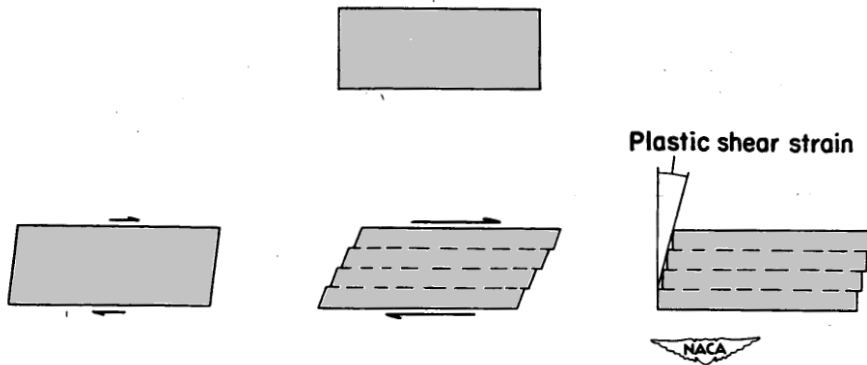


Figure 5 – The concept of slip in single crystal (schematic). (Batdorf and Budiansky, 1949)

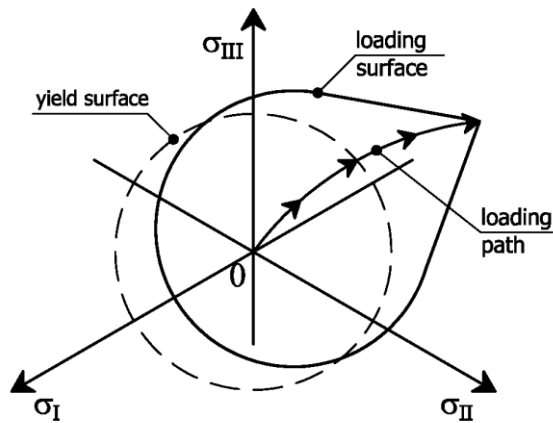


Figure 6 – A loading surface with a corner in stress space.

The total strain increment evolves along preferential directions depending on the material crystalline structure and on the amount but not on the direction of the applied load. At the same time, the strain increment can be decomposed into an elastic and a plastic part. The elastic part is reversible while the plastic part that corresponds to the slip between two adjacent crystalline blocks (see Figure 5) constitutes a permanent deformation. The strain hardening is also function of the

direction of the slip planes and it is therefore anisotropic. In this manner, the plastic function cannot be associated any more with a generic yield function but it depends on the loading surface which is not differentiable at any point and shows corners due to the particular directions of slip (see Figure 6).

Despite the fact that Batdorf and Budiansky theory is rationally based on the physical consideration that the slip is the principal mechanism of plastic deformation, the aim of the authors to give reason of several loading processes in plasticity resulted not entirely achieved. As demonstrated in many applications, as in case of circular tubes subjected to tension or torsion, the characteristic shear function based on the concept of slip is found to assume different and sometimes incorrect values in each simple loading case, so that the accuracy of the approach is not assured. Moreover, the slip theory involves some mathematical complexities in calculation that limit its application in many common cases.

In conclusion, in spite of the sound physical formulation of the slip theory with respect to the flow and deformation theories of plasticity, based on simplified assumptions about the exact orientation of the plastic strain tensor, the slip theory is not easily applicable to analytical calculations.

1.5. Experimental stress-strain curves

As stated in Section 1.2., the first objective in the study of the elastic-plastic behaviour of structures is the understanding of the material response under applied loads. This leads to the definition of constitutive relations which must be determined not only in the simple case of uniaxial state of stress but also in more general combined stress states. Ideally, the constitutive law for any state of stress should be deduced from a set of experimental tests but this is not always possible and hence reference is often made to simple uniaxial tension or compression test data. However, on the basis of some general principles it is possible to generalise the results from uniaxial stress states to multiaxial stress states. A large amount of stress-strain curves are available to determine the material parameters to use in the

multidimensional states and many material models have been developed accordingly.

One of the fundamental parameters is the elastic modulus E given that every stress-strain curve begins with an elastic path governed by the Young modulus E . Another fundamental parameter is the yield stress σ_y which represents the limit value of the stress in the transition from the elastic to the plastic range. However, in materials such as aluminium, the passage from the linear elastic region to the plastic region is so gradual that the identification of the limit yield stress cannot be well-defined.

In this respect, several material curves with a smooth transition between the elastic and plastic paths such as aluminium alloy, stainless-steel and carbon-steel curves are found to be accurately represented by the Ramberg-Osgood formula which defines the yield stress in the stress-strain plane as the intersection between the material curve and a line with the slope of the elastic modulus E shifted along the strain axis by a specified quantity between the 0.1% and the 0.5%. Generally, the amount of this shift, named “yield offset”, is taken as 0.2% and the corresponding yield stress, or proof stress, is hence conventionally defined $\sigma_{0.2\%}$, that is the stress that corresponds to a strain equal to 0.2%.

The general Ramberg-Osgood stress-strain curve is given by the equation:

$$\varepsilon = \frac{\sigma}{E} + K \left(\frac{\sigma}{E} \right)^n \quad (55)$$

in which the elastic strain is $\varepsilon^e = \frac{\sigma}{E}$ and the plastic one is given by the term $\varepsilon^p = K \left(\frac{\sigma}{E} \right)^n$. It is worth noticing that this exponential form does not provide a clear difference between the linear elastic region and the nonlinear plastic region, being the stress-strain curve nonlinear overall. This relation between stresses and strains is based on the three unknown parameters E , K and n derivable from the real stress-strain curve of the material.

As previously said, E is the well-known Young's modulus of the material, measured in the initial phase of the loading process and is related to the tangent to the stress-strain curve at the origin. The other two parameters, K and n , are obtained by tracing two straight lines passing through the origin and intersecting the stress-strain curve at two points, corresponding to two fixed stress values. The slopes of these two lines are respectively equal to $0.7E$ and $0.85E$ so that the stress values deduced by the intersection with the material curve are respectively $\sigma_{0.7E}$ and $\sigma_{0.85E}$ (see Figure 7).

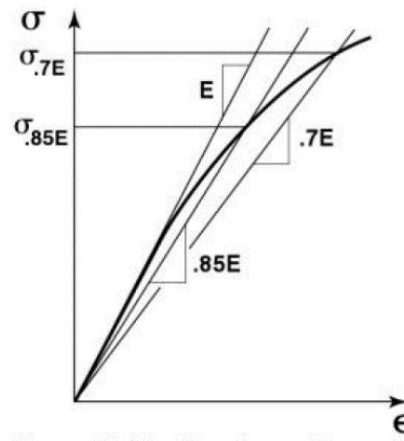


Figure 7 – Determination of K and n in the Ramberg-Osgood stress-strain curve. (Jones, 2009)

By means of simple calculations the parameters K and n are obtained and the stress-strain curve is effectively determined by the use of the three parameters E , $\sigma_{0.7}$ and $\sigma_{0.85}$. However, in practical applications it often appears preferable to deal with the yield strength σ_y rather than with the stress values $\sigma_{0.7}$ and $\sigma_{0.85}$ so that it is convenient to express the stress-strain curve as function of the three parameters E , σ_y and n where n graphically represents the best fit to the stress-strain curve data. (see Appendix 2).

By rewriting the Ramberg-Osgood formula using the three parameters E , σ_y and n , the well-known stress-strain curve expression can be obtained:

$$\varepsilon = \frac{\sigma}{E} \left(1 + \alpha \left(\frac{\sigma}{\sigma_y} \right)^{n-1} \right) \quad (56)$$

where the yield offset is defined as $\alpha = 0.002 E/\sigma_y$ and the hardening parameter n is correlated with the slope of the curve with particular respect to the plastic range.

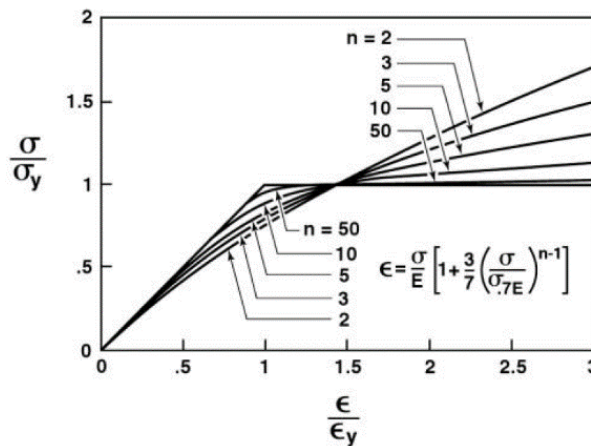


Figure 8 - Ramberg-Osgood stress-strain curves for various strain hardening values.(Jones, 2009)

It is of interest to note that high values of the hardening parameter n correspond to low slopes of the stress-strain curve in the plastic range. In this respect, by plotting several stress-strain curves for various values of n it can be seen that as n gets larger, the curve approaches to the elastic-perfectly plastic behaviour (see Figure 8).

As previously said, the Ramberg-Osgood curve is overall nonlinear so that no clear distinction exists between the elastic and the plastic ranges.

Early, in 1939, Nadai suggested to describe the nonlinear stress-strain behaviour paying particular attention to the limit between the linear elastic region below the yield stress and the nonlinear plastic region above. With respect to this aim, he

proposed a material model based on four parameters and he divided the curve equation in two distinct laws defining the elastic and the plastic regions, respectively. In the elastic range the governing law is:

$$\varepsilon = \frac{\sigma}{E} \quad \text{for } \sigma \leq \sigma_p \quad (57)$$

where E is the Young's modulus and σ_p is the proportional limit.

On the other hand, the plastic range is governed by the law:

$$\varepsilon = \frac{\sigma}{E} + \varepsilon_y \left[\frac{\sigma - \sigma_p}{\sigma_y - \sigma_p} \right]^n \quad \text{for } \sigma \geq \sigma_p \quad (58)$$

where σ_y is the yield stress, ε_y is the strain corresponding to the yield stress and n is a constant. By considering the yield strain at 0.002, the yield stress results to be $\sigma_{0.2\%}$ and the plastic equation becomes:

$$\varepsilon = \frac{\sigma}{E} + 0.002 \left[\frac{\sigma - \sigma_p}{\sigma_{0.2\%} - \sigma_p} \right]^n \quad \text{for } \sigma \geq \sigma_p \quad (59)$$

Consequently, by virtue of Eqs. (57) and (59), the Nadai stress-strain curve results ruled by four parameters: the Young modulus E , the proportional stress σ_p , the yield stress $\sigma_{0.2\%}$ and the constant n . As a consequence of introducing four parameters in the stress-strain relation there is an additional complexity in determining the exponent n with respect to the more straightforward procedure of the Ramberg-Osgood formula. Furthermore, Nadai have only displayed a series of material curves with various integer values of n but he did not state whether n should be an integer or not.

In order to find the value of the exponent which best fits the real material curve, besides the yield point $(\sigma_y, \varepsilon_y)$ other two points, $(\sigma_2, \varepsilon_2)$ and $(\sigma_3, \varepsilon_3)$, need to be chosen in the plastic range:

$$n = \log \frac{\varepsilon_2 - \sigma_2/E}{\varepsilon_3 - \sigma_3/E} + \log \frac{\sigma_2 - \sigma_y}{\sigma_3 - \sigma_y} \quad (60)$$

given that in the form of Eq.(59), the exponent n of the Nadai stress-strain curve cannot be determined by direct calculations.

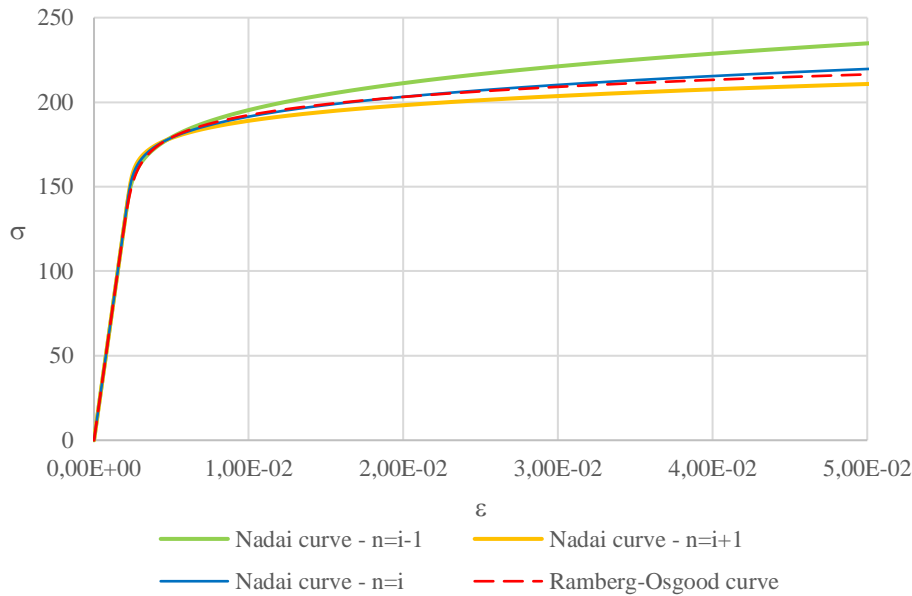


Figure 9 - Overlap of Ramberg-Osgood and Nadai stress-strain curves for an aluminium alloy.

As a matter of fact, in Figure 9 a real stress-strain curve of an aluminium alloy is represented by both the Ramberg-Osgood and Nadai material models. In particular, three Nadai curves are plotted with different values of the exponent n found by considering different points in the material plastic range. By this comparison it is evident that the accuracy of the Nadai stress-strain curve is much influenced by the value of the exponent n and also that constructing the material curve on the basis of two separated laws does not deliver a better accuracy since the Ramberg-Osgood curve fits well the elastic path at the advantage of a simpler

formula. Therefore, the accuracy of a material model does not really depend on the number of parameters taken into account but on its capacity of representing the real stress-strain curve. It is certainly true that a well-defined elastic law distinct from the plastic one as in the case of the Nadai model seems more physically sound with respect to the Ramberg-Osgood representation but, as seen in the previous example of the aluminium alloy, the nonlinearity of the elastic path in the Ramberg-Osgood case is largely acceptable also on account of the fact that for many materials a clear limit of the yield stress cannot be exactly defined in the real world.

In conclusion, it can be stated that determining an universal stress-strain curve must be done primarily in a convenient and sufficiently representative manner without impairing the mathematical treatment of the problem.

1.6. Uniaxial behaviour

For a simple uniaxial loading path, in the deformation theory of plasticity the total strain is directly related to the total stress by the secant modulus E_s which is a function of the actual value of the stress and not of how it has been attained. Conversely, in the flow theory of plasticity the increment of elastic strain is related to the increment of stress through the elastic modulus E while the increment of plastic strain is related to the increment of the plastic stress through the tangent modulus E_t which is a function of the actual stress.

As such, the following incremental strain-stress relationship, $d\varepsilon_{ij} = d\varepsilon_{ij}^e + d\varepsilon_{ij}^p$, holds in the J_2 flow theory of plasticity:

$$d\varepsilon_{ij} = d\varepsilon_{ij}^e + d\varepsilon_{ij}^p = \frac{1}{E} \left[(1 + \nu) d\sigma_{ij} - \nu d\sigma_{kk} \delta_{ij} + h_1(J_2) s_{ij} dJ_2 \right] \quad (61)$$

where E is the Young's modulus, ν is the Poisson's ratio, δ_{ij} is the Kronecker delta, $s_{ij} = \sigma_{ij} - \sigma_{kk} \delta_{ij} / 3$ is the stress deviator and $J_2 = s_{ij} s_{ij} / 2$ is the second invariant of the stress deviator. The term $h_1(J_2)$ is a hardening parameter, which

can be obtained from the one-dimensional stress-strain curve, $d\varepsilon = d\varepsilon(\sigma, d\sigma)$, in terms of the tangent modulus E_t after some manipulations:

$$d\varepsilon = \frac{d\sigma}{E} + h_1(J_2) \frac{4}{9} \sigma^2 \frac{d\sigma}{E} \quad \Rightarrow \quad h_1(J_2) = \frac{3}{4J_2} \left(\frac{E}{E_t} - 1 \right) \quad (62)$$

On the other hand, the following total strain-stress relationship, $\varepsilon_{ij} = \varepsilon_{ij}(\sigma_{ij})$, holds in the J_2 deformation theory:

$$\varepsilon_{ij} = \frac{1}{E} \left[(1 + \nu) \sigma_{ij} - \nu \sigma_{kk} \delta_{ij} + h_2(J_2) s_{ij} \right] \quad (63)$$

where the hardening parameter $h_2(J_2)$ can be obtained from the one-dimensional stress-strain curve, $\varepsilon = \varepsilon(\sigma)$, in terms of the secant modulus E_s :

$$\varepsilon = \frac{\sigma}{E} + h_2(J_2) \frac{2}{3} \frac{\sigma}{E} \quad \Rightarrow \quad h_2(J_2) = \frac{3}{2} \left(\frac{E}{E_s} - 1 \right) \quad (64)$$

The graphical meaning of tangent E_t and secant E_s moduli is shown in Figure 10.

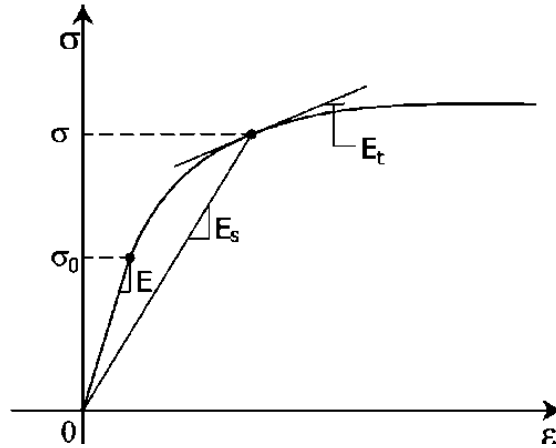


Figure 10: Tangent, E_t , and secant, E_s , moduli in a simple tension test.

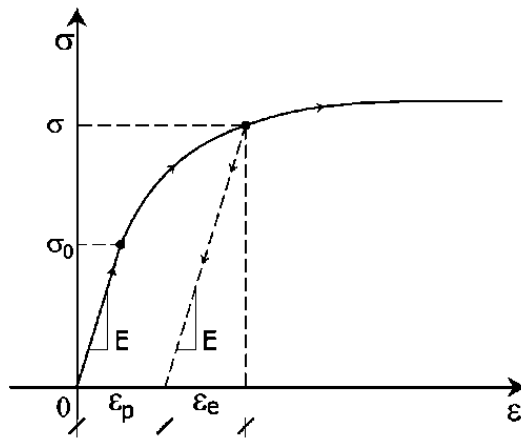


Figure 11: Unloading in the J_2 flow theory of plasticity.

The differences between the two theories of plasticity have been discussed in previous Sections but it is worth pointing out once again that the unloading in the J_2 flow theory of plasticity takes place according to the initial Young's modulus (see Figure 11), as it is experimentally found for most metals, while in the J_2 deformation theory it simply follows the total strain-stress path, making this theory substantially equivalent to a nonlinear elastic one, so that it can be reasonably applied to cases of monotonic proportional loading.

Section 2.

The “plastic buckling paradox”

2.1. The concept of buckling

Buckling is physical phenomenon which involves a sudden lost in strength of a structure due to its lost in shape.

Usually, this quick lost in shape involves consequently large deformations that, as it is generally known, are not recommendable for structural elements. Nevertheless, the most important state during the buckling is not the final widely deformed shape but the initially deformed configuration for which it is still possible to write equilibrium equations in order to obtain the critical load.

There are different types of buckling, the most important for structures are bifurcation buckling and nonlinear collapse. Bifurcation buckling consists in finding a particular state in load P and displacement Δ , called indeed “bifurcation point”, before that the structure is essentially in equilibrium in its undeformed shape and after that the structure changes rapidly its configuration maintaining equilibrium only with rapidly large displacements. The first equilibrium path before the buckling point is called pre-buckling path while the second equilibrium path after the buckling point is called post-buckling path (see Figure 12). There are three types of bifurcation buckling that will be described in detail later in Section 2.2. The investigation of the bifurcation load is conducted by an eigenvalue analysis.

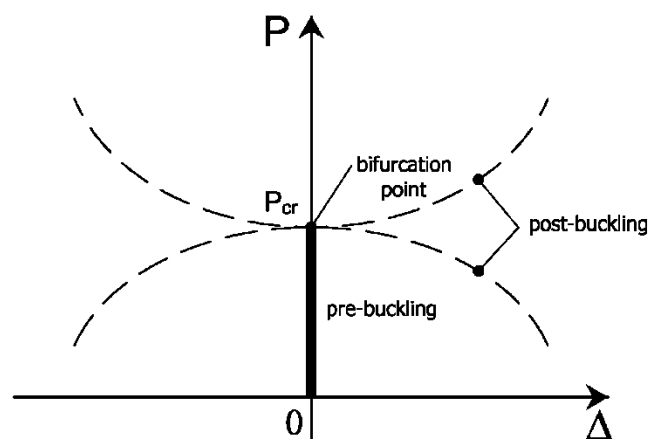


Figure 12: Bifurcation buckling.

The concept of bifurcation buckling is however too much conceptual in fact the most common real buckling phenomenon in structures is the nonlinear collapse. Differently from the bifurcation buckling analysis, the investigation of the nonlinear collapse is conducted by a nonlinear stress analysis in which the slope of the load-displacement curve decreases by increasing the load P until it reaches the critical value and the slope of the $P-\Delta$ curve becomes zero. In this manner, the loading process reaches a peak in correspondence of the critical load and immediately after the structure continues to deform showing quickly large displacements (see Figure 13).

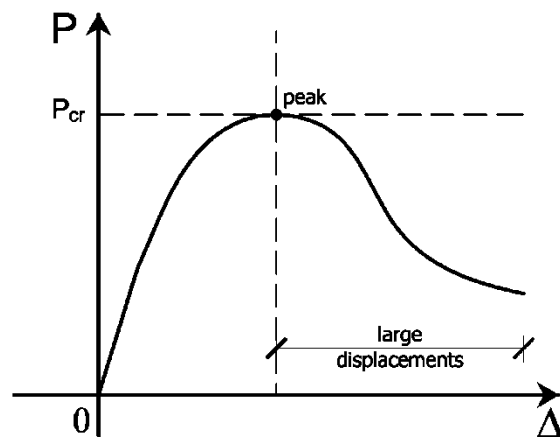


Figure 13: Nonlinear collapse.

Another important point is that buckling is a strongly nonlinear phenomenon, even for material as for geometry. This characteristic is of particular interest because including nonlinearities in the buckling analysis, even in bifurcation buckling as in nonlinear collapse, makes the investigation of the equilibrium paths more elaborate. From the material point of view, the nonlinearity depends on the nonlinearity of the stress-strain relationship of the considered material while the geometrical nonlinearity depends on the configurations before and during the loading process of the considered structural element, i.e. on the presence of some initial imperfections or on the second order effects, if large deformations occur. The effects of nonlinearities are decisive in the investigation of the critical load and also in the definition of the post-buckling behaviour.

Finally, depending on the material and the geometry of the structural element, elastic or plastic buckling may be exhibit. The difference between elastic and plastic buckling consists essentially in the region in which the buckling phenomenon occurs. Detailed examples and theories will be illustrated and discussed later in Section 2.3 and 2.4.

2.2. Bifurcation buckling

For a system with several degrees of freedom, classical stability analysis of a perfect structure develops in an eigenvalue problem that gives as a result a field of multipliers of the unit load where the smallest defines the bifurcation critical load P_{cr} .

A simple explanation of bifurcation buckling may be provided for a perfect column subjected to a compressive load: the concept of bifurcation arises in the fact that before reaching the critical value of the applied load the column is essentially undeformed in bending and then, immediately after the point of the critical load, the structure begins to exhibit deflections.

Stable or instable paths of equilibrium may show, depending on the possibility of increasing load after the bifurcation point. The Figures 14, 15 and 16 are three typical cases of possible load-deflection curves describing the static equilibrium configurations for perfect and imperfect structures. Starting from a perfect structure, Figure 14 displays the stable symmetric buckling where the structure is able to support more load than the bifurcation critical load and where it doesn't follow a particular direction for the deformed shape.

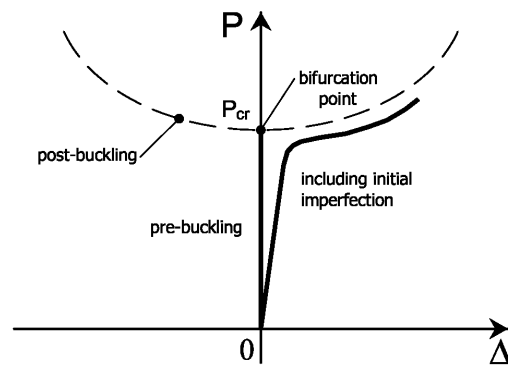


Figure 14: Stable symmetric buckling and influence of imperfections.

Conversely, Figure 15 displays the unstable symmetric buckling for which after the bifurcation point no more increments in loading are available and the structure is rapidly conducted to show large deflections.

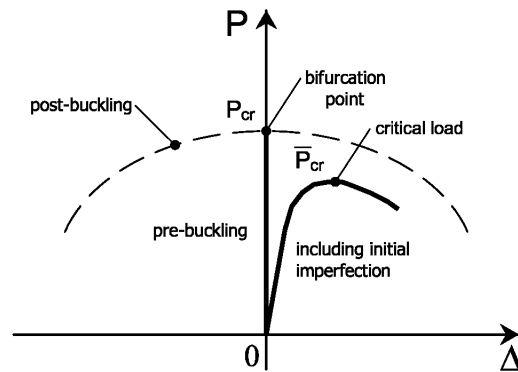


Figure 15: Unstable symmetric buckling and influence of imperfections.

Finally, Figure 16 displays asymmetric buckling where in the post-buckling path the structure shows at the same time a stable behaviour for positive deflections and unstable behaviour for negative deflections due to the asymmetry in loading application or in the geometry of the structure.

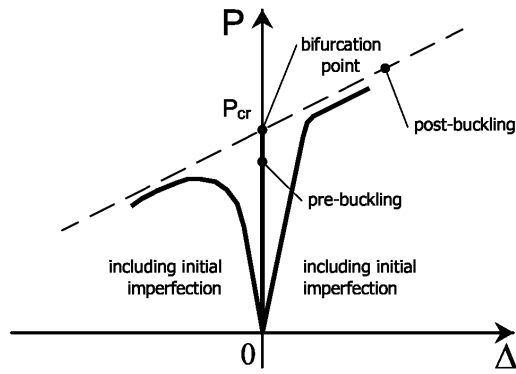


Figure 16: Asymmetric buckling and influence of imperfections.

The general theory of post-buckling behaviour of structures was developed by Koiter during World War II and diffused later, only in 1970. He argued that the classical bifurcation analysis does not give any indication about the character of the post-buckling behaviour or about the behaviour of imperfect structures. Thus, he conducted a careful investigation in the buckling of initially imperfect structures, finding that the presence of initial imperfections reduces significantly the critical load. In fact, any small increment of the applied load on the imperfect configuration produces non-avoidable deflections with a consequently loss in stiffness of the structure. Finally, the structure subjected to initial imperfections goes through a smoother transition between the pre-critical and the post-critical paths (see Figures 14, 15 and 16) so that it is not very simple to identify a clear bifurcation point.

2.3. Elastic buckling

In the elastic range, the first buckling problem investigated in the past was the elastic instability of columns for which Euler, in 1744, found the critical load by determining the value of the centred axial compressive force which caused large lateral deflections in a very slender column.

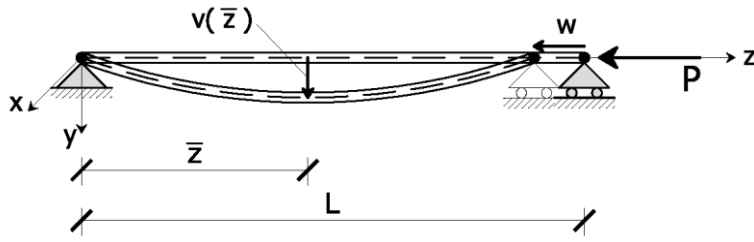


Figure 17: Critical load for a simply supported and uniformly compressed rod.

He wrote a simple equilibrium equation in the deformed configuration using the differential equation governing the deflection of a beam and derived a simple formula for the critical load of a slender ideal column with simply supported ends:

$$P_{cr} = \frac{\pi^2 EI}{l_0^2} \quad (65)$$

where l_0 is the effective length which, in the case of a simply supported rod, is equivalent to the total length L (Figure 17). In stresses terms, with respect to the cross section area, the critical load can be written as:

$$\sigma_{cr} = \frac{P_{cr}}{A} = \pi^2 E \frac{\rho^2}{l_0^2} = \frac{\pi^2 E}{\lambda^2} \quad (66)$$

where the slenderness ratio $\lambda = l_0/\rho$ is introduced. Particularizing the critical load in Eq. (66) for a rectangular cross section with dimensions $b \times h$, it is:

$$\sigma_{cr} = \frac{\pi^2 E b^2}{12 l_0^2} \quad (67)$$

Successively, the Euler formula was modified to describe different cross sections and boundary conditions and later, in 1890, the elastic buckling problem was extended also to the instability of plates, with reference to Bryan energy approach.

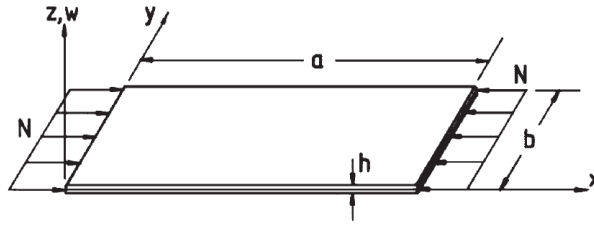


Figure 18: Plate subjected to in-plane compressive loading. (Singer, Arbocz and Weller, 1998)

Bryan investigated the elastic buckling of a supported rectangular plate subjected to a compressive load in its own plane (Figure 18). He described a displacement field normal to the middle surface of the plate that satisfies the boundary conditions. His work arose to the conclusion that the equilibrium stability of a given configuration depends on the total potential energy which must be minimum in that configuration. The critical compressive load for the rectangular plate was found to be:

$$\sigma_{cr} = \frac{\pi^2 E h^2}{12 a^2 (1 - \nu^2)} \quad (68)$$

Comparing the two expressions of the critical load for the column and the plate, it may be seen that replacing in the column equation (67) E by $E/(1 - \nu^2)$ the plate formula (68) results. The greater stiffness against bending in the plate is thus caused by biaxial stresses, identified in the $(1 - \nu^2)$ term.

Despite the fact that Bryan findings have become the foundations of the general theory of the stability of equilibrium for many years, his research includes some limitations. One was highlighted by Southwell in 1913: he showed that Bryan got to the conclusion that instability is possible only in the case of thin rods, plates and shells when no distortions are considered in the extension of the central line or middle surface of the plate. To remedy this limitations, Southwell proposed a general equation of elastic stability which is called “Equation of Neutral Equilibrium” which expresses that it may be equilibrium for a given configuration of slight distortion from the initial position. This equation is generally applicable to both materials of indefinite and finite strength taking as important advantage the

accuracy to follow the actual stress history in a structure which fails by instability under a gradually increasing stress.

The phenomenon of lateral buckling of compressed bodies illustrated by these authors is only a particular case of elastic instability. As it may be seen in the modern design of bridges, ships and aircraft there are a large variety of stability problems that includes torsional, flexural and local buckling. A simplest case is, indeed, the instability of columns with composed cross sections, i.e. cruciform columns that, if subjected to an axial compressive stress, show torsional buckling due to their low torsional stiffness. This simple example will be discussed later, in Section 2.5, in order to describe the “plastic buckling paradox”.

2.4. Plastic buckling

The buckling is one of the principal causes of collapse for plates and shells and, depending on the material and on the geometry of the element, elastic or plastic buckling may occur. For these kind of structures, the elastic buckling usually occurs quickly and catastrophically while the plastic buckling is generally a sequence of degenerating processes. The phenomenon of plastic buckling was firstly shown by thick cylindrical shells subjected to an axial compressive load. Bushnell, in 1982, examined the behaviour of thick cylindrical shells under axial compressive load during the loading process and he found that they firstly attain a critical state in which they deform axis-symmetrically and then, with no other increments in load, they meet the bifurcation point from which they start to deform non-axis-symmetrically showing more post-buckling paths (see Figure 19).

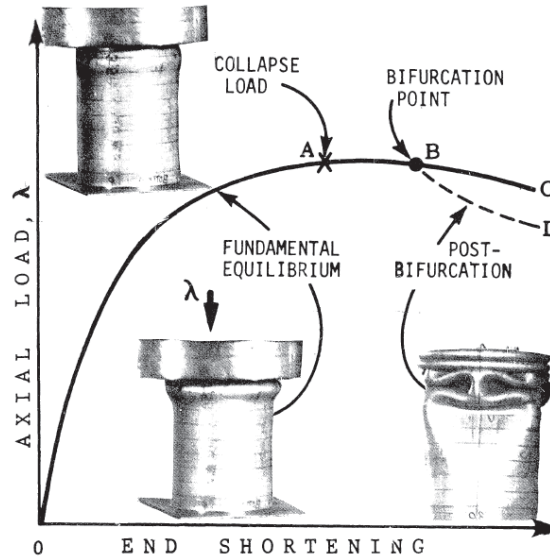


Figure 19: Plastic buckling of a cylindrical shell subjected to axial compression.

Since it is difficult to keep an eye on all the relevant literature about the plastic buckling of bars, plates and shells because of its fast and large development in years, only some of the important authors and publications involved in the field are briefly reported.

In order to appreciate the principal differences between elastic and plastic buckling in detail it may be useful to recall the simplest case of Euler rod subjected to a compressive load. By virtue of the Eq. (66), a hyperbole can be plotted in the $\sigma - \lambda$ plane (see Figure 20) and from this representation it is possible to identify a limit value of slenderness ratio, $\lambda_0 = \pi \sqrt{E/\sigma_0}$, for which the structure shows instability in elastic range. In fact, above the limit of slenderness λ_0 , the rod is considered slender and shows buckling in the elastic region with the corresponding critical load obtained from the Euler formula (65). Conversely, under the limit of slenderness λ_0 , the rod is considered stocky and shows buckling in the plastic range, i.e. the stresses exceed the elastic limit stress σ_0 so that the material has no more a linear behaviour and the critical load depends on the tangent modulus E_t (see Figure 10 in Section 1.6).

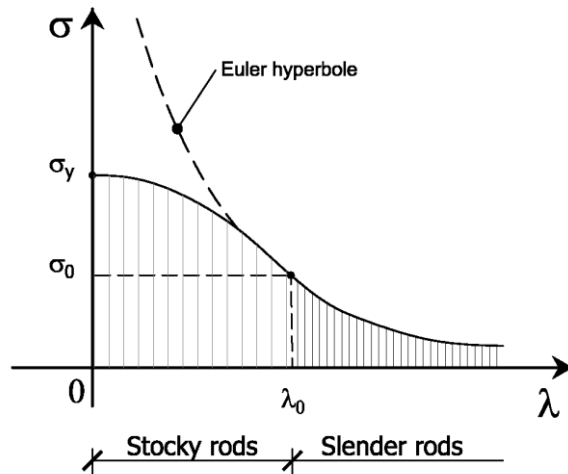


Figure 20: Euler's curve of instability.

The dependence of the critical load on the tangent modulus was discussed firstly in 1889 by Engesser who provided a simple formula for the plastic buckling of a compressed column replacing the elastic modulus E by the tangent modulus E_t in the Euler column formula:

$$P_{cr} = \frac{\pi^2 E_t I}{l^2} \quad (69)$$

He considered a perfect straight column also during the loading process and assumed that the axial strain increases everywhere with no strain reversal during buckling. Up to the critical load the column slightly deflects from the straight configuration of equilibrium. The bending stresses corresponding to these small deflections cause a slightly increase in the total compressive stress on the concave side of the column and a slightly decrease in the compressive stress on the convex side. The neutral axis coincides with the centroidal axis of the column so that bending stresses vary linearly across the whole section.

The tangent modulus theory is very easy to apply and it seems to work well with respect to some experimental results but it tends to underestimate the strength of the column since on the concave side of the column the stress exceeds the proportional limit while on the convex side it is still below it.

Furthermore, he simplified the inelastic buckling using only one value of the tangent modulus where, in reality, it depends on the stress which is a function of the bending moment that varies with the column deflection.

Many authors, included Engesser himself in 1898, proposed corrections to the tangent modulus theory by introducing the reduced modulus (or double modulus) that is a function of the elastic and the tangent moduli and is affected by the shape of the cross section. Among these proposals, finally in 1910 von Kármán presented the reduced modulus theory for a rectangular cross section assuming that, once attained the critical stress, the column starts to bend causing a decrease in strain on one side and an increase on the other one. In this manner, for the increasing strains the resulting stresses are given by the tangent modulus while for the decreasing strains the elastic modulus gives the relation between strain and stress so that the effective modulus all over the column lies between these two moduli in average. The elastic modulus E in the Euler column formula is thus replaced by the von Kármán reduced modulus E_r , so that the critical load takes the form:

$$P_{cr} = \frac{\pi^2 E_r I}{l^2} \quad (70)$$

The reduced modulus theory was accepted to be the exact theory for estimate the inelastic buckling of a perfect column. Nevertheless, experimental data showed that the critical load was generally closer to the tangent modulus one than to the reduced modulus one.

In 1946 Shanley investigated again the inelastic buckling of columns by conducting experiments on small aluminium columns and found some paradoxes in the reduced modulus theory. In particular, he opened a question about the von Kármán assumption that the column remains straight up to the critical load and in the meantime some strain reversal should be needed in order to provide the additional column stiffness required above the tangent modulus load. It is an evident paradox in that it is impossible to have strain reversal in a straight column.

Starting from that point, Shanley considered a discrete model of a rigid column with two degrees of freedom supported by two elastic-plastic springs at the bottom and subjected to an axial compressive force at the top. He concluded that the inelastic buckling of a column may be reviewed on the basis that bending proceeds simultaneously with increasing axial load. Consequently, his work led to a new column formula that includes both the tangent modulus and the reduced modulus formulas. It was shown that bending starts at the tangent modulus load and that the column load increases with increasing lateral deflection, approaching the reduced modulus load as an asymptotic limit if the tangent modulus is assumed to remain constant (Figure 21).

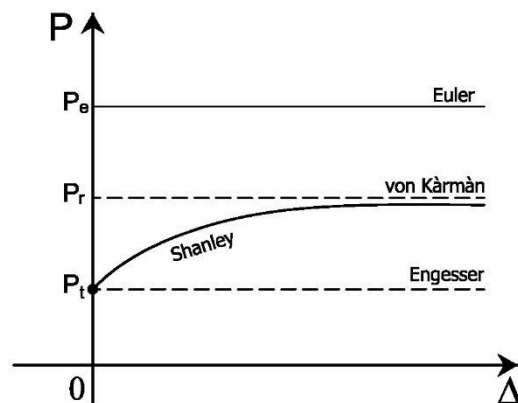


Figure 21: Shanley approach to inelastic column buckling.

The fact that bending proceeds simultaneously with increasing axial load attains particular interest in the case of an imperfect column. As back as 1886, it was described by Ayrton and Perry who analysed a centrally loaded and simply supported column with a small initial curvature. As expected, they found that if the column has an initial curvature of sinusoidal shape giving origin to a small displacement v at the middle section of the column, for any increment of the axial load the deflection also increases and the critical stress is given by the axial stress together with a bending stress produced by the axial force on account of the deflection ($v + \Delta v$).

In this manner, they found a quadratic equation for the critical stress depending on the Eulerian critical load σ_{eul} , as expressed in Eq.(66), on the elastic limit stress of the material σ_0 and on the slenderness ratio λ :

$$\sigma_{cr}^2 - \sigma_{cr} \left[\sigma_0 + \left(1 + \frac{\lambda}{l_0} \nu \right) \sigma_{eul} \right] + \sigma_0 \sigma_{eul} = 0 \quad (71)$$

On the basis of these important contributes, Timoshenko and Gere in 1963 extended the concept of buckling to many engineering problems, i.e. torsional buckling, buckling of frames, curved bars or arches and also to more complex structures as thin plates and shells. Later, in 1974, Hutchinson studied post-buckling behaviour of a large amount of plates and shells, highlighting important aspects about imperfection sensitivity in plastic buckling. He firstly investigated post-buckling behaviour of a simple discrete model, similar to Shanley's model for plastic buckling of column and then he examined a simple continuous model to bring out some aspects of the behaviour of continuous solids.

2.5. The “plastic buckling paradox”

The linear and nonlinear theories of elastic buckling have been thoroughly investigated in years and they have almost totally been completed so that the research about the buckling of structures directs on the plastic buckling and it is still ongoing in order to examine the motives of the diffuse paradox of plastic buckling.

The plastic buckling paradox shows that in the plastic buckling analysis the J_2 flow theory of plasticity seems to bring to a significantly overestimation of the critical buckling load while the J_2 deformation theory of plasticity seems to obtain more accurate results respect to the experimental data. The paradox insists due to the theoretical and physical differences between the two theories of plasticity (see Table 1) which should favour the use of flow theory of plasticity in practical applications.

Flow theory of plasticity	Deformation theory of plasticity
Dependence on the second invariant of stress deviator (J_2)	Dependence on the second invariant of stress deviator (J_2)
Incremental expression of the plastic strain	Total expression of the plastic strain
Dependence on the loading path	Independence on the loading path
Elastic unloading with residual deformations (irreversibility of plastic deformation)	Absence of residual deformations (nonlinear elastic behaviour)
Physical representation of the experimental loading and unloading behaviour of uniaxial tests	Best correspondence with the experimental data in many plastic buckling problems
Complexity in calculations	Simplicity in calculations
Wide applicability (step-by-step analysis)	Applicability in case of proportional or radial loading

Table 1 – Difference between flow and deformation theories of plasticity and the plastic buckling paradox.

The plastic buckling paradox firstly showed during investigations into the plastic buckling of flat plates subjected to uniform stresses. Since the 1940s, the critical load of a simply supported flat plate of infinite length has been obtained by using the J_2 flow theory of plasticity that is mathematically and physically more rigorous. However, in 1949, Bijlaard and Stowell, solved the same problem by using the J_2 deformation theory of plasticity that is commonly valid under the condition of proportional loading, and found an unexpected result: the critical load calculated with the deformation theory was in a very good agreement with the experimental evidence while that obtained by the flow theory tended to overestimate.

To completely understand this phenomenon, the applicability of the two theories of plasticity was further investigated in a large number of experiments.

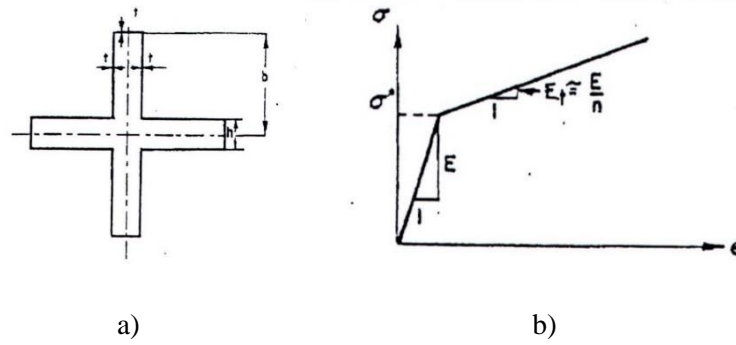


Figure 22: Onat and Drucker model (1953). a) simplified geometrical model. b) simplified material model.

In the 1953, Onat and Drucker found the paradox in the case of axially compressed cruciform column showing a torsional buckling. The critical compressive stress predicted by deformation theory was in better agreement with the experimental results than that predicted by the flow theory. The reasons for this discrepancy were found in the high value of the shear modulus in the flow theory formula. The solution was investigated by conducting an approximate analysis (Figure 22) in which small initial imperfections were taken into account. In this manner, assuming that there existed a very small imperfection in the column, the critical buckling load predicted by the flow theory was found to be reduced significantly, getting itself close to that predicted by the deformation theory. In any real structure, small initial imperfections can be observed thus the Onat and Drucker interpretation seems to be acceptable and was also supported by further theoretical studies and practical applications. Nevertheless, due to the imperfection sensitivity of the shear modulus in the flow theory formulation, the deformation theory remained to be suggested for practical applications.

The plastic buckling paradox of plates continued to be investigated from both analytical and numerical points of view. In 1974, Hutchinson and Budiansky pointed out a query about Onat and Drucker findings inquiring how and when it was possible for an unavoidable small imperfection to have a very large influence on the plastic buckling of a cruciform column. They gave an important contribution as they found that the effect of small imperfections depends on material properties: for different values of strain hardening the critical load becomes a function of the

imperfection amplitude. In particular, if the strain hardening of the material is sufficiently low (n is high, in the Ramberg-Osgood tensile relation, see Appendix 2), the numerical analysis confirms that in the use of the J_2 flow theory of plasticity the initial imperfections are effectively small and then unavoidable. However, when the strain hardening is high (n is low) the range of imperfections cannot necessarily be considered unavoidable (see Figure 23) so that it gave a limitation in the previous results.

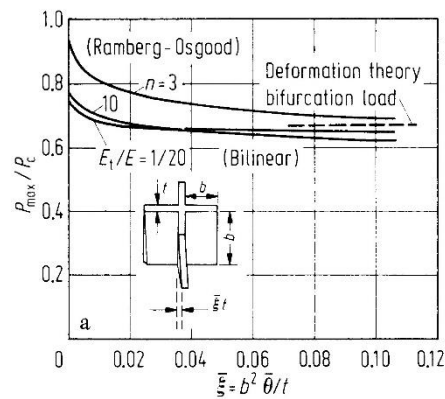


Figure 23: Hutchinson and Budiansky numerical results for critical load as a function of imperfection amplitude (1976).

Since the 1960s, the plastic buckling paradox also showed in the inelastic instability of cylindrical shells subjected to axial compression and, in the light of the latter findings, the effect of initial imperfections was also investigate.

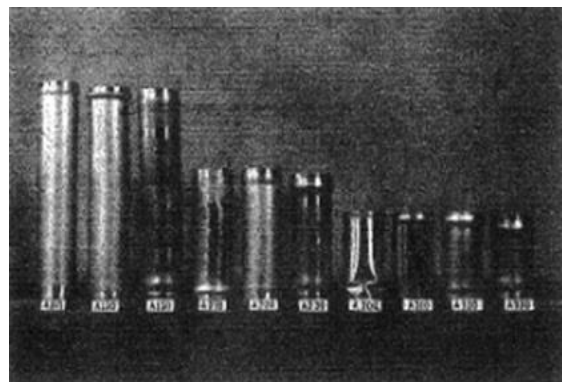


Figure 24: Modes of buckling of Lee's tests (1962).

In 1962, Lee conducted an analytical and experimental study concerning the plastic buckling of ten initially imperfect cylindrical shells of aluminium alloy 3003-0 subjected to an axial compressive stress (Figure 24). From the comparison between the theoretical and the experimental results he found that the deformation theory of plasticity provides a moderately accurate prediction of the buckling strength but fails to describe correctly the post-buckling behaviour, while the incremental theory leads to an overestimation of buckling strength, even though initial imperfections are taken into account. He proposed a procedure to determine the effect of initial imperfections on the buckling mode and on the critical stress using Donnell's equations and the principle of virtual work but he substantially concluded that the paradox remained to be solved.

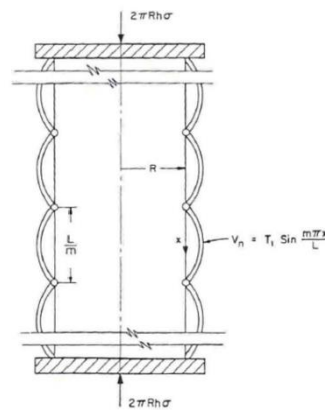


Figure 25: Batterman hinge model for cylindrical shells (1965).

In 1965, Batterman conducted analytical and experimental analyses on thirty cylindrical shells of aluminium 2024-T4 with different radius to thickness and length to radius ratios. He confirmed that it is necessary to include initial imperfections in the analysis in order to avoid the paradox but at the same time he argued that more attention has to be given to the nonlinearity of the material and to the effect of unloading. This was highlighted with reference to Shanley's concept of considering the growth of imperfections during the loading process until the critical load is attained. In this light, Batterman proposed a hinge model to investigate the effects of unloading (see Figure 25) and he found that the flow theory gives results very close to deformation theory. Finally, the incremental

theory was found to predict both the buckling strength and the geometry of buckling for thick or moderately thick shells in a good manner.

Later, starting from 1982, Bushnell proposed a strategy to eliminate much of the discrepancies between flow and deformation theories in many buckling problems and wrote some comments and suggestions about nonlinear collapse, bifurcation buckling and about a combination of these modes in order to avoid unexpected catastrophic collapse of structures composed by thin shells. He guided for years engineers to produce an efficient design of practical shell structures giving several examples and at the same time giving the basis for the determination of the buckling behaviour and of the imperfection sensitivity. Numerically, he gave a fundamental contribution with the code BOSOR5, a computer software able to predict the buckling of elastic-plastic complex shells of revolution including large deflections and creep.

After many practical and physical approaches, starting from the 1990s, analytical investigations were conducted in order to confirm theoretically the experimental findings. In 1992, Ore and Durban studied the buckling of axially compressed cylindrical shells in the plastic range for various boundary conditions. Unfortunately, they found that the analytical flow theory model overestimates the buckling compressive stress while the deformation theory predicts results very close to the measured test values. In the wake of Hutchinson and Budiansky observations, they also discovered that the strain hardening of the material was influent in the differences between the two theories in the way that the discrepancies reduce with increasing of the strain hardening parameter.

In 1999, Mao and Lu analysed the plastic buckling of cylindrical shells subjected to axial compression, comparing the theoretical results with the experimental ones obtained by Lee in 1962. The results were again in favour of deformation theory as the predicted critical stress was in good agreement with the experimental value while the flow theory tended to exceed in the buckling load.

The plastic buckling of cylindrical shells under an axial compressive stress was largely investigated in years and, as seen in Batterman or Bushnell works, some obtained results were of particular engineering interest. However, the plastic buckling paradox shows not only in the simple case of axial compression. In fact, it can be observed also with different loading conditions, i.e. in case of nonproportional loading. It is true that there are many interpretations of nonproportional loading but in the study of plastic buckling of cylindrical shells a simple nonproportional loading condition was frequently found in practical applications as the combination of axial tension and external pressure (considering for instance underwater or buried pipelines used to transport fluids).

At first, in 1988, Giezen investigated the plastic buckling paradox of cylindrical shells subjected to nonproportional loading in his thesis and concluded that, if reversing the loading path, the flow theory fails to predict buckling while the deformation theory summarily displays the same trend of the test results. Later, in 1991, Giezen et al. extended his early findings conducting experimental and numerical analyses on cylindrical shells subjected to combined axial tension and external pressure. For the investigation they chose two sets of specimens (Set A and Set B) of aluminium alloy 6061-T4 with length to diameter ratio equal to one. The condition of nonproportional loading were studied considering two different loading process: in the first, the axial tensile load was maintained constant and the external pressure increased while in the second one, the external pressure was maintained constant and the axial tensile load increased. As a result, considering the case of constant axial tension and increasing external pressure, the experiments showed that the axial tension reduces the strength of the cylinder moving the material in the plastic range, so that less external pressure is required to cause buckling. Conversely, from the numerical analyses conducted by the use of BOSOR5 computer program, the flow theory exhibits an increase in the external buckling pressure due to the axial tension and the deformation theory in some cases results to quite under-estimate the buckling pressure. In conclusion, Giezen et al. stated that both flow and deformation theories fail to predict the buckling load in case of nonproportional loading (see Figure 26).

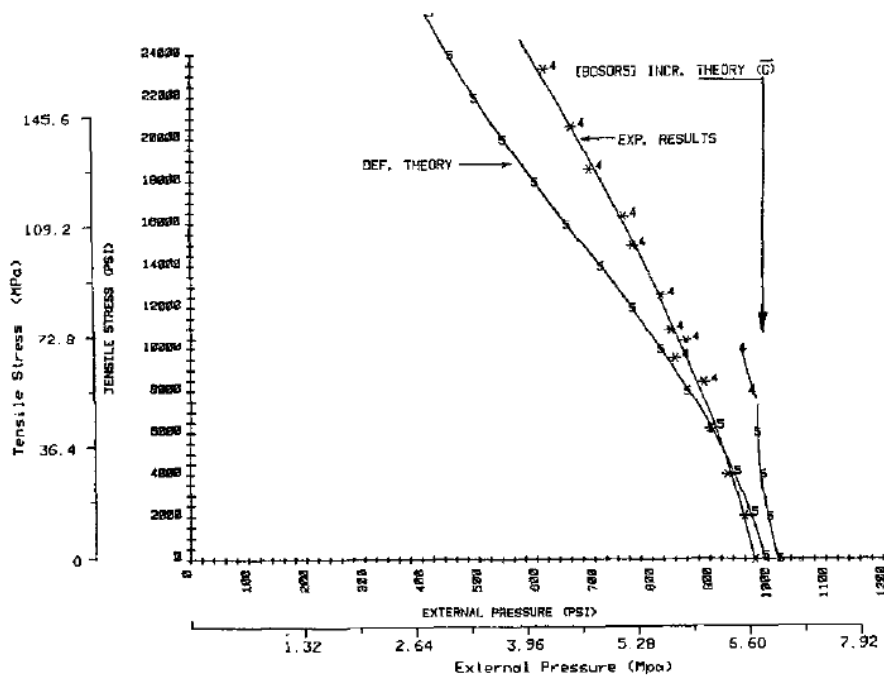


Figure 26: Numerical and experimental results for specimens (Set A). (Giezen, Babcock and Singer, 1991)

Moved from the Giezen et al. conclusions, Blachut et al. in 1996 thoroughly investigated the plastic buckling paradox for cylindrical shells under the same condition of nonproportional loading, i.e. axial tension combined with external pressure. They carried out numerical calculations employing the BOSOR5 program and conducted several experiments on a large amount of specimens with different material and geometrical characteristics. They tested thirty cylinders of mild-steel with length to diameter ratio of about 1, 1.5 and 2. As a matter of fact, it was noticed that the ratio L/D governs the accordance between the critical loads predicted by flow and deformation theories. In fact, the results showed that for $L/D=1$ the two theories coincide only for pure radial loading (sole external pressure) or with a negligible axial tension while in the other cases with increasing axial tension the flow theory tends to fail in predicting the critical load and the deformation theory is closer to the experimental value (Figure 27).

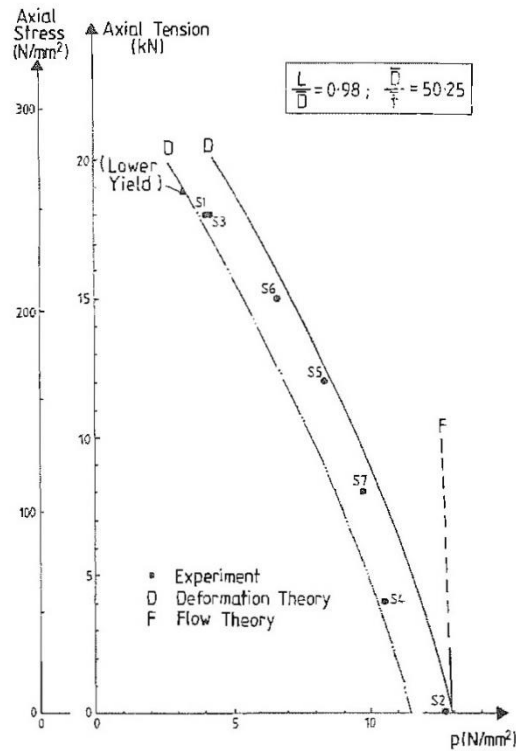


Figure 27: Theoretical and experimental results for $L/D = 1$ cylinders. (Blachut, Galletly and James, 1996)

On the other hand, for L/D from 1.5 to 2, flow and deformation theories are in a very good agreement together, depending on the amount of the axial tension applied. In any case, deformation theory results to agree reasonably well with the experimental evidence and moreover, differently from Giezen et al. findings, deformation theory predicts that, with increasing axial tension, the external pressure at which buckling occurs decreases, that is what observed in the experimental tests. Finally, another important point highlighted by Blachut et al. was the strong connection between the critical load and the number of waves in the buckling configuration. Indeed, they found numerically and confirmed experimentally that the critical load corresponds to the buckled configuration with the lowest number of circumferential waves.

The plastic buckling paradox for cylindrical shells thus resulted to be still unresolved and in years several experiments were conducted and many approaches proposed to archive the problem in all its shades. Between the experimental analyses, it may be recalled the contemporary work of Bardi and Kyriakides, in 2006, where they investigated the buckling of cylindrical shells due to axial compression. They designed and machined fifteen cylinders of stainless steel SAF 2507 with diameter to thickness ratio from 23 to 52. The result brought to a substantial confirm of Bushnell explanation about the evolution of plastic buckling for cylindrical shells: the first instability path causes axial axisymmetric mode of wrinkling (see Figure 28) and subsequently for some combinations the wrinkles amplify changing to a non-axisymmetric mode before the critical load is attained. The mode of wrinkling is by two or three circumferential waves and, with the gradual amplification of the wrinkles, the stiffness of the structure quietly reduces. Upon the critical load, phenomena of local collapse appears due to large deformations. In order to predict the beginning of buckling, a bifurcation analysis was conducted using the J_2 deformation theory of plasticity and by comparing the analytical and experimental results the authors found that the deformation critical stress was very close to the experimental one but at the same time the theory tends to overestimate the wrinkle wavelength.



Figure 28: Axisymmetric mode of wrinkling observed by Bardi and Kyriakides (2006).

From a numerical and theoretical point of view, Shamass et al. in 2014 investigated the plastic buckling paradox of cylindrical shells subjected to axial compression and also, in 2015, subjected to axial tension plus external pressure. Their contribution sheds a light on the plastic buckling paradox with respect to the common engineering practise of conducting nonlinear buckling analyses by the use of finite element models. In fact, in the case of simple axial loading they found that, contrary to previous statements, by employing a geometrically nonlinear finite element formulation and by choosing opportunely the constitutive laws, a satisfying concordance may be found between the experimental evidence and the numerical results obtained by the use of flow theory of plasticity (Figure 29).

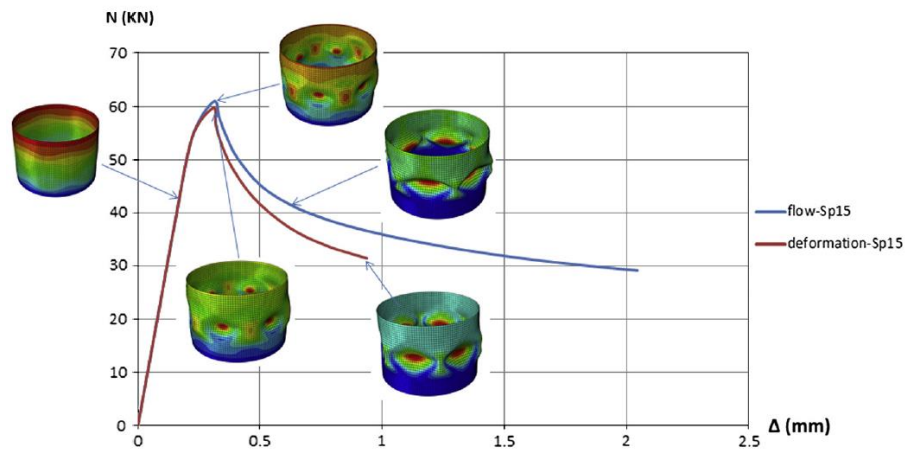


Figure 29: Results of axially compressed imperfect cylinders. (Shamass, Alfano and Guarracino, 2014).

Afterwards, in the case of nonproportional loading, they showed that the roots of the discrepancy between the two theories of plasticity resides in the harmonic buckling shapes assumed in the circumferential direction. As a matter of fact, the kinematic rigour of the incremental theory leads to an overestimation of the critical load while the more flexibility of the kinematic imposed by the deformation theory counterbalances the excessive stiffness, predicting critical loads more in accordance with the test values.

2.6. Open issues in the investigation of the plastic buckling paradox

In the previous Section 2.4 and 2.5, several examples of theories and applications about the plastic buckling of plates and shells have been presented. The plastic buckling paradox was found in many fields and, in particular, the simple case of the cruciform column and the case of cylindrical shells subjected to axial compressive load or nonproportional loading have been reported.

In any investigation, the authors highlighted the possible causes of the paradox and found their own solution to the problem, depending on the material, the geometry and the boundary conditions of the analysed structures. However, most of the time, open issues have persisted about these main topics: the imperfection sensitivity, the influence of the material curve, the applicability of the theories for different loading conditions and finally the numerical resolution by the use of finite element models.

About the imperfection sensitivity, since first studies about the paradox in plates, it was supposed that the presence of a small initial imperfection, which implies the presence of a shear stress, may be sufficient to reduce the shear stiffness modulus in the flow theory of plasticity leading to results more in accordance with the deformation theory ones and the experimental evidence (Onat and Drucker). Nevertheless, in several cases it was seen that imperfection amplitudes have to be considerable and thus no more compatible with those experimentally measured (Gerard and Becker, Hutchinson and Budiansky) so that there is still a difficulty in determining the magnitude of initial imperfection to take into account.

The imperfection sensitivity is strictly connected with the second open topic that is the influence of the material curve. In fact, as noticed by Hutchinson and Budiansky, when the strain hardening parameter of the material is high (n is low, in the Ramberg-Osgood tensile relation, see Appendix 2) the level of initial imperfection cannot be considered unavoidable. In this manner, the material curve assume an important role in the resolution of the problem.

Moreover, in the investigation of the plastic buckling for shells, it can be seen that there are different loading conditions under which the plastic buckling paradox occurs and it is not always possible to obtain reasonable results neither by the use of the flow theory and of the deformation theory of plasticity. Indeed, in case of nonproportional loading both the two theories fail to predict the critical load, as for instance in the condition of combined axial tension and external pressure investigated by Giezen and Blachut.

However, with the contemporary largely diffusion of powerful computational instruments able to conduct incremental analyses in the plastic range by the use of the Finite Elements, the discrepancy between flow and deformation theories has been reduced and many paradoxes have been resolved. But a doubt still remains: can a modern incremental analysis naturally avoid the plastic buckling paradox? Is that sufficient?

In the light of these open issues, the objectives in the study of the plastic buckling paradox for plates and shells remain:

- to introduce an initial imperfection in analytical and numerical flow and deformation models for the simple case of a cruciform column subjected to axial compression. The aim is to understand the effects of initial imperfections on the occurrence of the paradox depending on their amplitudes;
- to compare and validate the findings from the previous objective (the investigation of the cruciform column) for different material curves which show low and high strain hardening parameters;
- to thoroughly investigate the case of nonproportional loading in the plastic buckling of cylindrical shells in order to achieve a great correspondence between the flow theory and the deformation theory of plasticity and the experimental evidence;
 - to evaluate the results obtained by conducting numerical analysis on cylindrical shells subjected to nonproportional loading using finite element models in order to demonstrate whether or not an incremental nonlinear numerical analysis is sufficient to avoid the plastic buckling paradox.

Section 3.

Plastic buckling of a cruciform column

3.1. Historical background

Inelastic stability of structures has been the focus of many controversies since the end of the nineteenth century. In fact, as back as 1889, Engesser suggested the use of a variable tangent modulus into the classic Euler's equation for the study of the stability of a simple metal column in the plastic range. Two years later Considère indicated that a correct stability analysis in the plastic range would require the concept of strain reversal on one side of the bent section. As a result of this observation, Engesser in 1895 presented the reduced modulus theory. In the following years many carefully conducted column tests on both mild steel and aluminium alloys columns showed that the difference between the tangent modulus and reduced modulus theory is depending on the stress-strain curves for the materials and it was found that the results from experiments on aluminium alloy columns were generally in better accordance with the tangent modulus theory. Moreover, earlier in 1886 Ayrton and Perry had analysed the effect of initial imperfections and found that for a simply supported column with a small initial deflection, for any increment of the axial load the critical stress was given by the axial stress together with a bending stress due to the moment produced by the axial force on account of the increased deflection. On these bases in 1947 Shanley re-examined the basic assumptions of the analysis of the stability of columns in the plastic range and suggested that, if axial and bending straining proceed simultaneously at the buckling load, as it is the case even for a minimum level of imperfection, the tangent-modulus equation should be used as a basis for determining the buckling strength of members in the inelastic range. As a result, most of the work done thereafter in the inelastic stability of compressed metal struts has made reference to the Shanley's concept that axial straining and bending proceed simultaneously and the tangent-modulus theory has been seen as providing the critical stress of a strut with vanishingly small initial imperfections.

However, inelastic buckling is a complex phenomenon which occurs not only in simply compressed columns, but also in a variety of other structures such as plates, cylinders, torispherical domes and many others. Since buckling is a non-linear problem from both a geometrical and a material point of view, the material non-linearity requires the definition of appropriate strain-stress relationships, which for many cases of structural interest go beyond the results of a simple tensile test.

In general, based on whether path-dependence is accounted for or not, the plasticity models that have been proposed for metals in the strain hardening range can be divided into two main groups: the deformation and the flow theories of plasticity. In both of these theories the plastic deformations do not allow volume changes as plastic yielding is ruled by the second invariant of the deviatoric part of the stress tensor and in this respect they are both called J_2 theories of plasticity. The difference lays in the fact that the deformation theory of plasticity is based on the assumption that for continued loading the state of stress is uniquely determined by the state of strain and, therefore, it is essentially a special path-independent non-linear constitutive law, while the flow theory of plasticity assumes that an infinitesimal increment of strain is determined by the current stress and its increment. This leads to a path-dependent relationship in which the current strain depends not only on the value of the current total stress but also on how the actual stress value has been reached.

Notwithstanding the fact that there is a general agreement that the deformation theory of plasticity lacks physical rigour in comparison to the flow theory, the use of the deformation theory has been repeatedly reported to predict buckling loads that are in better agreement with the experimental results. This fact has become known in literature as the “plastic buckling paradox” and examined in a number of works and books in the past decades too abundant to be cited (see, for example Hutchinson, Lubliner or Bazant and Cedolin). It suffices to say that in the early and mid-90s, the plastic buckling paradox was considered still unresolved, for example, by Tuğcu and proposed explanations were judged still inconclusive by Teng who once again confirmed the better agreement between deformation theory and experiment.

Lately in a series of works on the plastic buckling of cylindrical shells Shamass et al. have shown that the results of geometrically nonlinear finite element analyses using flow theory with an associated flow rule are unaffected by the plastic buckling paradox, while a number of other analytical and numerical approaches are sensible to it. Their conclusion has been that there is actually no buckling paradox but, depending on the particular methodology, some inconsistencies might appear in the results.

In the light of these results and in order to investigate the roots of the plastic buckling paradox here reference is made to what is generally considered the simplest example of the discrepancy between the flow and deformation theory of plasticity, that is the torsional buckling of a cruciform column. This problem has been examined, among the others, by Cicala, Onat and Drucker, Hutchinson and Budiansky, Tuğcu and, very recently, by Becque. Cicala first and Onat and Drucker successively suggested that the plastic buckling paradox can be avoided by incorporating imperfections into the model since inevitable imperfections reduce the buckling load by the flow theory to levels close to those predicted by the deformation theory. Hutchinson and Budiansky confirmed this finding for low strain-hardening metals but found that for metals with significant strain-hardening the imperfections have to be of considerable magnitude in order to reduce the buckling load provided by the flow theory. In general, most of the published work has aimed, by various means, to reduce the shear modulus from the flow theory computations below its elastic value. In this respect Becque has proposed to circumvent the problem by apparently considering a perfectly straight column without initial imperfections but developing a relationship between shear stress and shear strain increments at the onset of buckling. In this manner he applied the plastic flow rule to an infinitesimal solid element in its deformed shape. As a matter of fact this approach makes reference to a configuration which is slightly past the buckling point and thus incorporates the deviation from the straight configuration to reduce the shear modulus of the flow theory.

In Section 3 an accurate analysis of the torsional buckling of a cruciform column is presented on the basis of the classic formulation of the flow and deformation theory of plasticity and it is shown that in order to overcome this apparent conundrum it is not only necessary to consider an imperfect column, as generally suggested in the past, but principally to account correctly for the effects of the imperfection up to the point where the critical load is attained. In such manner a very good agreement between the results from the flow theory of plasticity and other analytical and experimental results can be obtained also for metals with significant strain-hardening without the necessity of making reference to imperfections of significant magnitude.

In fact it is proven that, by properly computing the effects of imperfections until the critical load is attained, the flow theory of plasticity is capable of attaining a very good agreement with both the results from the deformation theory and from experiments. A new approach for the evaluation of the critical load according to the flow theory of plasticity is presented in detail.

Finally, an analysis of the effects of employing different stress-strain curves is carried out and the physical implications underlying the use of the flow and deformation theory of plasticity are discussed with particular attention to the variation in the shear modulus.

3.2. Torsional buckling: canonic results

It is known that doubly symmetric sections with low torsional rigidity may experience a pure torsional buckling mode. This is the case of a cruciform column which, for a certain range of dimensions, tends to buckle in the torsion mode under axial compression, as shown in Figure 30.

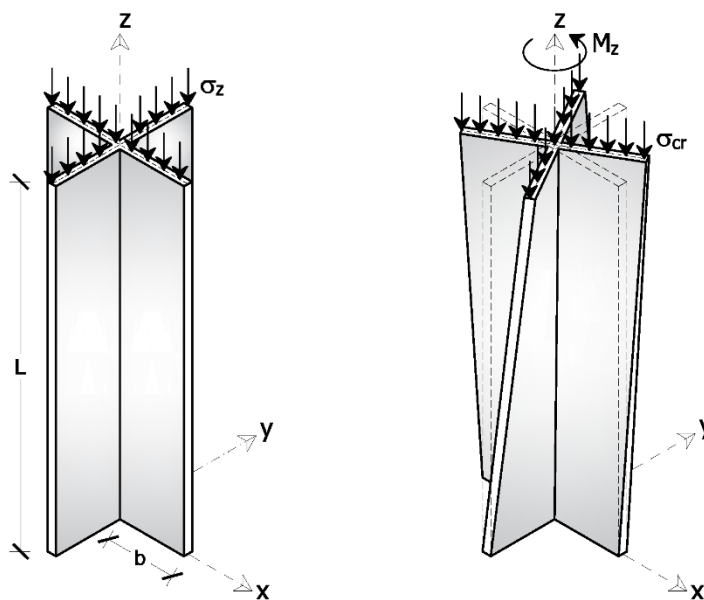


Figure 30: Torsional buckling of a cruciform column.

In the torsion mode the flanges of the cruciform column show twisting in addition to compression and change from simple compression to a combination of compression and shear. When the applied load exceeds the yield load, the twisted structure remains in the plastic state in the whole cross-section. This problem was originally studied by Stowell and, as said before, is one of the simplest examples of the problems of the J_2 flow theory in predicting buckling loads of perfect structures, that is of the plastic buckling paradox.

In the elastic range the critical stress, i.e. the value of the axial stress at which the torsional buckling takes place is:

$$\sigma_{cr} = G \frac{h^2}{b^2} \quad (72)$$

where G is the elastic shear modulus:

$$G = \frac{E}{2(1+\nu)} \quad (73)$$

and h and b are shown in Figure 31.

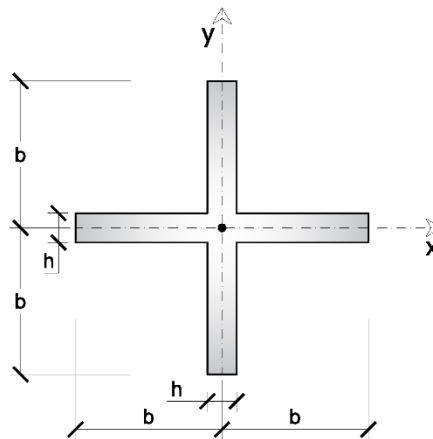


Figure 31: Cross section of a cruciform column.

In the plastic range, according to the classic J_2 flow theory of plasticity, Eq. (73) still holds true on account of the smooth yield surface, which makes the

increments in the components of shear stress and strain related, following uniaxial compression, by the elastic shear modulus. In fact, from Eq. (61), determining the shear strain where the Kronecker delta is zero and where the hardening parameter h_1 vanishes because of the void value of s_{ij} , it is:

$$d\gamma = 2d\varepsilon_{ij} = \frac{2}{E} \left[(1+\nu)d\sigma_{ij} - \cancel{\nu d\sigma_{kk}\delta_{ij}} + \cancel{h_1(J_2)s_{ij}dJ_2} \right] \quad (74)$$

and, being $d\tau = d\sigma_{ij}$, it follows:

$$G = \frac{d\tau}{d\gamma} = \frac{E}{2(1+\nu)} \quad (75)$$

that is Eq. (73).

On the other hand, in the case of the deformation theory of plasticity, the shear modulus following uniaxial compression can be derived from Eq. (63) as follows:

$$\gamma = 2\varepsilon_{ij} = \frac{2}{E} \left[(1+\nu)\sigma_{ij} - \cancel{\nu\sigma_{kk}\delta_{ij}} + h_2(J_2)s_{ij} \right] \quad (76)$$

and, being $\tau = \sigma_{ij}$, by virtue of Eq. (64) it is:

$$G_s = \frac{\tau}{\gamma} = \frac{E_s}{3 + (2\nu - 1)\frac{E_s}{E}} \quad (77)$$

The critical stress hence results:

$$\sigma_{cr} = G_s \frac{h^2}{b^2} \quad (78)$$

From these simple formulae it results evident that the critical load from the flow theory of plasticity does not account for the fact the column has attained the plastic status and provides the same result as the strut had remained in the elastic range, differently from the otherwise less physical sound deformation theory of plasticity. In fact, for a perfect straight column at the instant of buckling, shearing stress τ and shearing strain γ are added to the existing state of simple compression at the point P of the yielding curve $f(\sigma, \tau) = 0$ but according to the flow theory and its

associated rule the normal to the loading surface and therefore the plastic strain increment vector points along the negative $\sigma - \varepsilon$ axis (see Figure 32).

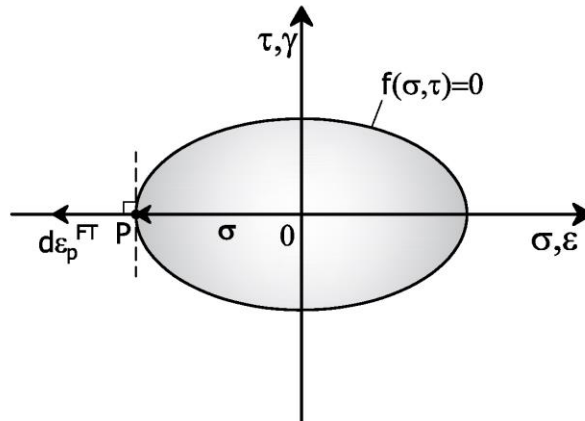


Figure 32: Strain increment for a perfect column according to the flow theory of plasticity.

As pointed out by Onat and Drucker, this means that all the associated incremental theories of plasticity which do not have a corner at P predict, according to Eq. (61), a purely elastic response to a shearing stress increment from point P .

This problem could be overcome by making reference to the slip theory by Batdorf and Budiansky, which predicts a vertex in the yield surface at the current stress point. However, the rationale of the present investigation is to show how the paradox does not take place by correctly accounting for the presence of small, unavoidable imperfections in the spirit of Shanley's approach and in the framework of the classic formulae of J_2 plasticity only. This route has been followed to some extent by Cicala, Onat and Drucker and Hutchinson and Budiansky, among the others, who all pointed out that, in order to avoid the overestimation of the shear stiffness of a compressed cruciform column given by the J_2 flow theory of plasticity, the introduction of an imperfection could help to obtain less inaccurate results.

However, in the case of the flow theory of plasticity these studies does not seem to have managed to calculate precisely the effects of the imperfection up to the point where the limit load is attained and have thus concluded that for materials with significant strain hardening the imperfections have to be of significant magnitude to reduce conveniently the buckling load.

3.3. A procedure for the evaluation of the critical load according to the flow theory of plasticity

The analytical procedure which will be developed in the present Section is intended to show that the observation by Shamass et al. that the results of incremental non-linear finite element analyses using flow theory with an associated flow rule are unaffected by the plastic buckling paradox, can be justified on the basis of straightforward equations in the case of a simple example like the one of a cruciform column.

Since an incremental approach naturally remedies the problem, it is natural to speculate that the difficulty in estimating the influence of small, unavoidable, imperfections lies in the procedure used to evaluate the actual state of stress in the vicinity of buckling. In fact, while on one hand the presence of a small shear stress τ is sufficient to reduce the value of the shear modulus for the flow theory of plasticity, given that in such a case the plastic strain increment vector do not point along the negative $\sigma - \varepsilon$ axis anymore (see Figure 33) on the other hand it is known that the buckling of structures in the plastic regime often exhibit a strong imperfection-sensitivity and so the evaluation of the equilibrium path must be precise in order to avoid inaccurate and unreliable results as it seems to have been the case for many past investigations.

In fact, in the canonical formulation of torsional buckling, Eq. (72) is simply a limit equilibrium equation involving the instability forces which tend to twist the column on account of the applied axial load and the warping resistance of the column. As such, it has been straightforwardly employed by the previously mentioned authors in order to evaluate the buckling load in the plastic range by

substituting the value of the elastic shear modulus, G , with those from the flow or the deformation theory of plasticity. In this respect, the analysis of the response of the structure to the imperfection is aimed to evaluate the value of the plastic shear modulus at buckling, that is at the limit axial load that the column can sustain before the induced twisting cannot be counteracted by the torsional stiffness and increases suddenly.

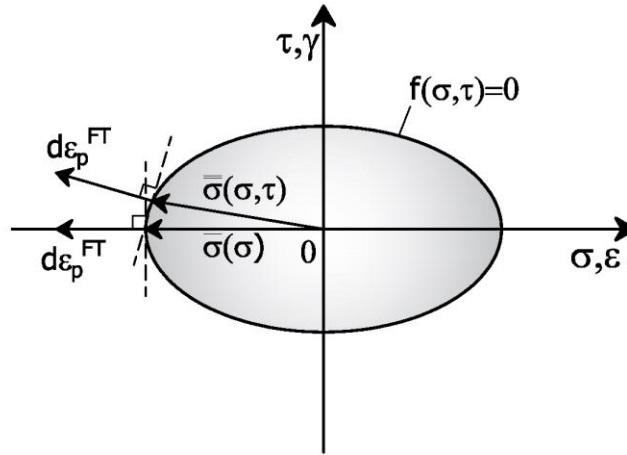


Figure 33: Strain increment for an imperfect ($\bar{\sigma}$) vs a perfect ($\bar{\sigma}$) column according to the flow theory of plasticity.

This said, the expression of the critical load in the flow theory of plasticity relies upon the value of the tangent shear modulus, which, by its own nature (see Figure 10 in Section 1.6), is much more sensible to the shape of the stress-strain curve than the value of the secant shear modulus in the deformation theory of plasticity. Therefore, inaccurate calculations tend to affect much more the predictions from the flow theory than those from the deformation theory.

To keep things as simple as possible, reference is made to the equation which links the rotation of the cross section in the plane x - y , ϕ , to the value of the applied compressive stress σ_z in presence of an initial imperfection ϕ_0 , as shown in Figure 34. Upon twisting, the axis of the column is thought to remain straight while each of the four flanges rotate about the z axis. The column is considered as an element fixed at one end and free at the other, in a manner that at $z = 0$ the cross section is

prevented to rotate but free to warp and at $z = L$ the section can rigidly rotate in its own plane and warp. Given that for the case at hand the warping rigidity C_1 vanishes, the equilibrium equation results:

$$C \frac{d^2\phi}{dz^2} = \sigma I_0 \frac{d^2(\phi + \phi_0)}{dz^2} \quad (79)$$

where $C = GI_t$ is the torsional rigidity, $I_t = \frac{4}{3}bh^2$ is the torsional inertia and $I_0 = \frac{4}{3}hb^2$ is the polar inertia. Introduce for simplicity $\sigma = \sigma_z$.

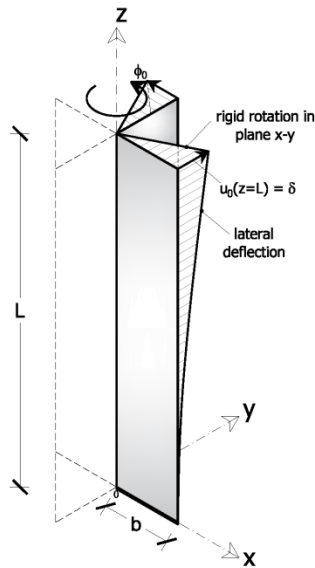


Figure 34: Twisted configuration of an imperfect cruciform column.

The angle of twist may be expressed in terms of the lateral deflection at the extremity of the flange, u , as $\phi = u(z)/b$. By choosing an initial imperfection shape in the sinusoidal form:

$$u_0(z) = \delta \sin \frac{\pi z}{2L} \quad (80)$$

Eq. (79) becomes:

$$(C - \sigma I_0) \frac{d^2 \phi}{dz^2} = -\sigma I_0 \delta \frac{\pi^2}{4L^2} \sin \frac{\pi z}{2L} \quad (81)$$

and the solution links the angle of twist of the generic cross-section, $\phi(z)$, to the applied compressive stress, σ , by:

$$\phi(z) = \frac{\delta I_0 \sigma \sin \frac{\pi z}{2L}}{C - I_0 \sigma} \quad (82)$$

or also, in terms of shear strain, $\gamma = h \frac{d\phi}{dz}$:

$$\gamma(z) = \frac{\delta I_0 \sigma h \pi}{2L(C - I_0 \sigma)} \cos \frac{\pi z}{2L} \quad (83)$$

Depending on the maximum amplitude of the initial imperfection, δ , for any increment of the applied compressive stress, σ , there will be increments in shear stress, $\tau = G\gamma$, so that the state of stress is never that of simple compression at any loading stage.

However, the key point is that at the beginning of the loading process, the shear modulus is simply the elastic one, G , whereas once the material has attained the plastic status, the shear modulus can be derived from the incremental stress-strain relationship in Eq. (61) in the case of the flow theory of plasticity and from the stress-strain relationship in Eq. (63) in the case of the deformation theory of plasticity.

Given that both a compressive axial stress, σ , and a shear stress, τ , exist at any stage of the loading process, in the case of the flow theory of plasticity, by virtue of Eqs. (61) and (62) it is:

$$d\gamma = \frac{2}{E} \left[(1 + \nu) d\tau + \frac{3}{4J_2} \left(\frac{E}{E_t} - 1 \right) \tau \left(\frac{2}{3} \sigma d\sigma + 2\tau d\tau \right) \right] \quad (84)$$

and, since the second invariant of the stress deviator may be expressed as $J_2 = s_{ij}s_{ij} / 2 = \sigma^2 / 3 + \tau^2$, Eq. (84) becomes:

$$d\gamma = \frac{2}{E} \left[(1+\nu)d\tau + \frac{3(E-E_t)\tau}{4E_t \left(\frac{\sigma^2}{3} + \tau^2 \right)} \left(\frac{2}{3}\sigma d\sigma + 2\tau d\tau \right) \right] \quad (85)$$

so that after some manipulation it is:

$$\frac{d\gamma}{d\tau} = \frac{1}{G_t} = \frac{2}{E} \left[(1+\nu) + \frac{(E-E_t)\tau\sigma}{2E_t \left(\frac{1}{3}\sigma^2 + \tau^2 \right)} \frac{d\sigma}{d\tau} + \frac{3(E-E_t)\tau^2}{2E_t \left(\frac{1}{3}\sigma^2 + \tau^2 \right)} \right] \quad (86)$$

It is worth noticing that Eq. (86), which represents the inverse of the tangent shear modulus, G_t , depends not only on the actual state of stress, (σ, τ) , but also on the ratio $d\sigma/d\tau$. However, it can be observed that, given the limit state of equilibrium represented by Eq.(72) at the point of buckling, the increment in the axial stress, if any, can be considered negligible when the swift progression of twist makes the increment in the shear stress much more significant than any possible increment in the axial loading, so that it can be assumed that $d\sigma/d\tau \approx 0$. Thus, the expression of the tangent shear modulus, G_t , can be written as:

$$G_t = \frac{EE_t \left(\frac{\sigma^2}{3} + \tau^2 \right)}{2E_t(1+\nu) \left(\frac{\sigma^2}{3} + \tau^2 \right) + 3(E-E_t)\tau^2} \quad (87)$$

Vice versa, with reference to the deformation theory of plasticity, from Eqs. (63) and (64) it is easy to verify that the expression of the secant shear modulus G_s in Eq. (77) holds the same at any stage of the loading process under a compressive axial stress, σ , and a shear stress, τ .

All this said, in order to evaluate the critical load for an imperfect column, for the deformation theory of plasticity reference can be made to Eqs. (78) and (77), while for the flow theory of plasticity reference can be made to the following equation:

$$\sigma_{cr} = G_t \frac{h^2}{b^2} \quad (88)$$

together with the expression in Eq. (87) of the tangent shear modulus, G_t , at buckling. In fact, as noticed before, Eq. (72) is simply a limit equilibrium equation involving the instability forces which tend to twist the column on account of the applied axial load and the warping resistance of the column. As such, it is here employed, as it has been previously done in literature by Onat and Drucker or Hutchinson and Budiansky and similarly to Euler's critical load for a column in the inelastic range, by substituting the value of the elastic shear modulus, G , with those from the flow or the deformation theory of plasticity, as it is done in Eqs.(78) and (88). Of course, the value of the actual shear modulus, G , at buckling has to account both for the initial imperfection and for the loading path.

This is the point that, in the view of the present authors, has mostly contributed to the controversies about the results from the flow and deformation theories and thus to the plastic buckling paradox.

In fact, the use of the secant shear modulus in Eq. (77) of the deformation theory of plasticity, which is, by its own nature, a total strain theory, naturally leads Eq. (83) to provide a value of the shear strain – and successively of the shear stress - which takes into account the loading path up to the considered value of the compressive stress σ . On this basis, and by making reference to the equivalent stress defined as:

$$\sigma_{eq} = \sqrt{\sigma^2 + 3\tau^2} \quad (89)$$

the simple procedure illustrated in the flow chart in Figure 35 gives straightforwardly the value of the critical load for an imperfect column according to the deformation theory of plasticity.

Things are different in the case of the flow theory of plasticity. In fact, being the flow theory of plasticity an incremental strain-hardening relationship, the tangent shear modulus cannot be directly employed in Eq. (83) to obtain a value of the shear strain – and successively of the shear stress – because this would not take correctly into account the loading path up to the considered value of the compressive stress σ . Instead, a non-linear incremental procedure would be required to reach the desired value of the compressive stress σ , which is what the finite elements incremental analyses do. Many analytical and numerical approaches in literature seem to have made reference to the elastic shear modulus to evaluate the effect of the initial imperfection on the progressive twisting of the column and this appears to be the main reason for which the imperfections have to be of significant magnitude in order to reduce the buckling load provided by the flow theory for materials with significant strain-hardening.

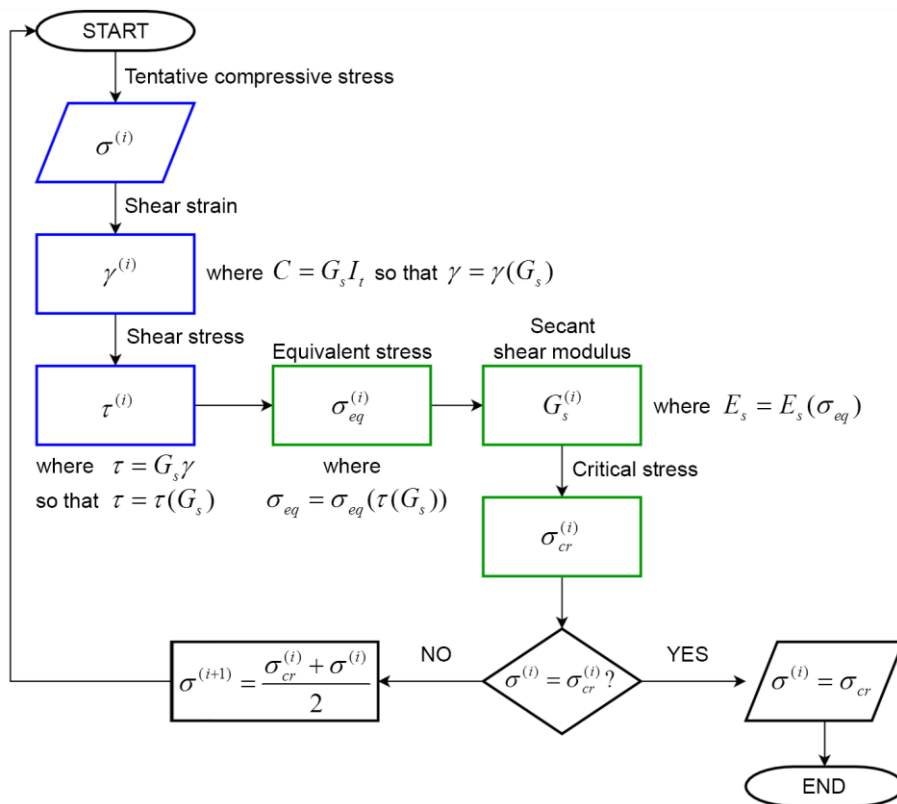


Figure 35: Iterative procedure for the evaluation of the critical twisting load of an imperfect cruciform column according to the deformation theory of plasticity.

Here the idea is to calculate the value of the shear strain induced by the imperfection on the basis of Eq. (83) and of the secant value of the shear modulus also in the case of the flow theory of plasticity. In such a manner, the loading path up to the considered value of the compressive stress σ is rationally taken into account in the elastic-plastic range and the simple procedure illustrated in the flow chart in Figure 36 is proposed to compute the value of the critical load for an imperfect column according to the flow theory of plasticity. It is worth underlining that, with the exception of the first three steps (in blue), relative to the evaluation of the value of the shear strain for an assigned value of the compressive stress, σ , the procedure uses the value of the tangent shear modulus G_t from Eq. (87). Also, it is worth noticing that the use of the secant modulus from the deformation theory of plasticity, generally restricted to proportional loading, is here justified by the fact that the column undergoes torsional instability following a monotonic process which does not involve strain or stress reversal.

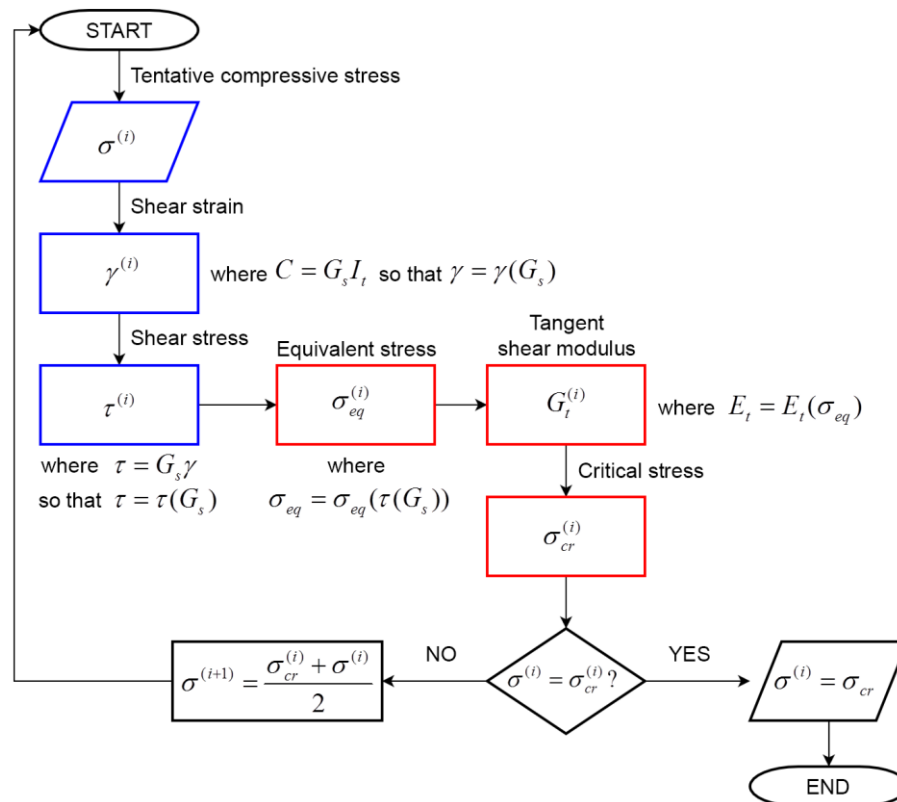


Figure 36: Iterative procedure for the evaluation of the critical twisting load of an imperfect cruciform column according to the flow theory of plasticity.

In both cases, the variation of the Poisson's ratio, ν , in the inelastic range can be estimated as reported by Hopperstad et al.:

$$\nu = \nu_p + \frac{E_s}{E}(\nu_e - \nu_p) \quad (90)$$

where the fully plastic value, ν_p , is generally set equal to 0.5 for incompressible, isotropic materials and ν_e is the elastic value. However, since buckling generally occurs for relatively small plastic strains, it has been usually found reasonable to take the current value of Poisson's ratio as the elastic one, ν_e .

In the following Section 3.3. a number of results from the presented procedures will be discussed and compared with those from experimental and numerical FE analyses.

3.4. Discussion of the results

The procedure presented in the previous Section 3.2. is applied here to a few selected examples and compared to the results from numerical and experimental tests.

Three different types of aluminium alloys have been taken into consideration, namely AA6082 tempers T4 and T6 and aluminum alloy 6061 temper T4. The first two alloys have been employed in the experimental tests by Hopperstad et al. who conducted torsional buckling tests on extruded aluminum cruciform columns, while the third one has been extensively employed in the studies by Shamass et al. on the buckling of circular cylindrical shells.

The uniaxial stress-strain relationships of the materials under monotonic loading are characterised by the well-known Ramberg-Osgood formula (see Appendix 2):

$$\varepsilon = \left(1 + \alpha \left(\frac{\sigma}{\sigma_y} \right)^{n-1} \right) \frac{\sigma}{E} \quad (91)$$

where σ_y is the nominal yield strength, sometimes called “proof stress” and denoted by $\sigma_{0.2\%}$, n is the strain hardening parameter and α is the “yield offset”, i.e.:

$$\alpha = 0.002 \frac{E}{\sigma_y} \quad (92)$$

	E (MPa)	σ_y (MPa)	n	α	σ_u (MPa)
AA 6082 T4	69 700	131	23	1.064	238
AA 6082 T6	67 900	267	45	0.509	290
AA 6061 T4	65 130	178	16	0.733	246

Table 2 - Ramberg-Osgood parameters for the considered aluminium alloys.

The material properties for the considered aluminium alloys are reported in Table 2. σ_u is the ultimate strength.

Figure 37 shows the plot of the Ramberg-Osgood curves for the considered aluminium alloys. Moreover, Figure 38 shows the same curves in a non-dimensional plot which highlights the low strain hardening ($n=45$) of AA6082T6 versus the relatively high ($n=16$ and $n=23$, respectively) of AA6061T4 and AA6082T4. This representation is useful with reference to the observations by previous investigations, especially by Hutchinson and Budiansky, which concluded that for metals with high strain-hardening the imperfections have to be of a much bigger magnitude with respect to low strain-hardening metals in order to reduce the buckling load provided by the flow theory.

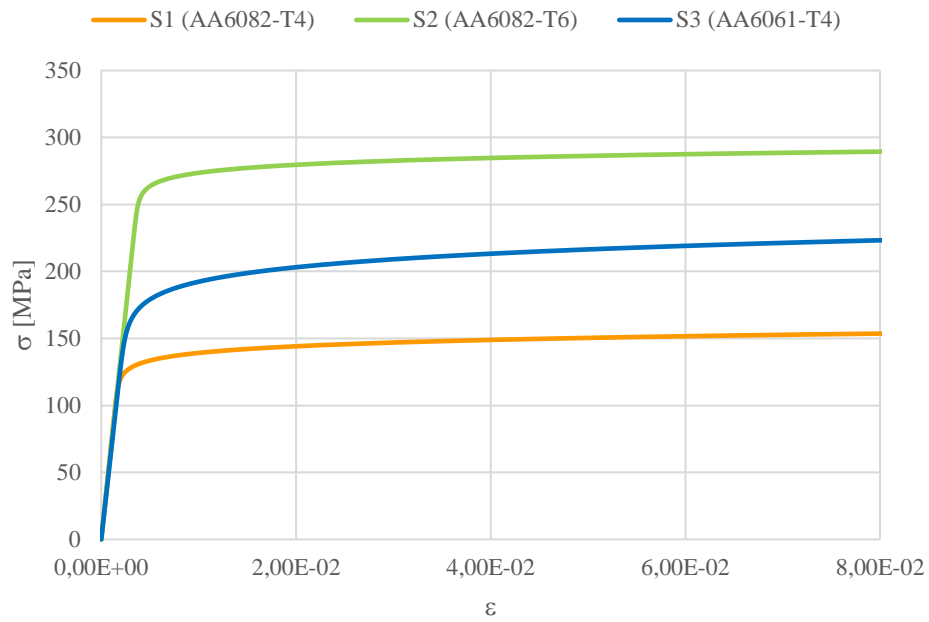


Figure 37: Plots of the Ramberg-Osgood curves for the considered aluminium alloys.

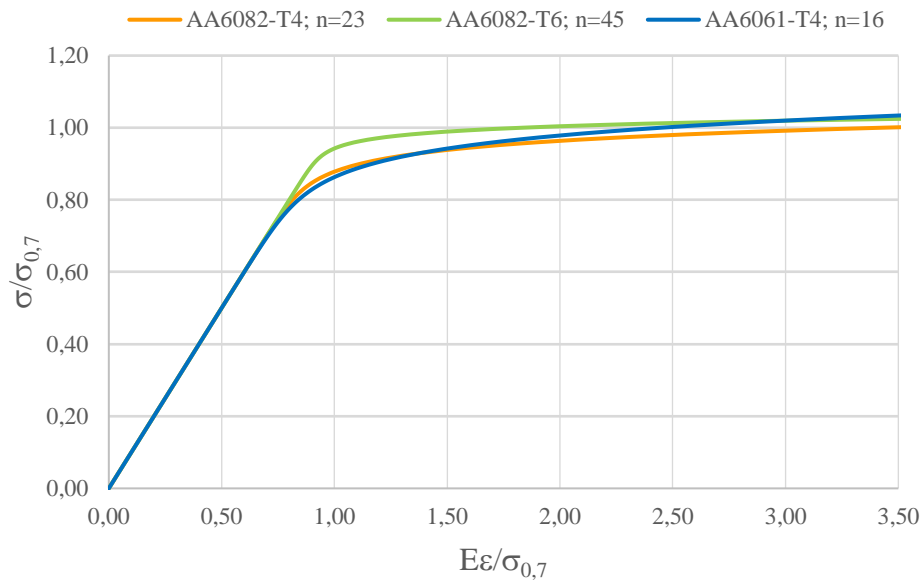


Figure 38: Non-dimensional plots of the Ramberg-Osgood curves for the considered aluminium alloys.

Three specimens have been considered for the present investigation: S1, S2 and S3. With reference to Figures 30 and 31, their respective dimensions and materials are listed in Table 3.

	h (mm)	b (mm)	L (mm)	L/b	b/h	Material
S1	25	262.5	1500	5.71	10.5	AA6082 T4
S2	25	262.5	1500	5.71	10.5	AA6082 T6
S3	24	200	1500	7.5	8.3	AA6061 T4

Table 3 - Characteristics of the analysed specimens.

For the numerical FE analyses, the examples under consideration have been modelled by means of the finite element commercial code ABAQUS. A general four-node shell element, S4R, for thin or thick shells with six degrees of freedom at each node, reduced integration, hourglass control and finite membrane strains has been used. This type of mesh element uses a normal integration rule with four integration points. A free quad-dominated mesh has been generated with an approximate size of 10 mm. Each flange of specimens S1 and S2 has been divided in 3938 elements. Each flange of specimen S3 has been divided in 3000 elements.

Both the end cross sections have been made undeformable by using the constraint type “MPC beam” and by setting the centre of the crux as Control Point and all the other points of the cross section as Slave Nodes. The control point at section $z=0$ has been modelled as fully fixed, i.e. with no allowed rotations and translations for all degrees of freedom, which implies that, differently from the analytical model of Section 3.2., the FE model displays some warping rigidity. At section $z=L$ a point compressive load is applied.

The FE model is shown in Figure 39.

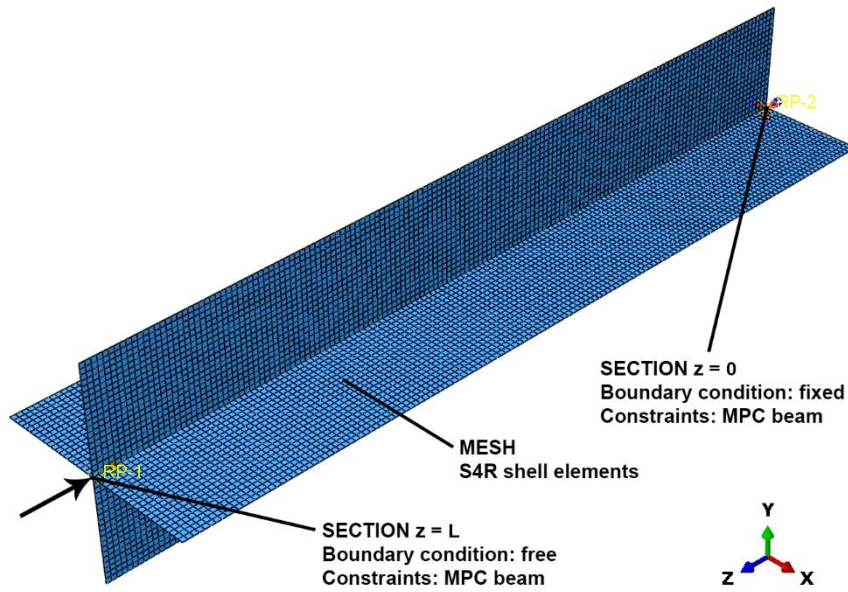


Figure 39: FE model of a cruciform column.

Table 4 shows the critical stress for a perfect specimen according to the flow deformation theory of plasticity, Eq. (72), and the deformation theory of plasticity, Eq. (78), compared to the results from an elastic buckling analysis by ABAQUS.

	Critical stress <i>Analytical</i>		Critical stress <i>Numerical</i> (ABAQUS)
	Flow	Deformation	Elastic
S1	243,15	129,06	253,99
S2	236,87	236,24	247,43
S3	360,72	179,82	362,57

Table 4 - Critical stress for a perfect specimen according to Eqs. (72), flow, and (78), deformation theory of plasticity vs ABAQUS elastic results.

It is evident that the results from the classic Eq. (72) for the flow theory of plasticity, which relies upon the elastic value of the shear modulus G , Eq. (73), and the FE ones by ABAQUS are in good agreement within a difference of at most 4.5% for specimens S1 and S2, a fact which can be attributed to the difference in the warping stiffness. On the contrary, as expectable, results from the classic Eq. (78) for the deformation theory of plasticity, are much lower than the elastic ones.

Also, it is worth pointing out that Table 4 shows a ratio of about 2:1 between the critical stresses from both ABAQUS and the flow theory of plasticity with respect to those from the deformation theory of plasticity for specimens S1 and S3, i.e. those made with AA6061T4 and AA6082T4 and therefore characterised by a relatively high ($n=16$ and $n=23$, respectively) strain hardening, see Figure 38. The same ratio is much lower for specimen S2, made by the low strain hardening ($n=45$) AA6082T6. This fact confirms the observation by Hutchinson and Budiansky that the difference between the results from flow and deformation theory of plasticity significantly increase for metals with high strain-hardening curves.

	Critical stress (MPa) <i>Analytical</i>		Critical stress (MPa) <i>Numerical (ABAQUS)</i>		Critical stress (MPa) <i>Experimental results by Hopperstad</i>
	Flow	Deformation	Flow	Deformation	
S1	125,89	126	128,17	125,58	124
S2	215,09	217,93	225,75	225,5	218
S3	175,93	175,89	181,57	175,05	-

Table 5 - Results obtained from the procedure proposed in this paper for an imperfection equal to 1/10 of the flange thickness, h , versus FE and experimental ones.

Table 5 collects the results obtained from ABAQUS and from the procedure proposed in this paper (see Figures. 35 and 36) for an imperfection of amplitude equal to 1/10 of the flange thickness, h . Table 5 shows also the results from the experimental tests conducted by Hopperstad et al., in 1999.

Hopperstad et al. did not measure the imperfection amplitude and the specimens were only examined by visual inspection. They were only believed to be small, at least within the tolerance ($\pm 0.005 b$) given by the extrusion producer.

It is evident that the proposed procedure achieves results using both the flow and the deformation theory of plasticity which are not only in very good agreement between each other, but also with the nonlinear FE analyses and the experimental results.

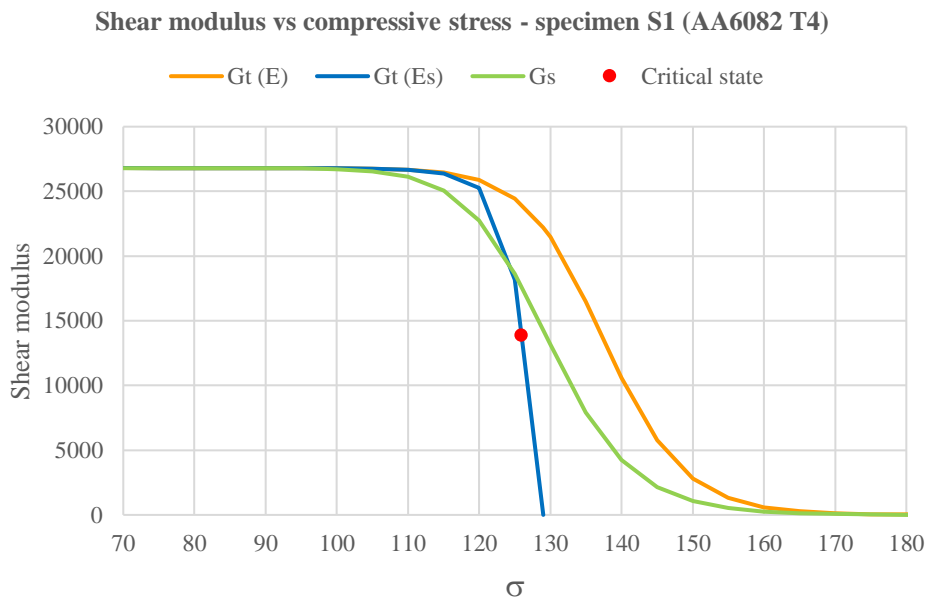


Figure 40: Plots of different shear moduli versus the compressive stress, σ for an imperfection amplitude $\delta = 1/10h$.

It is also worth underlining that the critical stresses from the flow theory of plasticity, according to the proposed solution and differently from the previous investigations, may results even lower than those from the deformation theory of plasticity. This finding can be understood by taking into consideration the fact that at buckling the tangent shear modulus can be lower than the secant one, see Figures 40,41 and 42.

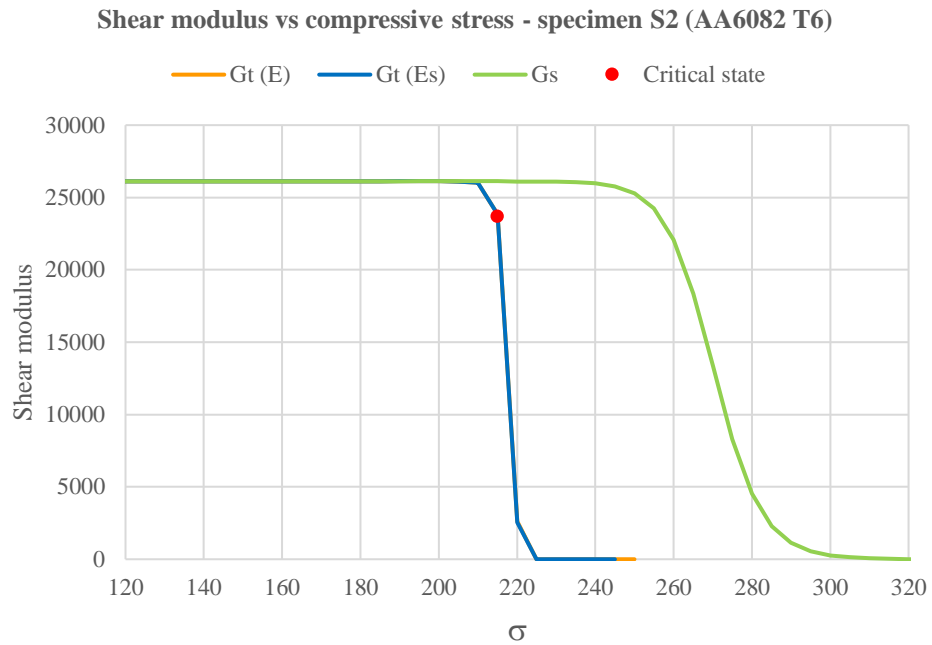


Figure 41: Plots of different shear moduli versus the compressive stress, σ for an imperfection amplitude $\delta = 1/10h$.

In fact, Figures 40,41 and 42 show the plots of different shear moduli versus the compressive stress, σ for an imperfection $\delta = 1/10 h$. The tangent shear modulus $G_t(E)$ is calculated by accounting for the effects of the initial imperfection on the basis of the elastic Young modulus, E , as it has generally been done in the past literature. The tangent shear modulus $G_t(E_s)$ is calculated according to the procedure proposed in the present paper (see Figure 36) and the secant shear modulus G_s is calculated according to the procedure shown in Figure 35.

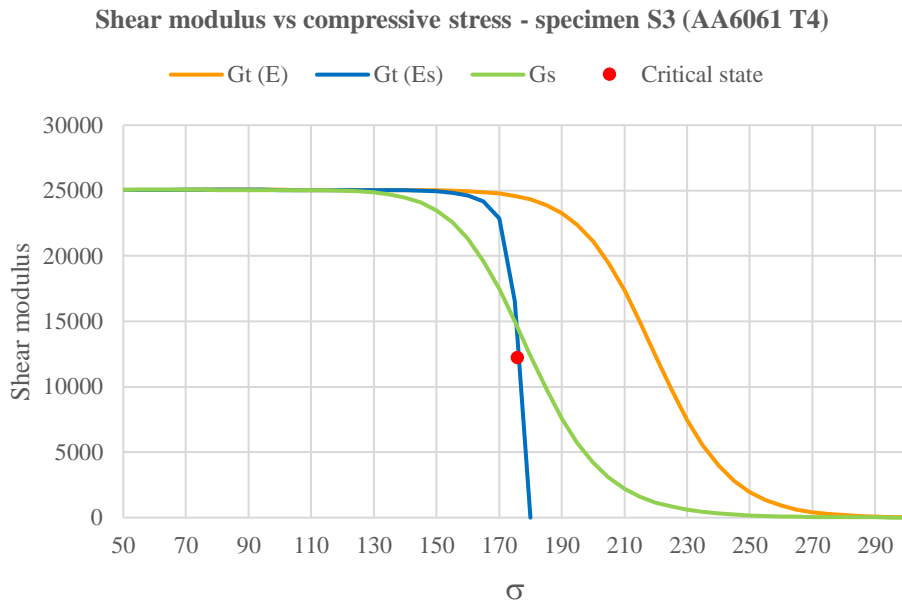


Figure 42: Plots of different shear moduli versus the compressive stress, σ for an imperfection amplitude $\delta = 1/10h$.

It is manifest that, to a different degree depending on the strain-hardening properties of the material, the tangent shear modulus $G_t(E)$ in the inelastic range results generally higher than the secant one, G_s , and this fact shows why, even in presence of imperfections, the flow theory of plasticity has been considered to deliver results in worse agreement with experimental tests than the less physical sound deformation theory of plasticity.

On the contrary, the tangent shear modulus $G_t(E_s)$ calculated accounting for the effects of the initial imperfection in a correct way, as proposed in the present paper, initially tends to follow the values of the secant modulus, G_s , but as the loading progresses in the inelastic range, takes values lower than G_s .

The robustness of the proposed procedure can be verified by repeating the calculations with reference to an imperfection amplitude equal to 1/100 of the flange thickness, i.e. $\delta = 1/100 h$.

The findings are collected in Table 6 and in Figures 43,44 and 45.

	Critical stress (MPa) <i>Analytical</i>		Critical stress (MPa) <i>Numerical (ABAQUS)</i>		Critical stress (MPa) <i>Experimental results by Hopperstad</i>
	Flow	Deformation	Flow	Deformation	
S1	128,73	128,47	134,04	128,67	124
S2	232,02	232,78	240,18	239,62	218
S3	177,75	177,75	191,55	179,38	-

Table 6 - Results obtained from the procedure proposed in this paper for an imperfection equal to 1/100 of the flange thickness, $\delta = 1/100 h$, versus FE and experimental ones.

Shear modulus vs compressive stress - specimen S1 (AA6082 T4)

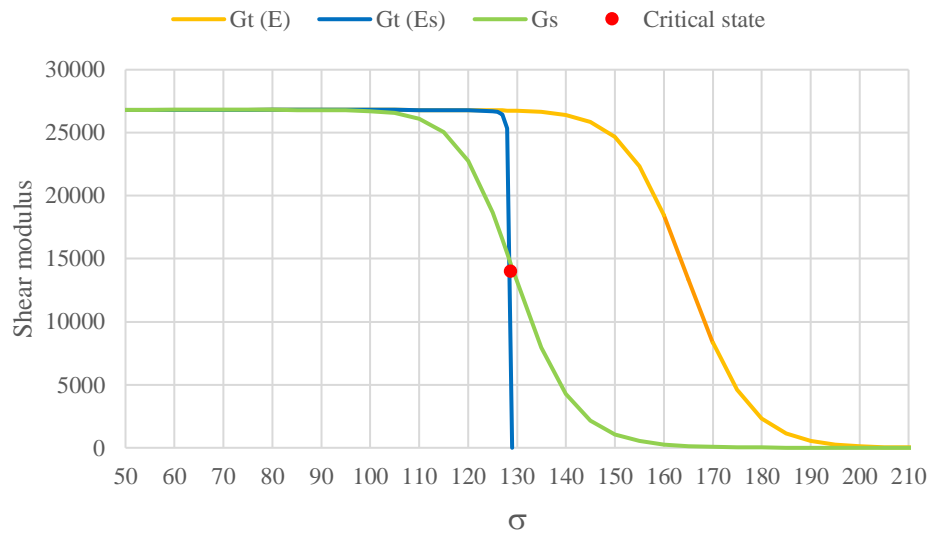


Figure 43: Plots of different shear moduli versus the compressive stress, σ for an imperfection amplitude $\delta = 1/100h$.

As it is physically expectable, the reduction in the imperfection amplitude leads to an increment in the critical stress, which is correctly captured by both the flow and the deformation theory of plasticity. Again, both theories result in nearly perfect agreement, also in the case of specimens S1 and S3, characterised by relatively high strain hardening curves.

Shear modulus vs compressive stress - specimen S2 (AA6082 T6)

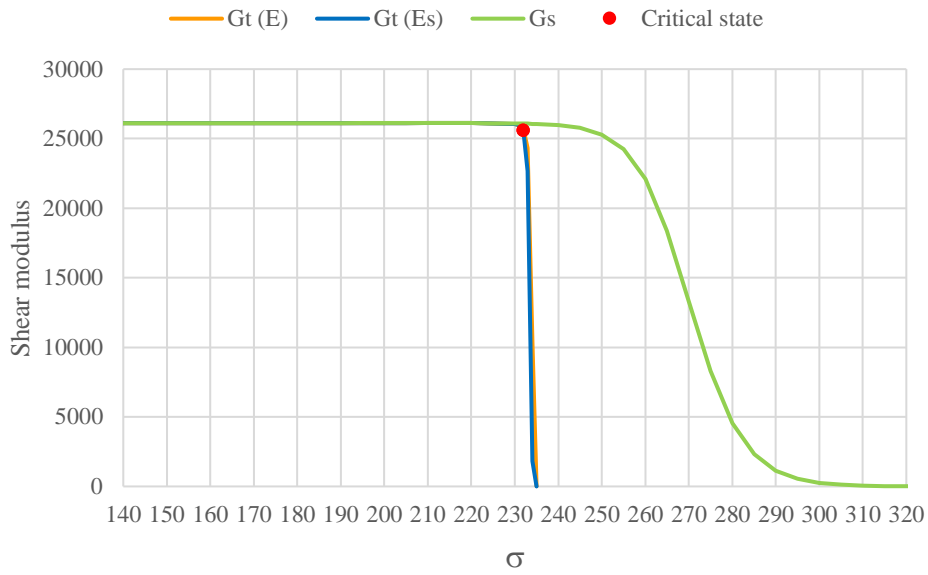


Figure 44: Plots of different shear moduli versus the compressive stress, σ for an imperfection amplitude $\delta = 1/100h$.

Shear modulus vs compressive stress - specimen S3 (AA6061 T4)

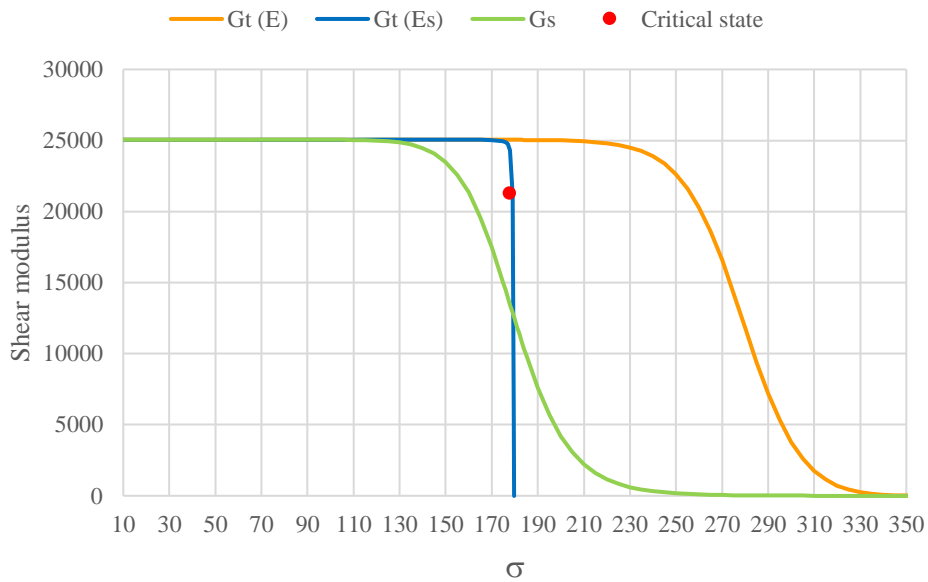


Figure 45: Plots of different shear moduli versus the compressive stress, σ for an imperfection amplitude $\delta = 1/100h$.

It can be thus concluded that the proposed procedure does not require imperfections of significant magnitude in order to reduce the buckling load provided by the flow theory.

The minor differences with nonlinear FE analyses by ABAQUS can be once again attributed to the effects of the warping rigidity deriving from the slightly different boundary conditions. To this purpose, Figures 46, 47 and 48 with Figures 49, 50 and 51 show the value of the axial load versus the torsional rotation, ϕ , in ABAQUS, together with the modes at impending collapse.

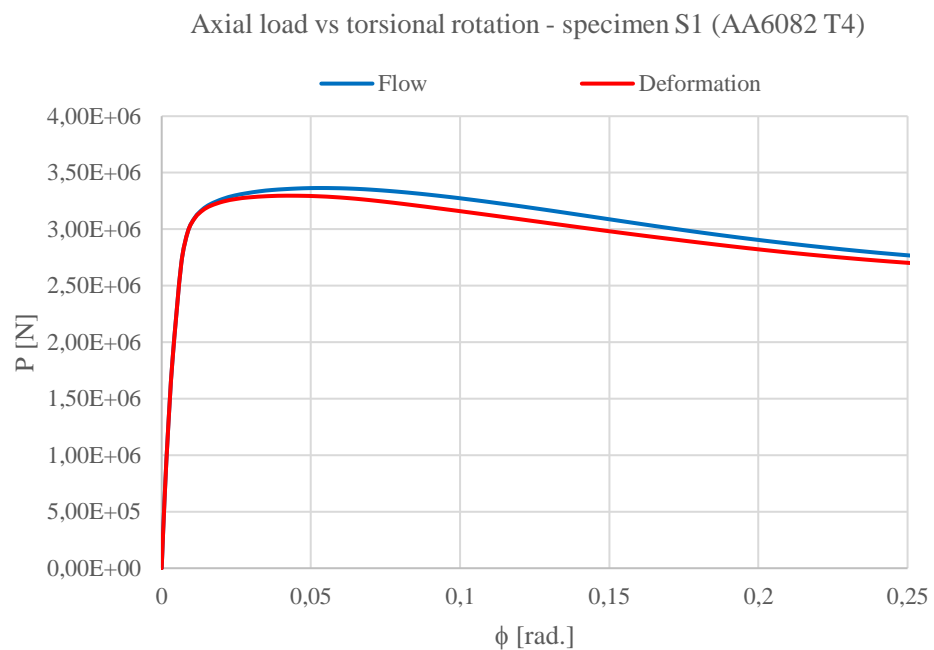


Figure 46: Axial load versus torsional rotation in ABAQUS, imperfection amplitude: $\delta = 1/10h$.

Figures 46, 47 and 48 with Figures 49, 50 and 51 clearly show that also in the case of the nonlinear FE analyses the most marked differences between the flow and the deformation theory of plasticity are found in the case of specimens S1 and S3, characterised by relatively high strain-hardening curves.

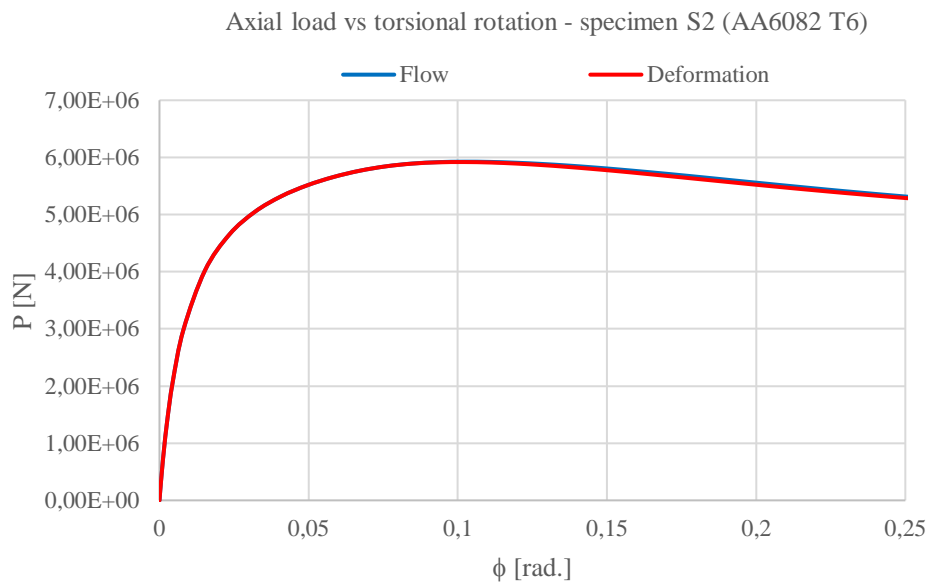


Figure 47: Axial load versus torsional rotation in ABAQUS, imperfection amplitude: $\delta = 1/10h$.

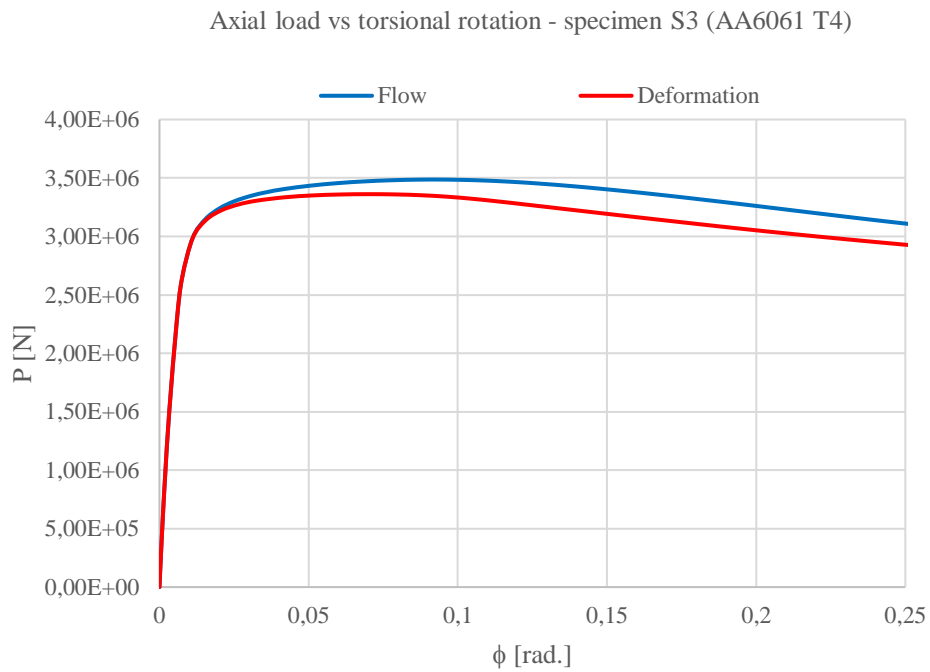


Figure 48: Axial load versus torsional rotation in ABAQUS, imperfection amplitude: $\delta = 1/10h$.

Axial load vs torsional rotation - specimen S1 (AA6082 T4)

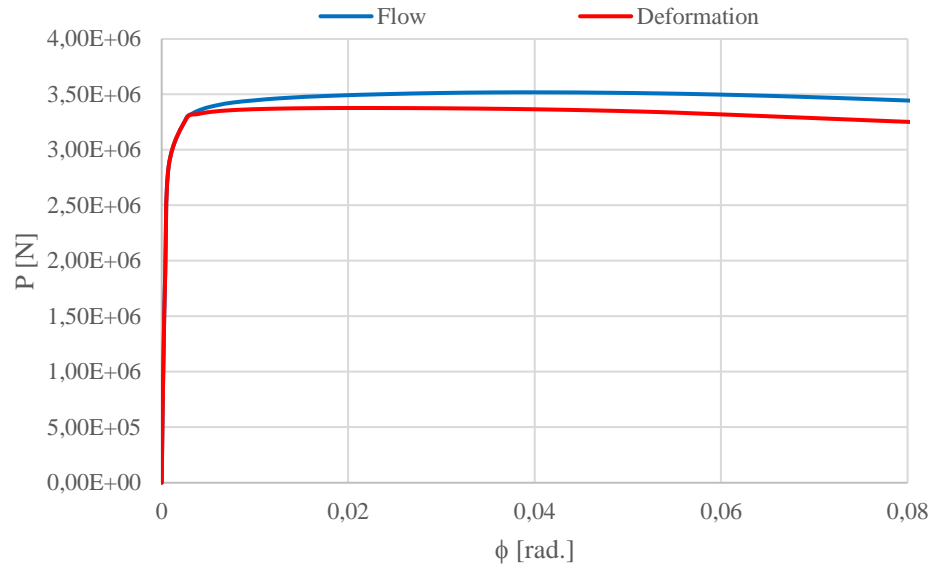


Figure 49: Axial load versus torsional rotation in ABAQUS, imperfection amplitude: $\delta = 1/100h$.

Axial load vs torsional rotation - specimen S2 (AA6082 T6)

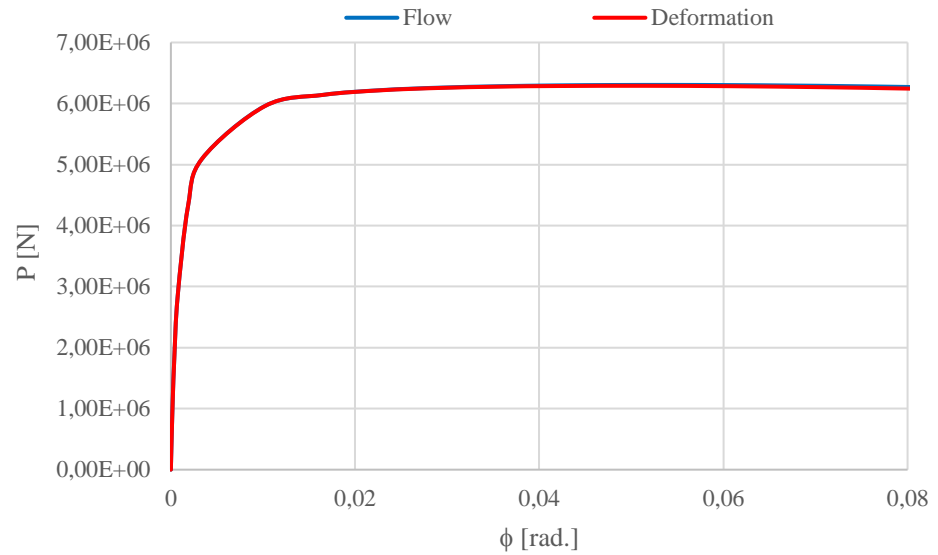


Figure 50: Axial load versus torsional rotation in ABAQUS, imperfection amplitude: $\delta = 1/100h$.

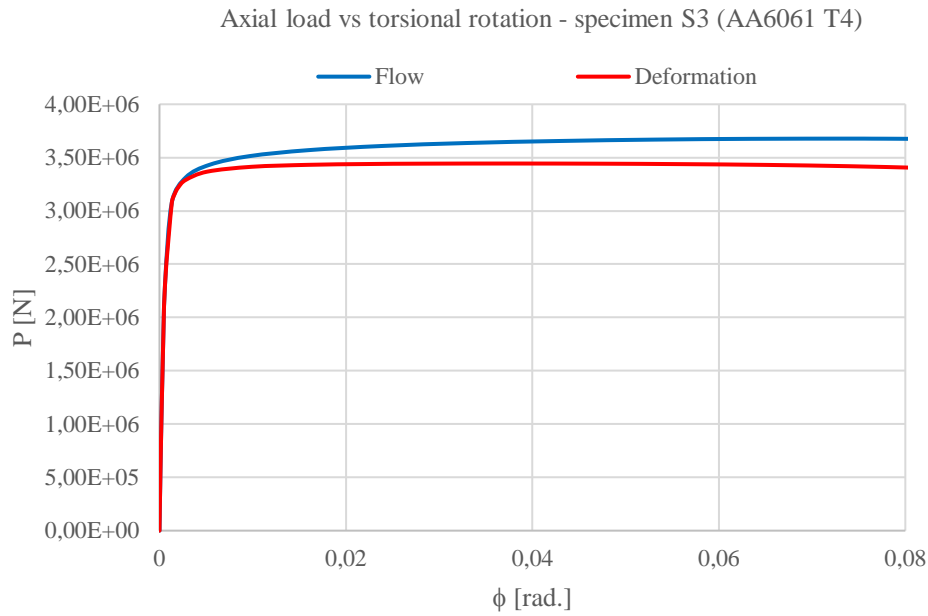


Figure 51: Axial load versus torsional rotation in ABAQUS, imperfection amplitude: $\delta = 1/100h$.

Finally, Table 7 shows the percent differences between the analytical solutions for the two different values of the imperfection amplitude, $\delta = 1/10h$ and $\delta = 1/100h$. The case of specimen S2, characterized by a relatively low strain-hardening curve, is the more sensible to the imperfection amplitude.

	Critical stress (MPa) <i>Analytical</i> $\delta = 1/100$		Critical stress (MPa) <i>Analytical</i> $\delta = 1/10$		Percentage increment between the critical stresses $\sigma_{\delta 100} = \sigma_{\delta 10} + \Delta\%(\sigma_{\delta 10})$	
	Flow	Deformation	Flow	Deformation	Flow	Deformation
S1	128,73	128,47	125,89	126	+2,26%	+1,96%
S2	232,02	232,78	215,09	217,93	+7,87%	+6,81%
S3	177,75	177,75	175,93	175,89	+1,06%	+1,06%

Table 7 - Percent differences between the analytical solutions for the two different values of the imperfection amplitude, $\delta = 1/10h$ and $\delta = 1/100h$.

In the present dissertation an accurate analysis of the torsional buckling of a cruciform column in the inelastic range has been conducted on the sole basis of the classic formulation of the flow and deformation theory of plasticity and in the spirit of Shanley's approach to the stability of columns in the plastic range. In this respect the column is considered to be affected by inevitably small initial imperfections.

The conclusions are the following:

- the discrepancies repeatedly reported in literature between the results from the flow and the deformation theory of plasticity, even in presence of imperfections, seem essentially due to the fact that the effects of imperfections are computed inaccurately up to the point where the limit load is achieved;
- by means of the presented analytical procedure, it is shown that the flow theory of plasticity is capable of attaining a very good agreement with the results from the deformation theory and the experimental results, as well as with nonlinear incremental FE analyses;
- the proposed solution is also capable of naturally overcoming the observation that for metals with significant strain-hardening the imperfections have to be of considerable magnitude in order to reduce the critical load provided by the flow theory;

Overall it can be affirmed that, by using a careful analytical procedure and in contrast to common understanding, in the case of the torsional buckling of a cruciform column in the inelastic range there is actually no plastic buckling paradox.

The present findings confirm and give a mechanical reason to the observation made in recent works on the plastic buckling of cylindrical shells by Shamass et al., who have shown that the results of incremental non-linear finite element analyses using flow theory with an associated flow rule are unaffected by the plastic buckling paradox while, depending on the particular methodology, other approaches are sensible to it.

Section 4

Plastic buckling of cylindrical shells

4.1. Historical background

The cylindrical shells have been one of the most commonly used elements in modern structures. Their relevance in structural design united with their simple shape have generated large interest in structural mechanics in recent times. This interest is evidenced by thousands of publications and books in this field and has led to many advances in the theory of thin shells.

The main difference between a plate and a shell element is that in the initial state the shell element has a natural curvature while the plate element is assumed to be flat. The presence of this initial curvature slightly affects the equilibrium equations for bending but it has significant consequences on the membrane action which is activated by in-plane forces. These latter may be distinguished in two groups: the primary in-plane forces generated by applied edge loads and the secondary in-plane forces produced by flexural deformations. Differently from plate elements in which secondary in-plane forces affect membrane action considerably only if bending deformations are large, for shell elements with initial curvature secondary in-plane forces have significant consequences on membrane action regardless of the amount of the bending deformations and thus they may be accounted for in both small and large deflection shell theories.

In the light of these basic considerations, more complexities are found out to be involved in the study of the plastic buckling of cylindrical shells diversely from the more simple formulation of flat plates, as for instance the case of the cruciform column discussed in Section 3. Moreover, beyond these geometrical complications, there is the evidence that in many shell problems the initially buckled configuration shows a condition of unstable equilibrium for which, once attained the buckling load, new equilibrium paths can exist only at a much lower load level (see Figure 52). In this manner, also due to the influence of inevitably initial imperfections, the theoretical buckling load calculated by the classical theories of stability may be hardly observed in experimental tests and in addition the analysis of the shell behaviour in the post-buckling path which is largely governed by the shape and the amount of initial imperfections is hence a fundamental issue to deal with in any buckling analysis.

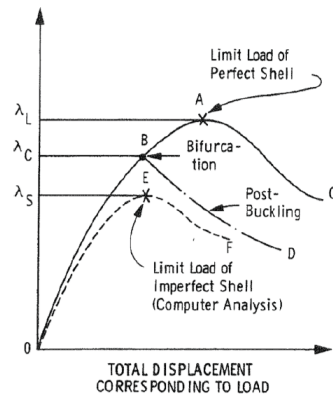


Figure 52: Load-deflection curves showing limit and bifurcation points. (Bushnell, 1984)

With reference to the study of buckling in the plastic range, there has been a considerable amount of works on the inelastic instability of initially imperfect cylindrical shells subjected to different loading conditions which takes into account the complexity of the material behaviour in the inelastic range respect to the particular geometry of the shell elements. In this direction, many studies have been conducted comparing experimental and analytical results with the application of the principal theories of plasticity, J_2 flow theory of plasticity and J_2 deformation theory of plasticity, and the same “plastic buckling paradox” has been found, i.e. the application of the flow theory of plasticity led to an overestimation of the buckling strength while the deformation theory of plasticity provided a more accurate prediction with respect to the experimental data.

The fact that many authors, such as Onat and Drucker, Mao and Lu, Durban and Ore and Bardi and Kyriakides, among the others, pointed out that the deformation theory tends to predict buckling loads that are smaller than those obtained by the flow theory and much closer to the experimental observations is essentially due to the fact that the associated incremental theories of plasticity which do not have a corner on the limit surface predict a purely elastic response to a shearing stress increment following a simple axial load, as discussed recently by Guarracino and Simonelli.

It is known that by introducing a certain degree of initial imperfection it is possible to overcome this problem and a number of recent studies conducted by Shamass et al. have shown that by means of accurately modelled and conducted FE analyses it is possible to obtain predictions based on the flow theory of plasticity that are in good agreement with the experimental findings.

This said, one may argue that making recourse to a properly constructed non-linear finite element model would naturally overcome any difficulty connected with this kind of analyses but unfortunately it is rather immediate to realise that this is not always the case. The present investigation goes deeper into the problem and shows that the material model is also capable to trigger a mode jumping from the initial imperfection which may reverse the predictions by the flow and deformation theories of plasticity and give origin to a sort of inverse buckling paradox. The study focuses on the plastic buckling of circular cylindrical shells under non-proportional loading which, on account of its importance in many engineering applications, has been the subject of intense research for many decades.

4.2. Buckling of cylindrical shells: an overview

The nonlinear equilibrium equations for thin cylindrical shells according to Donnell (1934) and von Kármán and Tsien (1941) are:

$$\begin{aligned} N_{x,x} + N_{xy,y} &= 0 \\ N_{xy,x} + N_{y,y} &= 0 \end{aligned} \tag{93}$$

$$\frac{\partial Q_x}{\partial x} + \frac{\partial Q_y}{\partial y} + N_x \frac{\partial^2 w}{\partial x^2} + N_y \left(\frac{\partial^2 w}{\partial y^2} + \frac{1}{R} \right) + 2N_{xy} \frac{\partial^2 w}{\partial x \partial y} + p = 0$$

where N_x, N_y, N_{xy}, N_{yx} are in-plane normal and shearing forces, Q_x, Q_y are transverse shearing forces, w is the displacement in the z-direction, i.e. normal to the middle surface directed toward the centre of curvature, R is the radius of curvature of the shell element and p is the applied load in z-direction, with reference to Figure 53.

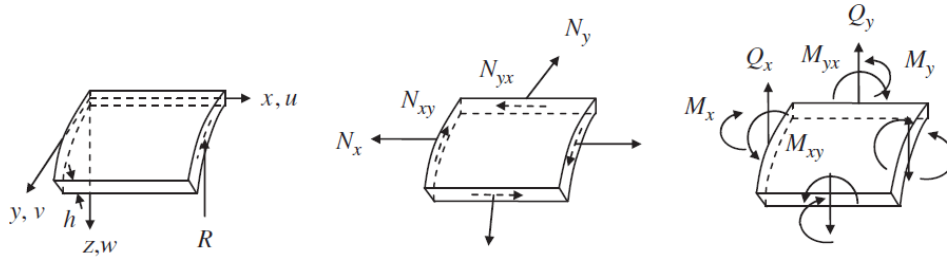


Figure 53: Cylindrical shell displacements and forces. (Yoo and Lee, 2011)

The constitutive equations for thin-walled isotropic elastic cylinders are:

$$\begin{aligned}
 N_x &= C(\varepsilon_x + \nu\varepsilon_y); & M_x &= -D\left(\frac{\partial^2 w}{\partial x^2} + \nu\frac{\partial^2 w}{\partial y^2}\right); \\
 N_y &= C(\varepsilon_y + \nu\varepsilon_x); & M_y &= -D\left(\frac{\partial^2 w}{\partial y^2} + \nu\frac{\partial^2 w}{\partial x^2}\right); \\
 N_{xy} &= \frac{C(1-\nu)\gamma_{xy}}{2}; & M_{xy} &= -D(1-\nu)\frac{\partial^2 w}{\partial x\partial y};
 \end{aligned} \tag{94}$$

C is the axial stiffness per unit thickness, defined as:

$$C = \frac{Et}{1-\nu} \tag{95}$$

where E is the Young's modulus, t is the thickness and ν is the Poisson's ratio. D is the bending stiffness per unit thickness, defined as:

$$D = \frac{Et^3}{12(1-\nu^2)} \tag{96}$$

The kinematic relations at the middle surface on which the Donnell equations are based are:

$$\begin{aligned}
\varepsilon_x &= \frac{\partial u}{\partial x} + \frac{1}{2} \left(\frac{\partial w}{\partial x} \right)^2; & \kappa_x &= -\frac{\partial^2 w}{\partial x^2}; \\
\varepsilon_y &= \frac{\partial v}{\partial y} - \frac{w}{R} + \frac{1}{2} \left(\frac{\partial w}{\partial y} \right)^2; & \kappa_y &= -\frac{\partial^2 w}{\partial y^2}; \\
\gamma_{xy} &= \frac{\partial u}{\partial y} + \frac{\partial v}{\partial x} + \frac{\partial^2 w}{\partial x \partial y}; & \kappa_{xy} &= -\frac{\partial^2 w}{\partial x \partial y};
\end{aligned} \tag{97}$$

where u, v, w and x, y, z are always referred to Figure 53.

Eq. (93), together with the constitutive and kinematic relations in Eqs. (94) and (97), govern all linear and nonlinear equilibrium conditions for cylindrical shells provided the deformations are not excessively large.

Buckling is a nonlinear problem from both material and geometrical points of view. Therefore, given that the investigation of the critical load of a thin cylindrical shell under any loading condition involves a large amount of computation, the reliability and efficiency of the incremental finite element analyses offer a tool which is facilitated by the availability of modern software packages. Nevertheless, many simple loading conditions as for example the axial compression or the lateral pressure (see Figure 54) have been solved using the governing equations for shells in Eq. (93) and by introducing some simplifications.

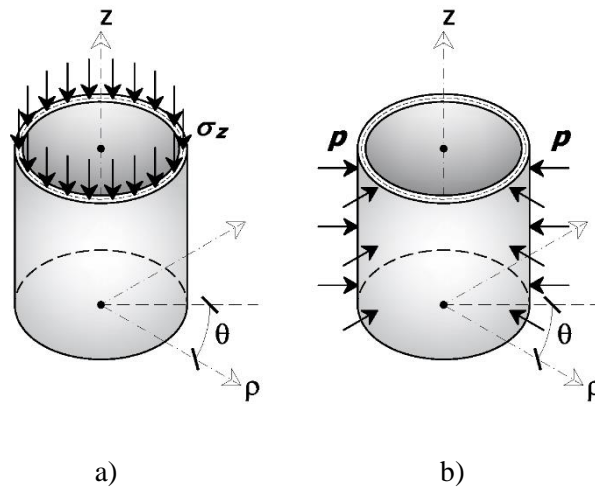


Figure 54: Cylindrical shells under simple loading conditions: a) axial compression;
b) external pressure.

By considering a symmetrical buckling of a cylindrical shell under the action of an uniform axial compression, Figure 54.a, the classical solution was obtained first by Lorenz in 1908 and lately discussed by Timoshenko in 1910 and by Southwell in 1914, in a modified form. The critical compressive stress, according to Timoshenko and Gere, was found to be:

$$\sigma_{cr} = \frac{Et}{R\sqrt{3(1-\nu^2)}} \quad (98)$$

where E is the elastic modulus and ν the Poisson ratio, t and R the thickness and the radius of the cylinder, respectively. It is of interest to note that the result is independent from the length of the cylinder, indicating that for very long cylinders the critical stress refers to local buckling. More accurate results for axially compressed cylinders may be obtained by considering the possible growth of eccentricities due to the increments of lateral deflection during the loading process.

The equilibrium paths for the perfect cylinder based on the solution in Eq. (98) and for a cylinder with a small initial imperfection subjected to axial compression are shown in Figure 55.

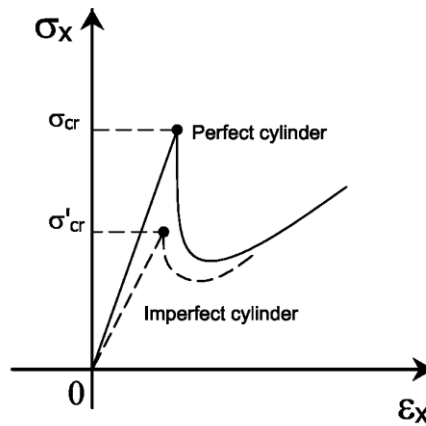


Figure 55: Equilibrium paths of axially compressed cylinder. (Yoo and Lee, 2011)

For the perfect cylinder, it can be observed that the pre-buckling path is linear static such as the underlying governing equilibrium equations while the post-buckling path is nonlinear. As a matter of fact, the nonlinear equations in Eq. (93) rule both the primary and the secondary paths and from their resolution the ultimate strength of the cylinder can be obtained, given that bifurcation point and critical load are coincident. On the other hand, in the case of an imperfect shell the critical load is substantially lower than that given by the perfect theory so that initial imperfections are believed to be the main reason of the discrepancy between the classical buckling solution and the experimental evidence.

In fact, in a cylinder with an initial imperfection, for any small increment of the axial load bending deformations slightly increase until, once a certain load is attained depending on the amplitude of the initial imperfection, bending deformations suddenly and rapidly grow and the load begins to reduce. In this manner, the maximum load for an initially imperfect cylindrical shell is significantly less than the critical load given by the classical theory and this circumstance denotes a strong imperfection sensitivity in the buckling prediction. In this respect, many progresses have been made in the study of axially loaded cylindrical shells by introducing initial imperfections into the buckling analysis.

Nevertheless, as seen in the work of Timoshenko among the others, the symmetrical buckling occurs within the elastic limit only for very thin cylindrical shells while for moderately thick cylinders subjected to various loading conditions as for example axial compression, external pressure, torsion or combinations of such loads, commonly plastic buckling occurs. Indeed, in the treatment of the plastic buckling, the material nonlinearity adds to the geometrical one and requires the use of the principal theories of plasticity, a fact which significantly affect the predictions for the critical load above the elastic limit. Additional computational difficulties may hence occur in resolving the buckling problem so that it is usually approached by conducting accurate linear and nonlinear finite element analyses by the use of the flow theory and the deformation theory of plasticity.

As seen in Section 2, also in the investigation of the plastic buckling of cylindrical shells the phenomenon of the “plastic buckling paradox” takes place and it has been object of extended research for many decades and by many authors. Focusing the attention on cylindrical shells subject to the simple case of axial compression, many theoretical and experimental results have been reported by Lee and Batterman and many analytical results have been reported by Mao and Lu and Ore and Durban, as seen in Section 2.5. Recently, Shamass et al. shed further light on the plastic buckling paradox for cylindrical shells subjected to axial compression and showed that, in contrast to common understanding, by using a careful geometrically nonlinear finite element analysis, a very good agreement between numerical and experimental results can be obtained in the case of the flow theory of plasticity.

Also for combined states of stress, as in the case of nonproportional loading, the flow and deformation theories seem to provide quite different results. A simple non-proportional path which combines more loading processes consists in applying first a fixed axial tension and then an increasing external lateral pressure. The instability of the cylindrical shell is hence activated by two principal phenomena: the axial tension moves the material farther into the plastic region and reduces the stiffness of the element while the external pressure induces structural instability because of the compressive circular stresses which increase the possibility of buckling.

This said, the differences in the prediction for plastic buckling between flow and deformation theories of plasticity are of particular interest. Blachut and Giezen, as seen in Section 2.5, conducted several experimental tests and also numerical analyses using the code BOSOR5 and Shamass et al. examined the sensitivity of the predicted critical pressures with respect to the applied tensile load. Similarly, as in the case of axially compressed cylinders, they concluded that the causes of the discrepancy between the two theories of plasticity lie substantially in the simplifying assumptions regarding the buckling modes used as the basis of many analytical studies. In particular, due to the evidence that the cylinders follow a constrained kinematics induced by predefined buckling modes, they have shown that the deformation theory of plasticity naturally counterbalances this excessive stiffness and thus provides results that are only apparently more in line with the experimental findings. Hence, by means of accurately modelled and conducted FE analyses it is possible to obtain predictions based on the flow theory of plasticity that are in good agreement with the experimental results.

4.3. Estimation of buckling strength in case of non-proportional loading

Since it has been extensively reported that the differences in the prediction of the buckling strength between the flow and the deformation theory are more evident in the case of non-proportional loading (see, for example, Giezen et al. and Blachut et al.) in the present dissertation reference is made to the simplest nonproportional loading procedure, which consists in applying first a fixed axial tension and then an increasing external lateral pressure, as reported in Figure 56.

The axial tension is such as to generate plasticity in the material, so that the subsequent lateral pressure can be increased until the specimen buckles in the plastic range. In fact Giezen et al. conducted experiments and numerical analyses on two sets of tubes made of aluminium alloy and subjected to combined axial tension and external pressure, making resort to the code BOSOR5 (Bushnell, 1986) for the numerical analyses.

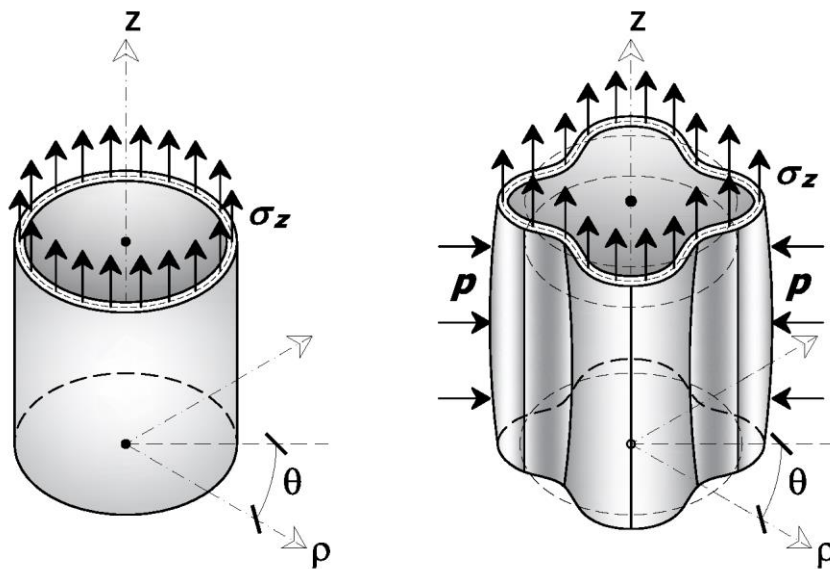


Figure 56: Buckling of a cylindrical shell subjected to a non-proportional loading.

Giezen, firstly in 1988, investigated the plastic buckling paradox of cylindrical shells subjected to nonproportional loading and found that upon reversing the loading path the flow theory failed to predict buckling while the deformation theory displayed the same trend of the test results. In 1991, Giezen et al. extended these early findings conducting experimental and numerical analyses on cylindrical shells subjected to combined axial tension and external pressure. For the investigation they chose two sets of specimens (Set A and Set B) of aluminium alloy 6061-T4 with a length to diameter ratio equal to one. The non-proportional loading was attained considering two different loading processes: in the first one, the axial tensile load was kept constant and the external pressure was progressively increased while in the second one the external pressure was kept constant and the axial tensile load was progressively increased. In the first case the experiments showed that the axial tension reduces the strength of the cylinder with respect to the application of the lateral pressure. However, the numerical analyses conducted by means of BOSOR5 showed that the flow theory predicts, contrarily to the experimental findings, an increase in the lateral buckling pressure on account of the axial tension preloading, while the deformation theory in some cases underestimates the lateral buckling pressure. Also in the second loading scheme with

increasing axial tensile load and constant lateral pressure the discrepancies between the test and the numerical results showed that both the flow and the deformation theory of plasticity were not able to provide satisfactory results. In conclusion, Giezen et al. stated that both the flow and the deformation theories fail to predict the buckling load under nonproportional loading.

Blachut et al., in 1996, conducted experimental and numerical analyses on 30 mild-steel machined cylinders of different dimensions, subjected to axial tension and increasing external pressure. Using once again the code BOSOR5 (Bushnell, 1986) for their numerical analyses, they showed that the agreement between the two plasticity theories was strongly dependent on the length of the cylindrical shell. For short cylinders, $L/D = 1$, the plastic buckling results predicted by the flow and deformation theories coincided only when the tensile axial load vanished. By increasing the axial tensile load, the buckling pressures predicted by the flow theory started to diverge quickly from those predicted by the deformation theory. Additionally, the flow theory failed to predict buckling for high axial tensile load while tests confirmed the buckling occurrence. For specimens with length-to-diameter ratio L/D ranging from 1.5 to 2.0 the results predicted by both theories were identical for a certain range of combined loading. However, for high values of the applied tensile load, the predictions of the flow theory began to deviate from those of the deformation theory and became unrealistic in correspondence to large plastic strains.

Consequently, in the case of cylinders subjected to axial tensile load and external pressure, Blachut et al. (1996) and Giezen et al. (1991) concluded that the flow theory tends to overpredict quite significantly the plastic strains and the buckling loads in the case of high values of the axial tensile loads, while the deformation theory leads to results that seem more in line with the experimental observations.

For the present investigation three different types of aluminium alloys have been taken into consideration, namely AA6082 tempers T4 and T6 and aluminium alloy 6061 temper T4. The first two alloys have been employed in the experimental tests by Hopperstad et al. (1999), who conducted torsional buckling tests on extruded aluminium cruciform columns, while the third one has been employed by

Giezen et al. in their study of on the buckling of circular cylindrical shells under non-proportional loading.

The uniaxial stress-strain relationship of the material under monotonic loading has been characterised by means of the Ramberg-Osgood law, i.e.:

$$E\varepsilon = \sigma + \alpha \left(\frac{\sigma}{\sigma_y} \right)^{n-1} \sigma \quad (99)$$

where σ and ε denote uniaxial stress and strain, E is the Young's modulus, σ_y is the nominal yield strength, α is the yield offset and n is the hardening parameter (see Appendix 2).

The Ramberg-Osgood parameters of the considered aluminum alloys are reported in Table 8 where σ_u is the ultimate strength. The Ramberg-Osgood stress-strain curves of the considered aluminum alloys are shown in Figure 57.

	E (MPa)	σ_y (MPa)	n	α	σ_u (MPa)
AA 6082 T4	69 700	131	23	1.064	238
AA 6082 T6	67 900	267	45	0.509	290
AA 6061 T4	65 130	178	16	0.733	246

Table 8 - Ramberg-Osgood parameters for the considered aluminium alloys.

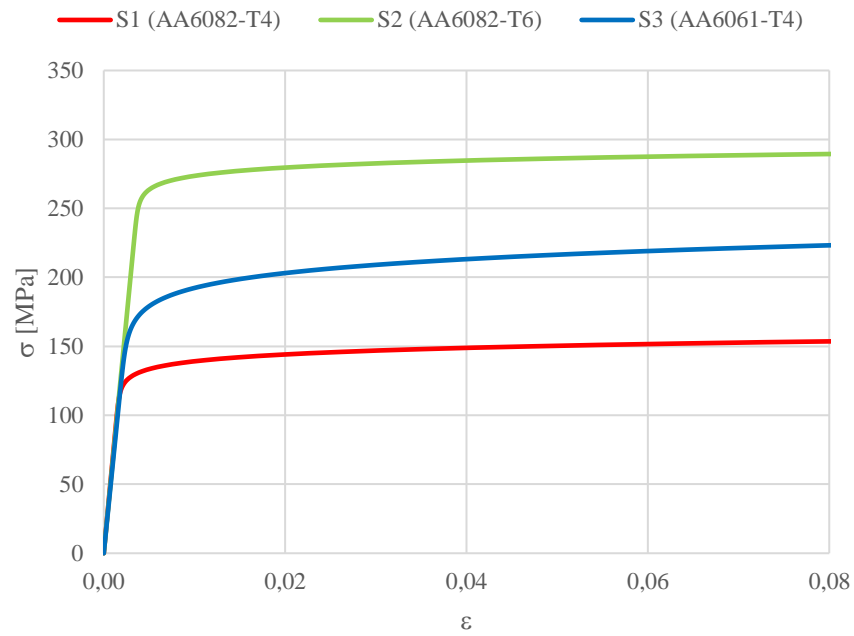


Figure 57: Ramberg-Osgood stress-strain curves of the considered aluminium alloys.

Four different specimens have been studied, which have been derived from the geometry of the specimen Set A analysed by Giezen: S1, S2, S3 and S4. Their dimensions, with reference to Figure 58, and materials are listed in Table 9.

	D (mm)	R (mm)	L (mm)	t (mm)	L/D	D/t	Material
S1	38.1	19.05	38.1	0.76	1	50	AA6082 T4
S2	38.1	19.05	38.1	0.76	1	50	AA6082 T6
S3	38.1	19.05	38.1	0.76	1	50	AA6061 T4
S4	38.1	19.05	57.2	0.76	1.5	50	AA6061 T4

Table 9 - Characteristics of the analysed specimens.

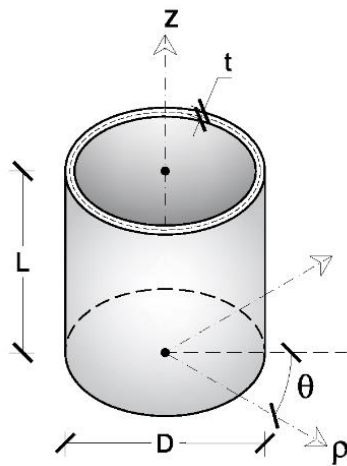


Figure 58: Dimensions and coordinate system of a cylindrical shell.

The plastic buckling of the case studies has been numerically analysed using both the flow theory and the deformation theory of plasticity by means of the FE code ABAQUS, version 6.11-1 (Simulia, 2011).

A general four-node shell element, S4R, for thin or thick shells with six degrees of freedom at each node, reduced integration, hourglass control and finite membrane strains was used. This type of mesh element adopts a normal integration rule with four integration points. A free quad-dominated mesh was generated with an approximate size of 1.07 mm. Consequently, the circumferential number of divisions was 100 and therefore the specimens S1, S2 and S3 resulted divided in 3800 elements, while the specimen S4 was divided in 5400 elements.

Both the end cross sections were made undeformable by using the constraint type “MPC beam” and by setting the centre of the circumference as Control Point and the all the other points of the border as Slave Nodes. The control point at section $z=0$ was modelled as fully fixed, i.e. with no allowed rotations and translations for all degrees of freedom while at section $z=L$ only the uniform component of the displacements along the z -axis are allowed. Moreover, in order to prevent local buckling phenomena at each end of the cylinder a stiffener was added so that the effects of the end constraints and of the applied loads would not alter the overall behaviour of the specimen. In this respect, two rings of 4 mm length characterised by a flexural and torsional stiffness ten folds larger than an equal

length of the cylinder wall were added. The stiffeners were modelled employing the same four-node element, S4R, with an approximate size of 1.07 mm.

The layout of the constraints was made in accordance to the experimental setting of Giezen et al. displayed in Figure 59.

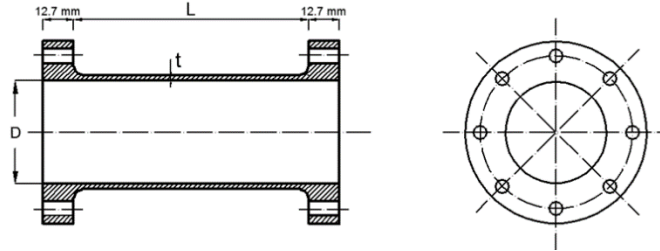


Figure 59: Experimental setting by Giezen et al.. (Giezen, Babcock and Singer, 1991)

The loading consisted, according to the nonproportional sketch of Figure 56, first of an axial tensile stress at section $z = L$ and successively of an increasing external pressure on the lateral surface of the cylinders. The value of the applied axial tensile loads are reported in Table 10.

	D (mm)	Material	σ_y (MPa)	$\bar{\sigma}$ (MPa)	$\bar{\sigma}/\sigma_y$
S1	38.1	AA6082 T4	131	20.33	0.16
S2	38.1	AA6082 T6	267	41.43	0.16
S3	38.1	AA6061 T4	178	27.58	0.16
S4	38.1	AA6061 T4	178	27.58	0.16

Table 10 – Applied axial loads, $\bar{\sigma}$.

The FE model is shown in Figure 60.

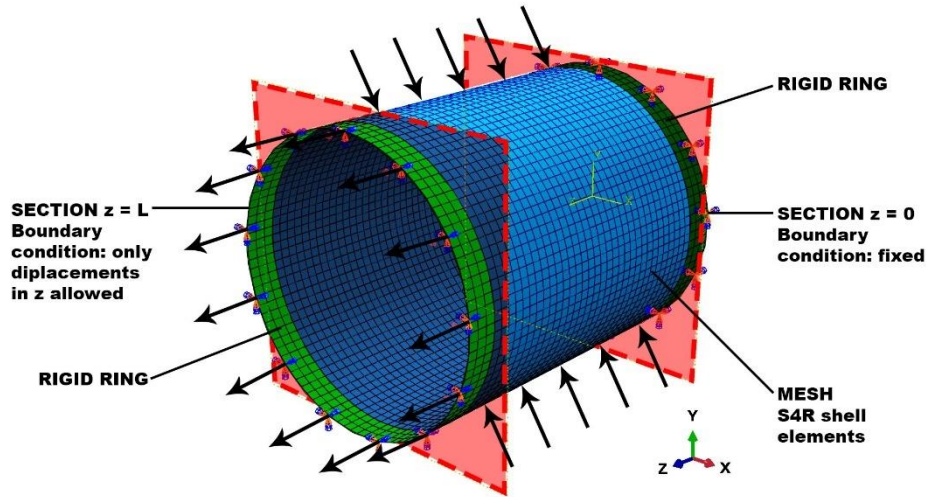


Figure 60: FE model of cylindrical shells.

The numerical analyses were performed in the realm of large-strains by using spatial co-rotational stress and strain measures and a hypo-elastic relation between the rates of stress and elastic strain (Simulia, 2011). Even if hypo-elastic laws may occasionally tend to lead to fictitious numerical dissipation, as noticed by Simo and Hughes in 1998, the adopted large-strain formulation is widely implemented in many commercial codes, including ABAQUS, and it is generally accepted that the hypo-elasticity of the formulation has limited influence on the results because, even when strains are large, the elastic part of the strain is typically still very small and close enough to the limit where hypo-elastic and hyper-elastic formulations coincide.

In order to follow the structural response beyond the buckling load, that is a limit point when load control is applied, the Riks arc-length method, proposed by Riks himself in 1979, was used in the version implemented in ABAQUS (Simulia, 2011). In this method both the nodal displacement increments Δu and the increment $\Delta \lambda$ of the load multiplier are assumed unknown in each increment. The Riks' formulation iterates along a hyperplane orthogonal to the tangent of the arc-length from a previously converged point on the equilibrium path (Falzon, 2006).

Following these assumptions, in the present investigation the external pressure is set as $\Delta\lambda p_0$, where p_0 denotes a reference inward external pressure and λ is a scalar multiplier. The critical load is determined by the point at which the load-arc length curve reaches a maximum.

The bifurcation point is the intersection of secondary and primary paths, which are the post-buckling and pre-buckling paths, respectively. To avoid such discontinuous response at bifurcation, geometric imperfections are generally introduced in order to remove bifurcation points (Falzon, 2006; Simulia, 2011). In this way, the post-buckling problem analysed using Riks method turns into a problem with a continuous loading-deformation path. The critical point determined on the equilibrium path is the limit point and there are no bifurcations prior to collapse. Ideally, with the progressive reduction of the amplitude of the imperfection, the limit point should represent a reliable approximation of the bifurcation load but, as it will be pointed out in the discussion, this does not turn to be always the case.

Accounting for imperfections was achieved by scaling and adding buckling eigenmodes to a perfect geometry in order to create a perturbed initial configuration. The scaling factor was set as a percentage of the shell thickness t and the buckling analyses useful to find the eigenmodes were conducted assuming linear elastic material behaviour and small displacements, under constant axial tensile loading. It is worth noticing that Giezen et al. reported that the average measured imperfection, Δ , of the specimens was about 10% of the shell thickness.

4.4. Discussion of the results

Table 11 shows that for all the considered specimens the buckling lateral pressure is essentially the same according to both the Hencky's deformation theory of plasticity and the Lévy-Mises flow theory of plasticity for an initial imperfection with the shape of the lowest buckling mode given by the eigenvalue analysis and an imperfection amplitude of 1%.

Once again this result would seem to contribute to support the supposition that making recourse to a properly constructed nonlinear finite element model naturally overcomes any difficulty connected with the different theories of plasticity. However, by making reference to the experimental tests by Giezen et al., one can notice that the critical load for specimen S3 was obtained with a buckling shape of five circumferential waves and one longitudinal wave (first eigenmode), with a measured amplitude of the initial imperfection equal to 10% of the shell thickness.

Specimen	Initial imperfection mode	Initial imperfection amplitude Δ	p_{cr}^n (MPa) (numerical)		p_{cr}^{exp} (MPa) (experimental)
			Deformation theory	Flow theory	
S1	1	1%	4.62	4.68	-
S2	1	1%	8.82	8.84	-
S3	1	1%	6.08	6.19	6.27
S4	3	1%	5.50	5.53	-

Table 11 – Calculated limit values of the lateral pressure.

By repeating the numerical nonlinear analysis with an imperfection amplitude equal to 10% of the shell thickness, the buckling pressure results 5.18 MPa for the deformation theory and 5.21 MPa for the flow theory, with a 17% difference from the previous analysis and the experimental measured buckling load.

Table 12 shows the results of the nonlinear FE analyses for specimen S3 for different initial imperfection modes and amplitudes.

Specimen	Initial imperfection mode	Initial imperfection amplitude Δ	P_{cr}^n (MPa)		P_{cr}^{exp} (MPa)	$P_{cr}^n / P_{cr}^{\text{exp}}$
			Deformation theory	Flow theory		
S3	1	1%	6.08	6.19	6.27	0.98
S3	1	10%	5.18	5.21	6.27	0.83
S3	3	10%	5.74	5.77	6.27	0.92
S3	5	10%	5.10	5.14	6.27	0.82

Table 12 – Influence of the initial imperfection shape and amplitude on the buckling loads.

In order to obtain a value of the buckling pressure more in line with the experimental findings by Giezen, it is necessary to assume, for an imperfection amplitude of 10% an initial imperfection mode corresponding to the third eigenvector. However, contrary to what one would expect, an initial imperfection mode corresponding to the fifth eigenvector does not lead to a further increase in the predicted buckling pressure. Moreover, by progressively reducing the amplitude of the initial imperfection to a very low value, such as to consider a nearly perfect cylinders, it is found that the deformation theory predicts buckling pressures which are much higher than the ones predicted by the flow theory, contrary to the common agreement and overturning the results which have given origin to the plastic buckling paradox. These results are shown in Table 13.

A deeper insight into the behaviour of the numerical solutions can be obtained by making reference to Figures 61-64, which show the lateral pressure vs. arc length plots for different amplitudes of the initial imperfection (first eigenmode) for Specimens S1, S2, S3 and S4. All these plots have been drawn considering the initial imperfection in the shape of the first eigenmode and show that the Lévy-Mises flow theory of plasticity tends to provide buckling pressures which are lower than those predicted by the Hencky's deformation theory of plasticity for perfect or nearly perfect specimens.

Specimen	Initial imperfection mode	Initial imperfection amplitude Δ	P_{cr}^n (MPa) (numerical)		P_{cr}^{exp} (MPa) (experimental)
			Deformation theory	Flow theory	
S1	1	0.005%	6.78	5.43	-
S2	1	0.2%	12.43	9.33	-
S3	1	0.1%	8.24	6.50	6.27
S4	3	0.07%	7.28	5.89	-

Table 13 – Calculated limit values of the lateral pressure for low imperfection amplitudes.

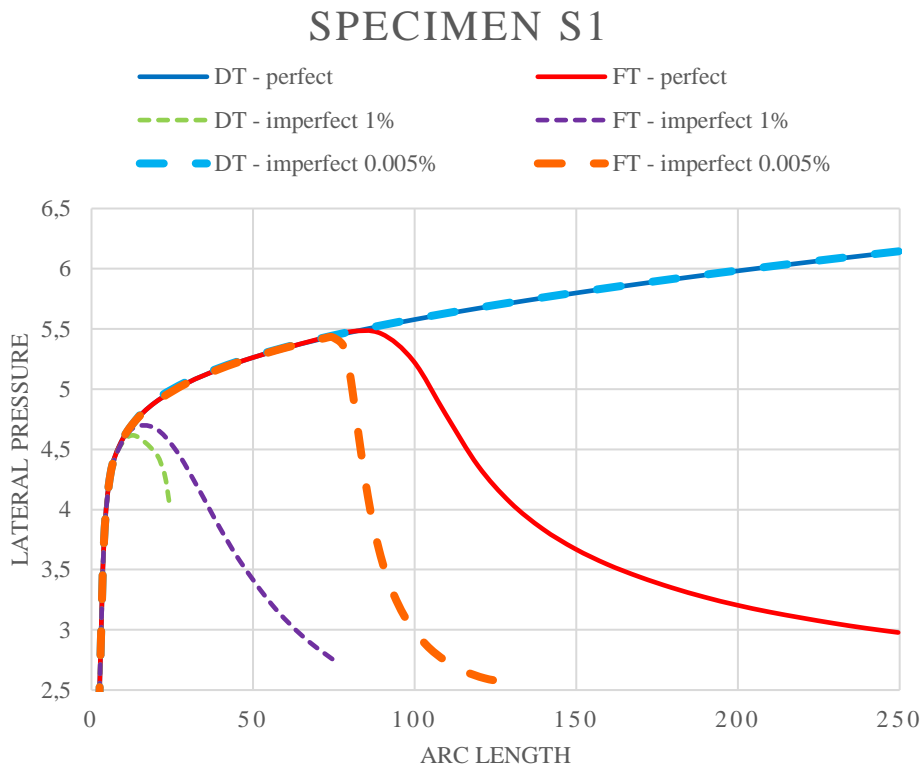


Figure 61: Load arc length paths for specimen S1.

SPECIMEN S2

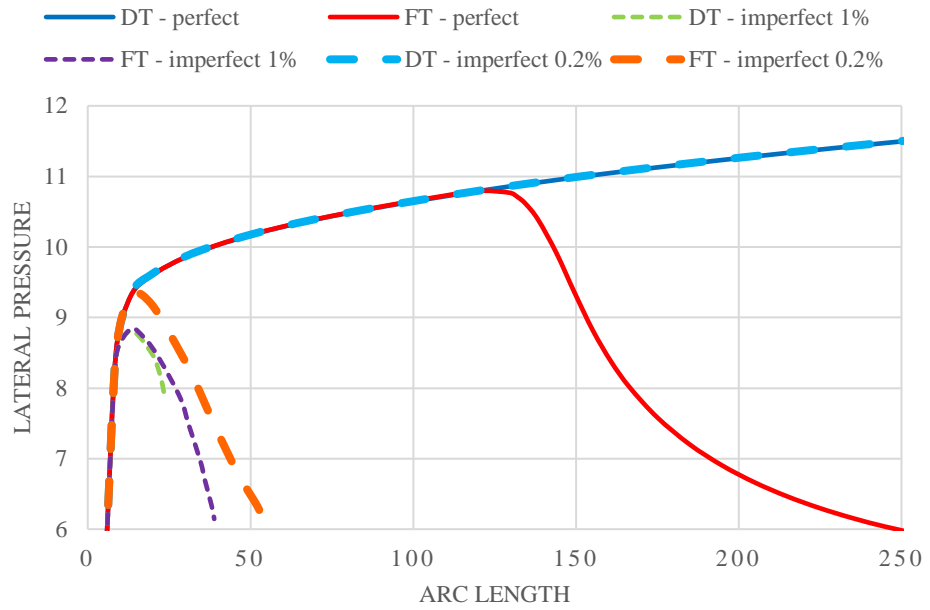


Figure 62: Lateral pressure-arc length paths for specimen S2.

SPECIMEN S3

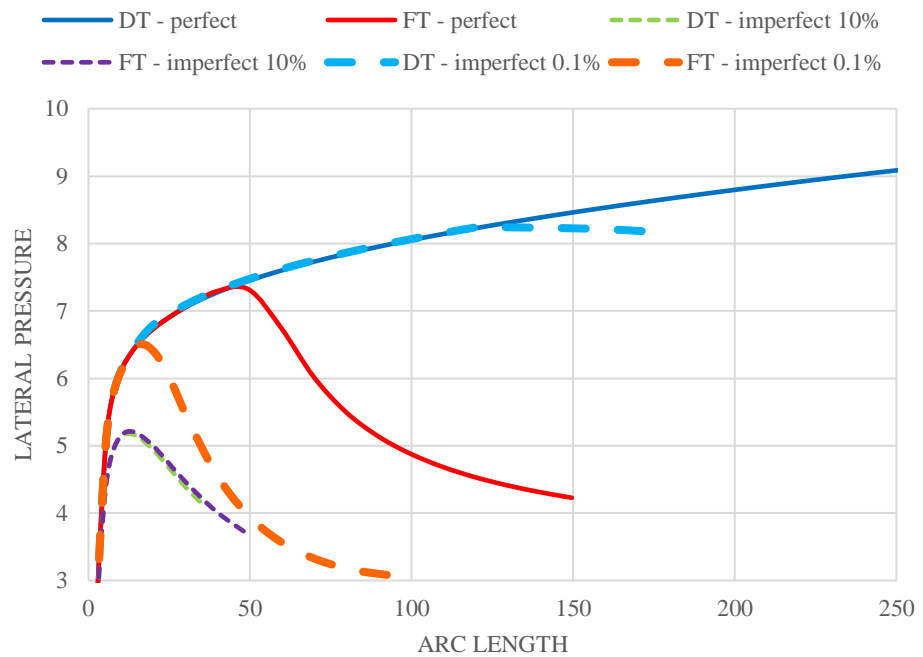


Figure 63: Lateral pressure-arc length paths for specimen S3.

SPECIMEN S4

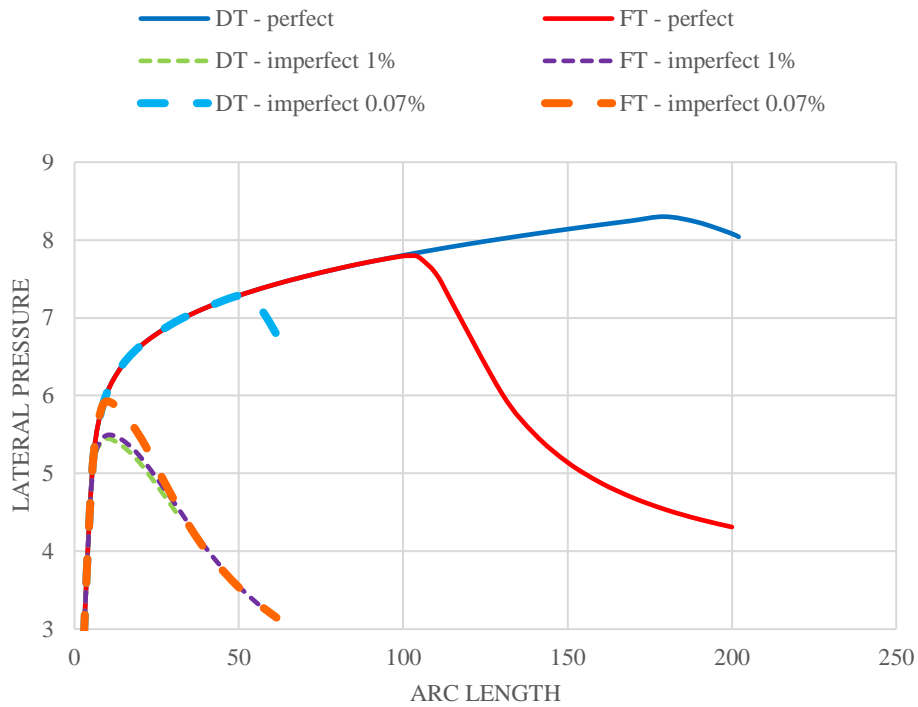


Figure 64: Lateral pressure-arc length paths for specimen S4.

It is normally accepted that the “plastic buckling paradox” is essentially due to the fact that the associated incremental theories of plasticity which do not have a corner on the limit surface predict a purely elastic response to a shearing stress increment following a simple axial load and it is thus necessary to introduce a certain degree of initial imperfection in order to overcome this problem (Onat and Drucker, 1953, Hutchinson and Budiansky, 1974, Guarracino and Simonelli, 2017). Given that, the fact that in the presented cases the behaviour of the solution appears to be the opposite, needs some additional considerations which are presented in the next Section 4.5.

4.5. The role of the mode switching

The critical load of shells of revolution is known to exhibit complex phenomena, characterised by mode switching and mode interaction. Many analyses of the non-axisymmetric buckling configurations of spherical domes, as for instance those conducted by Blachut and Galletly in 1993, have suggested that the collapse is mostly determined by the form of the imperfections, rather than by their magnitude. However, it is also generally believed that the circular cylindrical shells object of the present dissertation, especially in the case of nonproportional loading, does not exhibit such kind of behaviour. In fact, in the performed numerical analyses, the R/t ratio of the cylinders was about 25, thus placing the buckling in a substantially pure plastic range, where imperfect shells are less prone to show a reduced collapse load with respect to perfect ones (Shamass et al., 2015).

From the analyses presented in the previous Section 4.4, it is on the contrary found that the shape of the buckling mode and its relation with that of the initial imperfection plays a major role in determining the predictions from the flow and deformation theories of plasticity. In fact, it can be noticed that both theories predict the same value of the critical pressure when the buckling shapes result the same.

The flow theory models tend to exhibit the same number of circumferential waves at the critical state of the imposed initial imperfection, regardless of its initial amplitude, while in the deformation theory models the number of circumferential waves at buckling tend to differ from the one of the initial imperfection, particularly when the amplitude of the initial imperfections is low.

The different behaviour of the two plasticity theories can be thus attributed to the phenomenon of the mode switching (Supple, 1968, Guarracino and Walker, 2007). In order to have a jump in the buckling mode along the loading path, it is necessary that the linear perfect model has two rather close eigenvalues which may give origin to different secondary bifurcations if small perturbations act in the neighbourhood of some critical parameter values. Mode jumping is perhaps the most noteworthy feature of experimental studies of the stability behaviour of plates and shells. In fact, a rectangular plate can show a number of different buckled configurations which can be distinguished by their wave number. Experiments

have shown that the wave number do not need to remain constant as the load is gradually increased and there might be values of the load parameter at which a sudden and violent change in buckling pattern takes place. The new mode typically has a wave number greater than the previous one. Such a phenomenon has also been pointed out in the buckling analysis of circular rings (Fraldi and Guarracino, 2014).

In order to investigate the effects of the mode switching in the present study, it is thus opportune to consider the elastic buckling problem with its eigenvalues and modal shapes for each specimen. The specimens S1, S2 and S3 are characterised by the same geometry and, following a linear eigenvalue analysis, it is immediate to realise that their modal shapes are characterised by the same number of circumferential and longitudinal waves. Specimen S4 has a different geometry and its modal shapes are different. Table 14 collects the eigenmodes, the elastic critical loads and the number of corresponding circumferential waves for each specimen. The eigenmodes are characterised by a single longitudinal wave for all the case studies.

In particular, as seen in Figure 65, the first two modes show the same number of circumferential waves and present the same elastic critical load. The same happens for modes 3 and 4 and for modes 5 and 6 so that only modes 1, 3 and 5 are reported in Table 14 and in the subsequent tables and figures.

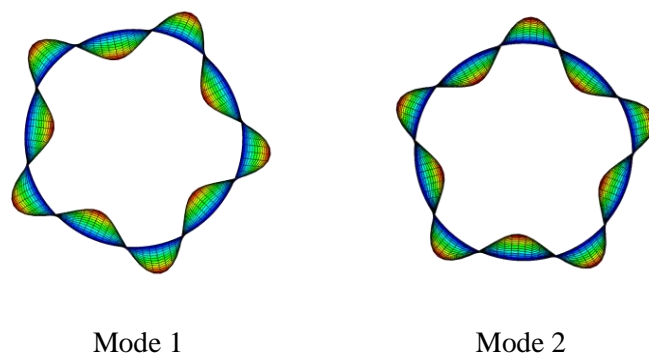


Figure 65: Representation of first two circumferential modes for specimens S1-S3.

	L/D	Material	Mode	Number of waves	$P_{buckling}$ (MPa)
S1	1	AA6082 T4	1	5	15.18
S2	1	AA6082 T6	1	5	14.79
S3	1	AA6061 T4	1	5	14.18
S4	1.5	AA6061 T4	1	4	9.07
S1	1	AA6082 T4	3	4	17.05
S2	1	AA6082 T6	3	4	16.61
S3	1	AA6061 T4	3	4	15.93
S4	1.5	AA6061 T4	3	5	10.84
S1	1	AA6082 T4	5	6	17.85
S2	1	AA6082 T6	5	6	17.39
S3	1	AA6061 T4	5	6	16.68
S4	1.5	AA6061 T4	5	3	14.01

Table 14 – Elastic buckling modes.

Figures 66 and 67 show the circumferential modes 1, 3 and 5 for the specimens object of the present study.

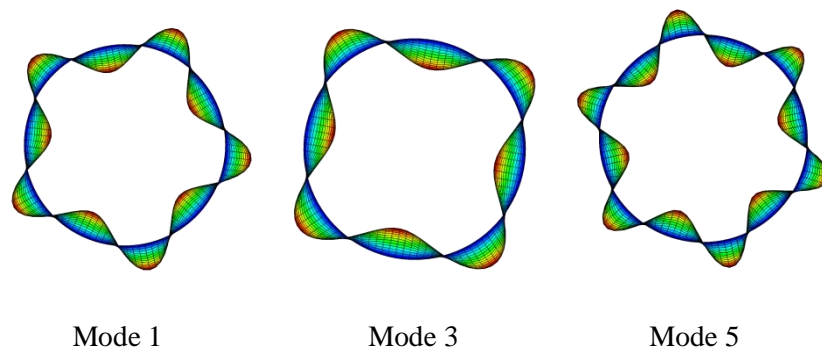


Figure 66: Representation of circumferential modes for specimens S1-S3.

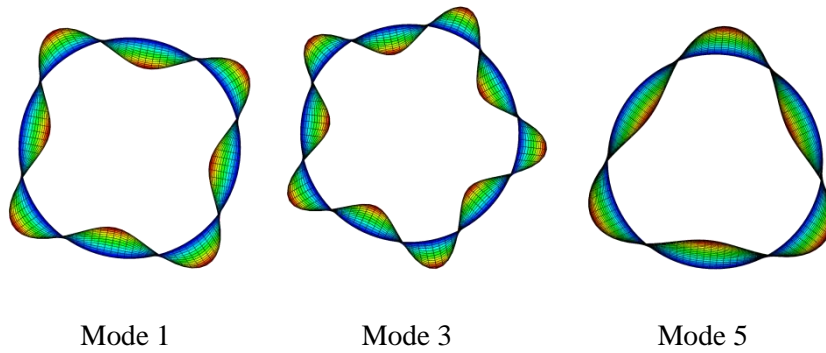


Figure 67: Representation of circumferential modes for specimen S4.

On these bases it is possible to making reference to Table 15 and notice that, notwithstanding the fact that the initial imperfection considered for both theories of plasticity is in the shape of the first eigenmode (five circumferential waves), for an imperfection amplitude of 0.2% in the case of specimen S2 the flow theory of plasticity attains a critical pressure of 9.33 MPa with a buckling mode which retains the shape of the injected imperfection, while the deformation theory attains a critical pressure of 12.43 MPa with a buckling mode characterised by 20 circumferential waves.

The longitudinal buckling is shown in Figure 68.

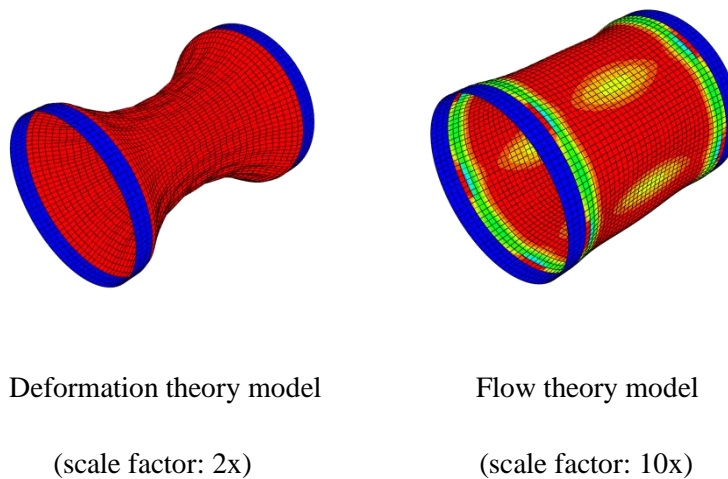


Figure 68: Representation of circumferential modes for specimen S2.

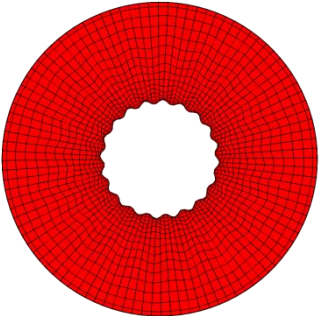
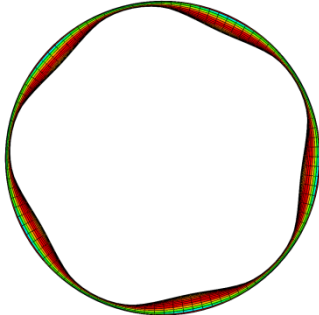
Deformation theory results		
Imperfect cylinder (Mode 1, $\Delta = 0.2\%$)		
$t = 0.76$	mm	
$R = 19.05$	mm	
$n = 20$	-	
$p_{buckling} = 157.53$	MPa	
$p_{cr}^n = 12.43$	MPa	
Flow theory results		
Imperfect cylinder (Mode 1, $\Delta = 0.2\%$)		
$t = 0.76$	mm	
$R = 19.05$	mm	
$n = 5$	-	
$p_{buckling} = 9.48$	MPa	
$p_{cr}^n = 9.33$	MPa	

Table 15 – Results of non-linear buckling analysis for specimen S2.

Moreover, always referring to Table 15, the values of the elastic buckling pressure load corresponding to the same number of waves showed by the numerical models are also reported and calculated according to Timoshenko and Gere formula:

$$p_{buckling} = \frac{Et^3(n^2 - 1)}{12R^3(1 - \nu^2)} \quad (100)$$

where E is the elastic modulus, n the number of circumferential waves, t and R the thickness and the radius of the cylinder, respectively, and ν the Poisson ratio.

In Figures 69-72 the loading curves of the specimens S1-S4 are showed only with reference to the low initial imperfection amplitudes reported in Table 13.

SPECIMEN S1

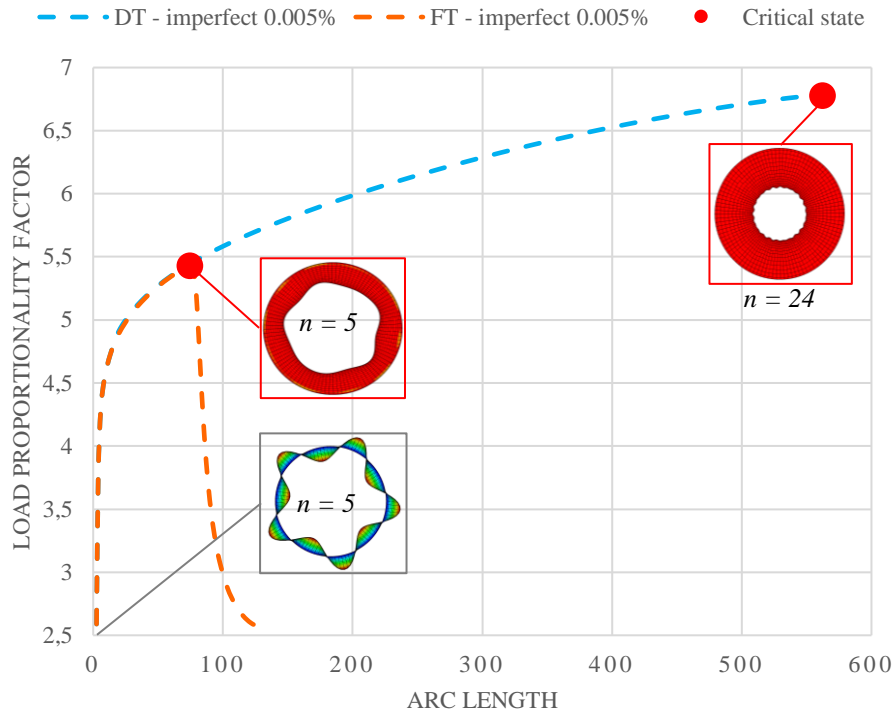


Figure 69: Lateral pressure-arc length paths for specimen S1.

SPECIMEN S2

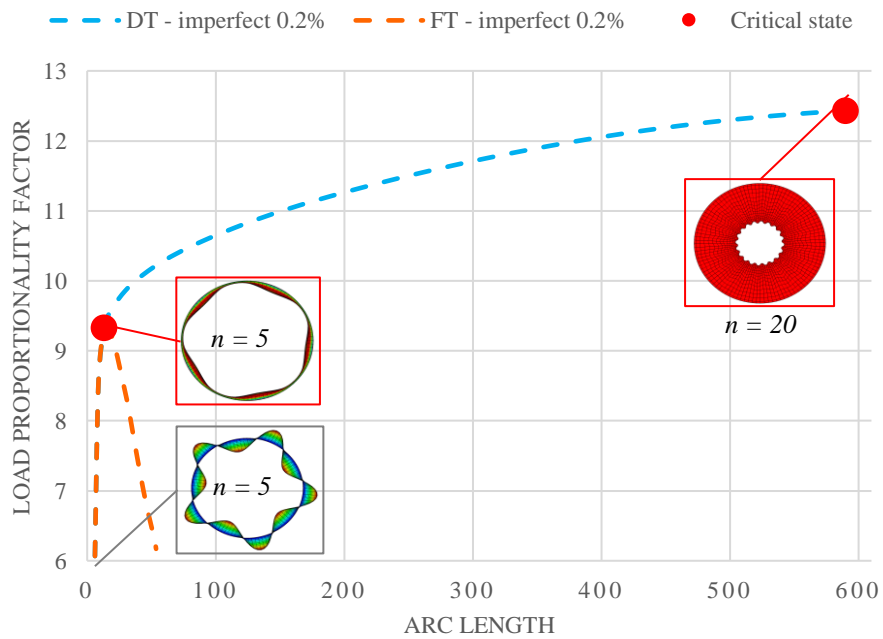


Figure 70: Lateral pressure-arc length paths for specimen S2.

SPECIMEN S3

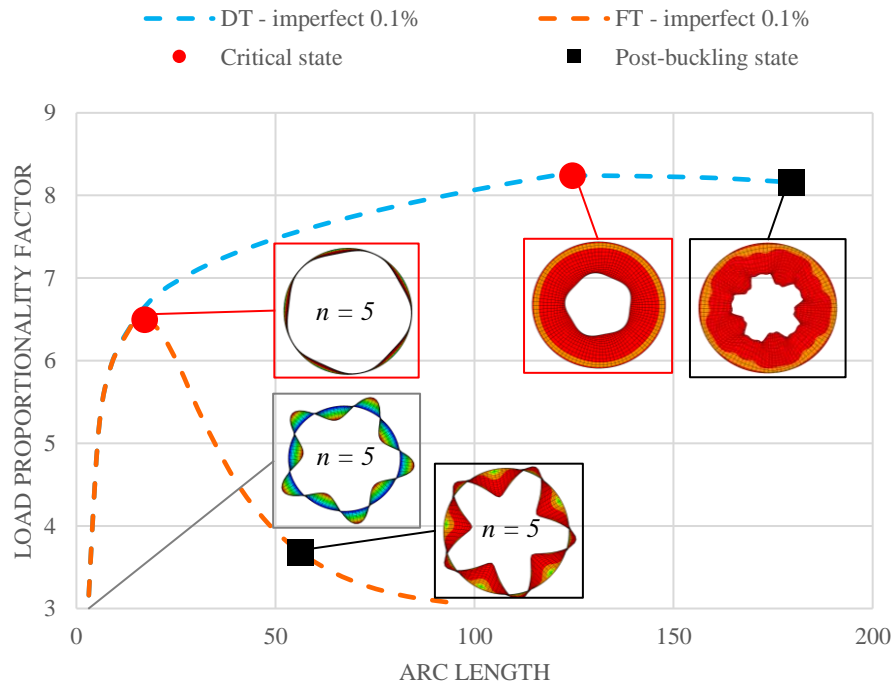


Figure 71: Lateral pressure-arc length paths for specimen S3.

SPECIMEN S4

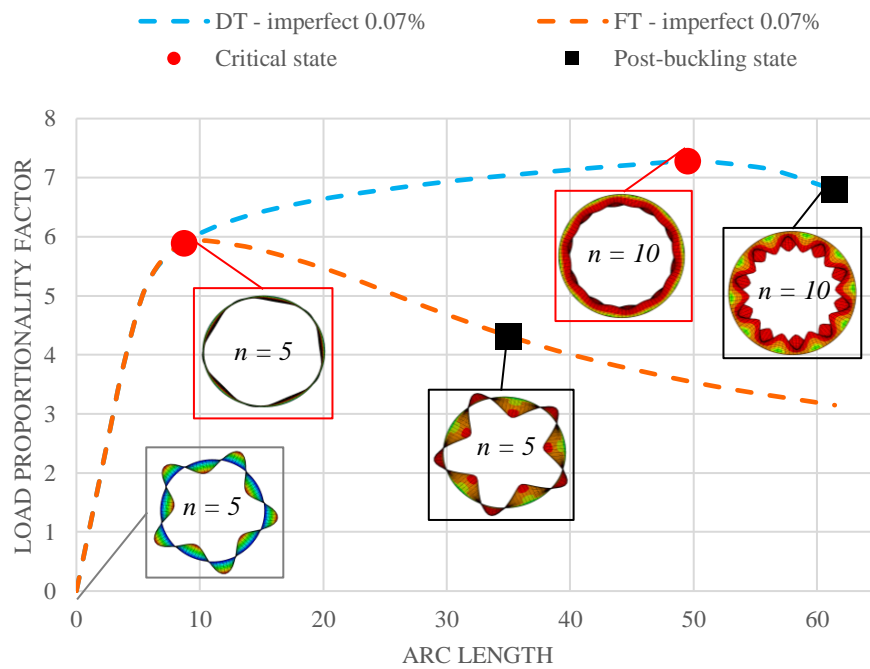


Figure 72: Lateral pressure-arc length paths for specimen S4.

It can be clearly seen that for any specimen the flow theory maintains the same shape of the initial imperfection while the deformation theory changes form attaining more elevated critical loads. In several cases the system does not forget the initial imperfection shape also in largely deformed post-buckling configurations, as it may be seen in Figures 71 and 72 which show the loading curves of the specimens S3 and S4 with an initial imperfection amplitude of 0.1% and 0.07%, respectively, and a 5 waves initial imperfection shape. In fact, for the specimen S4 in Figure 72, in the post-buckling configuration the deformation theory model displays 10 circumferential waves until the ultimate load is attained, while the flow theory model maintains along the whole loading process the 5 circumferential waves of the initial imperfection.

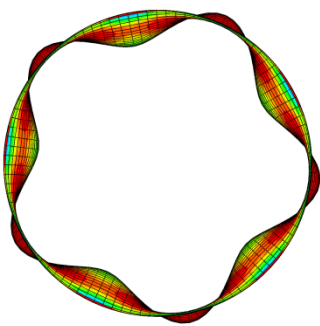
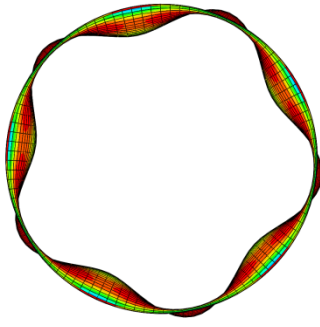
Deformation theory results		
Imperfect cylinder (Mode 1, $\Delta = 1\%$)		
$t = 0.76$	mm	
$R = 19.05$	mm	
$n = 5$	-	
$p_{buckling} = 9.48$	MPa	
$p_{cr}^n = 8.82$	MPa	
Flow theory results		
Imperfect cylinder (Mode 1, $\Delta = 1\%$)		
$t = 0.76$	mm	
$R = 19.05$	mm	
$n = 5$	-	
$p_{buckling} = 9.48$	MPa	
$p_{cr}^n = 8.84$	MPa	

Table 16 – Results of non-linear buckling analysis for specimen S2.

Table 16 shows the results for the specimen S2 again with an initial imperfection with the shape of the first eigenmode (five circumferential waves) but an imperfection amplitude of 1%. In this case both theories of plasticity attain essentially the same critical pressure with the same buckling mode, which retains the shape of the injected imperfection with no mode switching in the case of the deformation theory. Therefore the amplitude of the initial imperfection is decisive in maintaining the shape of the initial imperfection for the whole loading path up to the buckling load.

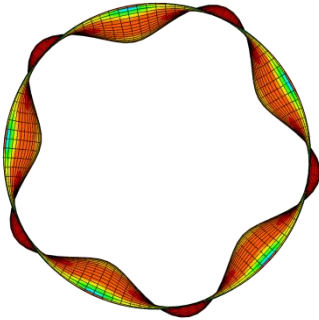
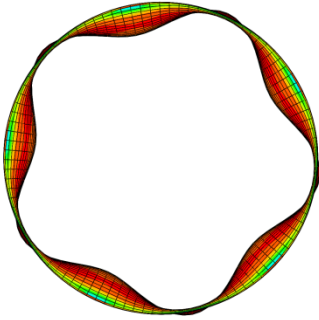
Deformation theory results		
Imperfect cylinder (Mode 1, $\Delta = 1\%$)		
$t = 0.76$	mm	
$R = 19.05$	mm	
$n = 5$	-	
$P_{buckling} = 9.09$	MPa	
$P_{cr}^n = 6.08$	MPa	
Flow theory results		
Imperfect cylinder (Mode 1, $\Delta = 1\%$)		
$t = 0.76$	mm	
$R = 19.05$	mm	
$n = 5$	-	
$P_{buckling} = 9.09$	MPa	
$P_{cr}^n = 6.19$	MPa	

Table 17 – Results of non-linear buckling analysis for specimen S3.

Table 17 shows the results of both theories of plasticity for the specimen S3 tested by Giezen for an initial imperfection with the shape of the first eigenmode (five circumferential waves) and an imperfection amplitude of 1%.

It is immediate to notice that both theories of plasticity attain essentially the same critical pressure with the same buckling mode, which retains the shape of the injected imperfection with no mode switching in the case of the deformation theory. The predicted buckling load corresponds to the one found experimentally by Giezen, who also counted five circumferential waves at buckling.

Table 18 shows the results of both theories of plasticity for the specimen S3 for an initial imperfection again with the shape of the first eigenmode (five circumferential waves) but an imperfection amplitude of 10%. Once again both theories of plasticity attain essentially the same critical pressure with the same buckling mode, which retains the shape of the injected imperfection with no mode switching in the case of the deformation theory. As it was expectable, the predicted buckling load results about 15% less than the one calculated for an imperfection amplitude of 1% .

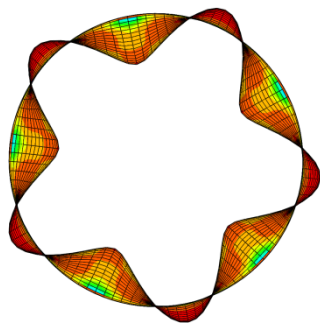
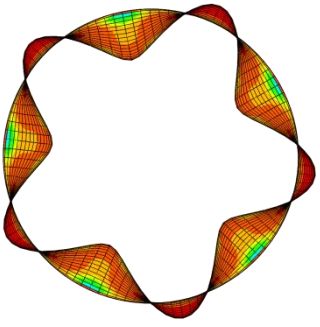
Deformation theory results		
Imperfect cylinder (Mode 1, $\Delta = 10\%$)		
$t = 0.76$	mm	
$R = 19.05$	mm	
$n = 5$	-	
$P_{buckling} = 9.09$	MPa	
$p_{cr}^n = 5.18$	MPa	
Flow theory results		
Imperfect cylinder (Mode 1, $\Delta = 10\%$)		
$t = 0.76$	mm	
$R = 19.05$	mm	
$n = 5$	-	
$P_{buckling} = 9.09$	MPa	
$p_{cr}^n = 5.21$	MPa	

Table 18 – Results of non-linear buckling analysis for specimen S3.

It is worth noticing that Giezen et al. (1991) did not report the amplitude of the measured initial imperfection for each tested specimen but simply observed that the maximum measured imperfection was about 0.03 in., that is 10% of the thickness.

It results thus clear that in all the examples under consideration the discrepancy between the flow and the deformation theory of plasticity, which for low values of the imperfection amplitude leads to results contrary to those of the plastic buckling paradox, can be attributed to a switching in the initial imperfection mode which takes place, in the case of the deformation theory of plasticity, along the loading path.

In conclusion, the following considerations may be observed:

- depending on the value of the amplitude of the initial imperfection injected into the model, a mode switching can take place along the loading path which is even capable of reversing the results which in the past have given origin to the plastic buckling paradox. In fact, a sort of inverse buckling paradox may occur in which the deformation theory provides buckling load which are sensibly higher than those obtained by the flow theory of plasticity;
- differently from the common beliefs for which the use of deformation theory of plasticity in the investigation of the inelastic buckling of shells is however recommended despite its some obvious inadequacies, so that many researchers attempted to elaborate revised formulations of the deformation theory, for instance including unloading (Peek, 2000) or redefining it as a sequence of linear loadings in case of nonproportional loading (Jahed et al.,1998), the results from the present dissertation highlight a superior reliability of the use of the flow theory of plasticity which is in contrast to what is normally agreed in literature and suggests that a geometrically nonlinear finite element formulation for imperfect shells is used with great attention to constitutive laws and imperfection amplitudes and a preference for the physically more sound flow theory of plasticity.

Conclusions

The present dissertation has investigated the plastic buckling of thin and moderately thin plates and shells with particular reference to the phenomenon of the “plastic buckling paradox” which occurs in these structures under various loading conditions. Old controversies in classical literature and new perspectives have been examined and thoroughly discussed with the aim of providing an explanation of the paradox.

In this respect, the study of the main theories of the plasticity has been of fundamental importance as many of the controversies reported in literature derive from the theoretical assumptions and from the limits of applicability of the proposed formulations. In fact, it is generally accepted that the incremental theory of plasticity is more in line with the experimental behaviour of engineering materials than the deformation theory and hence, under a physical point of view, it is more widely applicable, even if it implies a higher complexity in calculations. Therefore, despite the fact that there is a general agreement that the deformation theory of plasticity lacks of physical rigour in comparison to the flow theory, the use of deformation theory is practically motivated by its capability to solve certain problems without the mathematical complications of the flow theory. Moreover and importantly, in the study of plastic buckling problems of plates and shells under multiaxial stress the use of deformation theory has been repeatedly reported to predict critical loads that are in better agreement with the experimental results while the flow theory is often incorrect. This fact is generally named “plastic buckling paradox”

In 1953, Onat and Drucker investigated the plastic buckling paradox in the case of an axially compressed cruciform column showing torsional buckling. The solution was investigated by the authors by means of an approximate analysis in which small initial imperfections were taken into account. In this manner, assuming that a very small degree of imperfection was present in the column, the critical load predicted by the flow theory could be reduced significantly, getting it closer to that predicted by the deformation theory.

In the light of these findings, in the present dissertation first an accurate analysis of the torsional buckling of a cruciform column in the inelastic range has been

conducted on the sole basis of the classic formulation of the flow and deformation theory of plasticity and in the spirit of Shanley's approach to the stability of columns in the plastic range. It has been shown that the discrepancies repeatedly reported in literature between the results from the flow and the deformation theory of plasticity, even in presence of imperfections, seem essentially due to the fact that the effects of imperfections are computed inaccurately up to the point where the critical load is achieved. Furthermore, by means of the analytical procedure presented in Section 3.3, it has been shown that the flow theory of plasticity is capable of attaining a very good agreement with the results from the deformation theory and the experimental results, as well as with nonlinear incremental FE analyses. The proposed solution is also capable of naturally overcoming the observation that for metals with significant strain-hardening the imperfections have to be of considerable magnitude in order to reduce the critical load provided by the flow theory. Overall it can be affirmed that, in contrast to common understanding, by using a careful analytical procedure in the case of the torsional buckling of a cruciform column in the inelastic range there is actually no plastic buckling paradox. The present findings confirm and give a mechanical reason to the observation made in recent works on the plastic buckling of cylindrical shells by Shamass et al., who have shown that the results of incremental nonlinear finite element analyses using flow theory with an associated flow rule are unaffected by the plastic buckling paradox while, depending on the particular methodology, other approaches are sensible to it.

Also in presence of a more complex state of stress, as it is the case of non-proportional loading, the flow and deformation theories seem to provide quite different results. In the case of circular cylindrical shells, a simple non-proportional loading process can be obtained by applying first a fixed axial tension and then an increasing external lateral pressure. The inelastic instability of the cylindrical shell subjected to this kind of non-proportional loading has been investigated in depth by authors such as Blachut (1996) and Giezen (1991) which conducted several experimental tests and numerical analyses using the code BOSOR5. Recently, Shamass et al. (2014-2017) examined the sensitivity of the predicted critical pressures with respect to the applied tensile load. By means of accurately modelled and conducted FE analyses, they concluded that it is possible to obtain predictions

based on the flow theory of plasticity that are in good agreement with the experimental results. However, a deeper insight into the problem, presented in Section 4, has shown that, depending on the value of the amplitude of the initial imperfection injected into the model, a mode switching can take place along the loading path which is even capable of reversing the results which in the past have given origin to the plastic buckling paradox. In fact, it has been shown that the deformation theory, far from predicting critical loads lower than the flow theory and more in line with experimental findings, might provide critical loads which are sensibly higher than those by the flow theory of plasticity.

Notwithstanding the fact that the adoption of the deformation theory of plasticity in the investigation of the inelastic buckling has been recommended by many researchers, despite its obvious inadequacies (Jones, 2009; Peek, 2000; Jahed et al.,1998), the results from the present dissertation indicate that the use of the flow theory of plasticity, contrarily to what is normally agreed in literature, is generally more reliable for this kind of problems. Thus, the results of the present investigation suggest that a geometrically nonlinear finite element formulation for imperfect shells should be used paying particular attention to constitutive laws and imperfection amplitudes even in presence of the physically more sound flow theory of plasticity.

References

References for Section 1.

Batdorf, S.B and Budiansky, B. (1949). A mathematical theory of plasticity based on the concept of slip. National Advisory Committee for Aeronautics Technical Note- 1871, pp. 1-36.

Chen, W.F. and Han D.J. (1988). Plasticity for structural engineers. Springer-Verlag, New York Inc.

Hill, H.N. (1944). Determination of stress-strain relations from “offset” yield strength values. Technical Note No. 927, National Advisory Committee For Aeronautics, Washington.

Hill, R. (1950) The mathematical theory of plasticity. Oxford university press Inc., New York.

Jones, R. M. (2009). Deformation theory of plasticity. Bull Ridge Corporation.

Khan, A.S and Huang, S. (1995). Continuum theory of plasticity. John Wiley & Sons, Inc.

Lubliner, J. (1990). Plasticity theory. Macmillan Publishing Company.

Ramberg, W. and Osgood, W. R. (1943). Description of stress–strain curves by three parameters. Technical Note No. 902, National Advisory Committee For Aeronautics, Washington DC.

References for Section 2.

Ayrton, W.E. and Perry, J. (1886). On struts. The Engineer, 62, 464-5, 513-15.

Bardi, F.C. and Kyriakides, S. (2006). Plastic buckling of circular tubes under axial compression - Part I: Experiments. International Journal of Mechanical Sciences, 48(8), pp. 830-841.

Batterman, S.C. (1965). Plastic buckling of axially compressed cylindrical shells. *AIAA Journal*, 3(2), pp. 316-325.

Blachut, J., Galletly, G.D. and James, S. (1996). On the plastic buckling paradox for cylindrical shells. *Proceedings of the Institution of Mechanical Engineers, Part C*, 210(5), pp. 477-488.

Bryan, G.H. (1890). On the stability of elastic systems. *Proceedings of the Cambridge Philosophical Society*, 4, pp. 199-286.

Engesser, F. (1889). Die Knickfestigkeit gerader Stäbe. *Z. Architektur Ingenieurw*; 455.

Engesser, F. (1895). Über Knickfragen, *Schweizerische Bauzeitung*; 26: 24-26.

Gerard, G. and Becker, H. (1957). *Handbook of Structural Stability*. NACA TN 3781 to 3785.

Giezen, J.J. (1988). Plastic buckling of cylinders under biaxial loading. (Ph.D. thesis), California Institute of Technology, Pasadena, CA, February.

Giezen, J.J., Babcock, C. D. and Singer, J. (1991). Plastic buckling of cylindrical shells under biaxial loading. *Experimental Mechanics journal*, 31(4), pp. 337-343.

Huchinson, J.W. and Koiter, W.T. (1970). Postbuckling Theory. *Applied Mechanics Reviews*, 23, pp. 1353-1366.

Hutchinson, J.W. (1972). On the postbuckling behavior of imperfection-sensitive structures in the plastic range. *Journal of Applied Mechanics – Transactions of ASME*, 39, pp. 155–162.

Hutchinson, J. W. (1974). Plastic Buckling. *Advances in Applied Mechanics*, 14(67).

Hutchinson, J. and Budiansky, B. (1976). Analytical and numerical study of the effects of initial imperfections on the inelastic buckling of a cruciform column. In: Budiansky, B. (Ed.), *Proceedings of IUTAM Symposium on Buckling of Structures*. Springer; 98-105.

Koiter, W.T. (1945). On stability of elastic equilibrium. (Ph.D. thesis), Technical Sciences at the Technische Hooze School.

Shanley, F.R. (1946). The column paradox. Lockheed Aircraft Corporation, p.678.

Shanley, F. R. (1947). Inelastic column theory. Journal of the Aeronautical Science, 14, pp. 261-267.

Singer, J. , Arbocz J. and Weller, T. (1998). Buckling Experiments: Experimental Methods in Buckling of Thin-Walled Structures: Basic Concepts, Columns, Beams and Plates – Volume 1. John Wiley & Sons, Inc.

Southwell, R.V. (1913). On the general theory of elastic stability. Philosophical Transactions of the Royal Society of London. Series A , 213, pp. 187-244.

Timoshenko, S. P. and Gere, J. M. (1961). Theory of Elastic Stability. McGraw-Hill. New York.

von Kàrmàn, T. (1910). Untersuchungen über Knickfestigkeit, Mitteilungen über Forschungsarbeiten auf dem Gebiet des Ingenieurwesens, Verein Deutscher Ingenieure, Heft 81, Berlin.

References for Section 3.

Ayrton, W.E. and Perry, J. (1886). On struts. The Engineer, 62, 464-5, 513-15.

Batdorf, S.B and Budiansky, B. (1949). A mathematical theory of plasticity based on the concept of slip. National Advisory Committee for Aeronautics Technical Note- 1871, pp. 1-36.

Bazant Z.P. and Cedolin L. (1991). Stability of Structures. Oxford University Press, Oxford, U.K.

Becque, J. (2016). The application of plastic flow theory to inelastic column buckling. Int J Mech Sci; 111/112: 116–124.

Budiansky, B. (Ed.), Proceedings of IUTAM Symposium on Buckling of Structures. Springer 1976; 98-105.

Bushnell, D. (1986). BOSOR5 – Program for Buckling of Complex, Branched Shells of Revolution Including Large Deflections, Plasticity and Creep. In Structural Analysis Systems – 2, edited by Niku-Lari, A. Pergamon; 25-54.

Cicala, P. (1950). On Plastic Buckling of a Compressed Strip. Readers' Forum, J. Aero. Sci.; 17(6): 378.

Considère, A. (1891). Résistance des pièces comprimées. Congr. intern. procédés construct. Paris; 3: 371.

Engesser, F. (1889). Die Knickfestigkeit gerader Stäbe. Z. Architektur Ingenieurw; 455.

Engesser, F. (1895). Über Knickfragen, Schweizerische Bauzeitung; 26: 24-26.

Guarracino, F. , Simonelli, M.G. , The torsional instability of a cruciform column in the plastic range: Analysis of an old conundrum. Thin-Walled Struct. J. 2017; 113:273–286.

Hopperstad, O.S. , Langseth, M. , Tryland, T. (1999). Ultimate strength of aluminium alloy outstands in compression: experiments and simplified analysis. Thin-Walled Structures; 34: 279-294.

Hutchinson, J. W. (1974). Plastic Buckling. Advances in Applied Mechanics, 14(67).

Hutchinson, J. and Budiansky, B. (1976). Analytical and numerical study of the effects of initial imperfections on the inelastic buckling of a cruciform column. In: Budiansky, B. (Ed.), Proceedings of IUTAM Symposium on Buckling of Structures. Springer; 98-105.

Lubliner, J. (1990). Plasticity theory. Macmillan Publishing Company.

Onat, E. and Drucker, D. (1953). Inelastic Instability and Incremental Theories of Plasticity. J. Aeronaut. Sci.; 20 (3): 181–186.

Ramberg, W. and Osgood, W. R. (1943). Description of stress–strain curves by three parameters. Technical Note No. 902, National Advisory Committee For Aeronautics, Washington DC.

Shamass, R. , Alfano, G. , Guarracino, F. (2013). A numerical investigation into the plastic buckling of circular cylinders, *Shell Structures: Theory and Applications- Proceedings of the 10th SSTA 2013 Conference*, Gdansk, Poland; 441-444.

Shamass, R. , Alfano, G. , Guarracino, F. (2014). A numerical investigation into the plastic buckling paradox for circular cylindrical shells under axial compression, *Engineering Structures*; 75: 429-447.

Shamass, R. , Alfano, G. , Guarracino, F. (2015). An analytical insight into the buckling paradox for circular cylindrical shells under axial and lateral loading. *Mathematical Problems in Engineering*; Article ID 514267: 1-11, doi: 10.1155/2015/514267.

Shamass, R. , Alfano, G. , Guarracino, F. (2015). An investigation into the plastic buckling paradox for circular cylindrical shells under non-proportional loading, *Thin-Walled Structures*; 95: 347-362.

Shamass, R. , Alfano, G. , Guarracino, F. (2016). On the elastoplastic buckling analysis of cylinders under non-proportional loading by differential quadrature method. *Int. J. of Structural Stability and Dynamics*; ID: 1750072; <http://dx.doi.org/10.1142/S0219455417500729>

Shanley, F. R. (1947). Inelastic column theory. *Journal of the Aeronautical Science*, 14, pp. 261-267.

Simulia (2011). *ABAQUS User's and Theory Manual*. Version 6.11-1. Dassault Systems, Johnston, RI 02919, USA.

Stowell, E. (1956). *A Unified Theory of Plastic Buckling of Columns and Plates*. NACA Technical Note, NACA, Washington 1948.

Teng, J.G. (1996). Buckling of thin shells: recent advances and trends. *Applied Mechanics Reviews*; 49(4): 263-274.

Timoshenko, S. P. and Gere, J. M. (1961). Theory of Elastic Stability. McGraw-Hill. New York.

Tuğcu, P. (1991). On plastic buckling predictions. International Journal of Mechanical Sciences, 33(7), pp. 529-539.

Tuğcu, P. (1991). Plate buckling in the plastic range. Int. J. Mech. Sci.; 33(1): 1-11.

Wang, C.M. , Xiang, Y. , Chakrabarty, J. (2001). Elastic/plastic buckling of thick plates. Int J Solids Struct; 38: 8617-8640.

References for Section 4.

Bardi, F.C. and Kyriakides, S. (2006). Plastic buckling of circular tubes under axial compression - Part I: Experiments. International Journal of Mechanical Sciences, 48(8), pp. 830-841.

Batterman, S.C. (1965). Plastic buckling of axially compressed cylindrical shells. AIAA Journal, 3(2), pp. 316-325.

Blachut, J. and Galletly, G. D. (1993). Influence of local imperfections on the collapse strength of domed end closures. Proceedings of the Institution of Mechanical Engineers, Part C J Mech Eng Sci,; 207:197-207.

Blachut, J., Galletly, G.D. and James, S. (1996). On the plastic buckling paradox for cylindrical shells. Proceedings of the Institution of Mechanical Engineers, Part C, 210(5), pp. 477-488.

Bushnell, D. (1982). Plastic buckling, in pressure vessels and piping: Design Technology – 1982, A Decade of Progress, edited by Zamrik, S. Y. and Dietrich, D. ASME:47-117.

Bushnell, D. (1984). Computerized analysis of shells-governing equations. Comput Struct; 18:471 - 536.

Bushnell, D. (1986). BOSOR5 – Program for Buckling of Complex, Branched Shells of Revolution Including Large Deflections, Plasticity and Creep. In *Structural Analysis Systems – 2*, edited by Niku-Lari, A. Pergamon; 25-54.

Bushnell, D. Bifurcation buckling of shells of revolution including large deflections, plasticity and creep. *Int J Solids Struct* 1974;10:1287-1305.

Donnell, L. H. (1934). New Theory for Buckling of Thin Cylinders Under Axial Compression and Bending. *Transactions, ASME*, Vol. 56, 795–806.

Falzon, B.G. (2006). An introduction to modelling buckling and collapse. Glasgow, UK, NAFEMS Ltd.

Fraldi, M. and Guarracino, F. (2014). Stability Analysis of Circular Beams with Mixed-Mode Imperfections under Uniform Lateral Pressure, *Advances In Mechanical Engineering*, pp. 294507-1-7.

Giezen, J.J. (1988). Plastic buckling of cylinders under biaxial loading. (Ph.D. thesis), California Institute of Technology, Pasadena, CA, February.

Giezen, J.J., Babcock, C. D. and Singer, J. (1991). Plastic buckling of cylindrical shells under biaxial loading. *Experimental Mechanics journal*, 31(4), pp. 337-343.

Guarracino, F. , Simonelli, M.G. (2017). The torsional instability of a cruciform column in the plastic range: Analysis of an old conundrum. *Thin-Walled Struct. J.*; 113:273–286.

Guarracino, F. and Walker, A.C. (2008). Some Comments on the Numerical Analysis of Plates and Thin-Walled Structures. *Thin-Walled Structures*, 46, pp. 975-980.

Hopperstad, O.S. , Langseth, M. , Tryland, T. (1999). Ultimate strength of aluminium alloy outstands in compression: experiments and simplified analysis. *Thin-Walled Structures*; 34: 279-294.

Lee, L. (1962). Inelastic buckling of initially imperfect cylindrical shells subjected to axial compression. *Journal of Aerospace Science*, 29, pp. 87-95.

Lorenz, R. (1908). Achsensymmetrische Verzerrungen in dhnnwandigen Hohlzylindern, Zeitschrift des Vereines Deutscher Ingenieure, Vol. 52(No. 43), 1766.

Mao, R. and Lu, G. (1999). Plastic buckling of circular cylindrical shells under combined in-plane loads. *Int J Solids Struct*;38:741-757.

Onat, E. and Drucker, D. (1953). Inelastic Instability and Incremental Theories of Plasticity. *J. Aeronaut. Sci.*; 20 (3): 181–186.

Ore, E. and Durban, D. (1992). Elastoplastic buckling of axially compressed circular cylindrical shells. *IJMS*;34:727-742.

Peek, R. (2000). An incrementally continuous deformation theory of plasticity with unloading. *Int J Solids Struct*;37:5009–5032.

Riks, E. (1979). An incremental approach to the solution of snapping and buckling problems. *Int J Solids Struct*;15:529-551.

Shamass, R. , Alfano, G. , Guarracino, F. (2014). A numerical investigation into the plastic buckling paradox for circular cylindrical shells under axial compression, *Engineering Structures*; 75: 429-447.

Shamass, R. , Alfano, G. , Guarracino, F. (2015). An analytical insight into the buckling paradox for circular cylindrical shells under axial and lateral loading. *Mathematical Problems in Engineering*; Article ID 514267: 1-11, doi: 10.1155/2015/514267.

Shamass, R. , Alfano, G. , Guarracino, F. (2015). An investigation into the plastic buckling paradox for circular cylindrical shells under non-proportional loading, *Thin-Walled Structures*; 95: 347-362.

Simo, J.C. and Hughes, T.J.R. (1998). *Computational inelasticity*. Springer.

Simulia (2011). *ABAQUS User's and Theory Manual*.Version 6.11-1. Dassault Systems, Johnston, RI 02919, USA.

Supple WJ. On the change of buckle pattern in elastic structures. *Int.. J. Mech. Sci.* 1968; 10: 737-745.

Yoo, C. H., and Lee, S. (2011). Stability of structures: principles and applications. Elsevier.

Timoshenko, S. P. and Gere, J. M. (1961). Theory of Elastic Stability. McGraw-Hill. New York.

Tuğcu, P. (1991). On plastic buckling predictions. International Journal of Mechanical Sciences, 33(7), pp. 529-539.

von Kármán, T., Tsien, H. S. (1941). The Buckling of Thin Cylindrical Shells under Axial Compression. Journal of the Aeronautical Sciences, Vol. 8(No. 8), 303–312.

Appendixes

Appendix 1. Plastic work in Prandtl-Reuss material

The concept of plastic work is very important in plasticity due to its large and simple use in determining some quantities related to the material behaviour. For instance, as seen in Section 1.2, it would be very helpful in order to determine the scalar factor $d\lambda$ present in the yield function formulation.

Basically, the total work at the end of a loading process is simply the product between the stress and the strain while during a loading process the increment of work per unit volume is the product between the stress and the increment of strain:

$$dW = \sigma_{ij} d\varepsilon_{ij} \quad (101)$$

Recollecting that the increment of strain undergoes the additive decomposition property, it will be replaced by the sum of the elastic and plastic increments:

$$dW = \sigma_{ij} (d\varepsilon_{ij}^e + d\varepsilon_{ij}^p) = dW^e + dW^p \quad (102)$$

where dW^e is the increment of elastic work and dW^p is the increment of plastic work. If the loading process reverses or unloads, the increment of elastic work, or the increment of elastic strain energy, totally recovers while the increment of plastic work dW^p remains as dissipated energy because of the irreversibility of plastic deformations. Substituting instead the stress σ_{ij} by the sum of its hydrostatic and deviatoric parts, the increment of plastic work becomes:

$$dW^p = \sigma_{ij} d\varepsilon_{ij}^p = (p\delta_{ij} + s_{ij}) d\varepsilon_{ij}^p \quad (103)$$

and for another property of plastic deformation that is the incompressibility, i.e. no dependence on volume change exists, it follows that: $p\delta_{ij} d\varepsilon_{ij}^p = 0$ and then the increment of plastic work reduces to:

$$dW^p = s_{ij} d\varepsilon_{ij}^p \quad (104)$$

In vector form, the Eq. (104) may be expressed as the inner product of the stress deviator vector with the increment of plastic strain one. In the principal stress space for isotropic materials, it becomes:

$$dW^p = |\mathbf{s}| |\mathbf{d}\boldsymbol{\varepsilon}^p| \cos \beta \quad (105)$$

where $|\mathbf{s}|$ and $|\mathbf{d}\boldsymbol{\varepsilon}^p|$ are the norms of the stress deviator and of the plastic strain increment, respectively, and β is the angle between them. In order to explicit the terms in the increment of plastic work expression, the norms of the stress deviator and of the plastic strain increment are given, respectively:

$$|\mathbf{s}| = \sqrt{s_I^2 + s_{II}^2 + s_{III}^2} = \sqrt{s_{ij}s_{ij}} = \sqrt{2J_2} \quad (106)$$

$$|\mathbf{d}\boldsymbol{\varepsilon}^p| = \sqrt{(d\varepsilon_n^p)^2 + (d\varepsilon_m^p)^2 + (d\varepsilon_l^p)^2} = \sqrt{d\varepsilon_{ij}^p d\varepsilon_{ij}^p} \quad (107)$$

and the effective stress and effective strain increment are recalled as:

$$\sigma_{ef} = \sqrt{3J_2} = \sqrt{\frac{3}{2}s_{ij}s_{ij}} \quad (108)$$

$$d\varepsilon_{ef} = \frac{2}{\sqrt{3}} \sqrt{\frac{1}{2}d\varepsilon_{ij}d\varepsilon_{ij}} \quad (109)$$

From this point, after some manipulations it results possible to connect the norms with the effective stress and effective strain increment by introducing the expressions:

$$|\mathbf{s}| = \sqrt{\frac{2}{3}}\sigma_{ef} \quad (110)$$

$$|\mathbf{d}\boldsymbol{\varepsilon}^p| = \sqrt{\frac{3}{2}}d\varepsilon_{ef}^p \quad (111)$$

and in this manner the equation for the increment of plastic work simply becomes:

$$dW^p = \sigma_{ef} d\varepsilon_{ef}^p \cos \beta \quad (112)$$

Under the assumption of Prandtl-Reuss constitutive relations, it is known that the increment of plastic strain vector is coaxial with the stress deviator so the angle $\beta = 0$, $\cos \beta = 1$ and the increment of plastic work reduces to:

$$dW^p = \sigma_{ef} d\varepsilon_{ef}^p \quad (113)$$

After these calculations, the Prandtl-Reuss equation may be rewritten taking into account the amount of the increment of plastic work, as seen in Eq. (113), and the expression of the increment of plastic work, as seen in Eq. (104), so that:

$$dW^p = s_{ij} d\varepsilon_{ij}^p = d\lambda s_{ij} s_{ij} = d\lambda 2J_2 = 2d\lambda k^2 \quad (114)$$

and the unknown parameter $d\lambda$ may be obtained:

$$d\lambda = \frac{dW^p}{2k^2} \quad (115)$$

as already seen in Section 1.2. in Eq. (23).

Finally, the complete expression for the plastic strain increment may be showed substituting the scalar $d\lambda$ in the flow rule:

$$d\varepsilon_{ij}^p = d\lambda s_{ij} = \frac{dW^p}{2k^2} s_{ij} \quad (116)$$

Appendix 2. Description of Ramberg-Osgood stress-strain curve

As discussed in Section 1.5., the Ramberg-Osgood stress-strain formula is based on the determination of three parameters in order to express approximatively the relation between stresses and strains in the plastic range for a given material. Its general expression already seen in Eq. (55) in Section 1.5. is following reported:

$$\varepsilon = \frac{\sigma}{E} + K \left(\frac{\sigma}{E} \right)^n$$

where E is the Young modulus, K and n are material parameters.

In the first edit of the work, the two unknown parameters, K and n , are obtained by tracing two straight lines passing through the origin and intersecting the real stress-strain curve at two points, corresponding to two precise stress values. The slopes of these two lines are respectively of $0.7E$ and $0.85E$ so that the stress values deduced by the intersection with the material curve are respectively $\sigma_{0.7E}$ and $\sigma_{0.85E}$ (see Figure 50 in Section 1.5). Nevertheless, since determining the stresses by means of the offset method along the strain axis is much more used than by means of that secant method, it may be convenient to evaluate the two parameters K and n by assuming other two stresses related to adequate offset stress values.

Consider to have two generic stress and offset values: σ_1 related to the offset d_1 and σ_2 related to the offset d_2 . In the Eq. (55) the first term represents the elastic amount of the strain while the second term is the plastic one. In this respect, a generic strain offset over the yield point may be rewritten as:

$$d = K \left(\frac{\sigma}{E} \right)^n \quad (117)$$

from which by introducing a logarithmic scale and using the additive property of the logarithm it may be obtained:

$$\log d = \log K + n \log \left(\frac{\sigma}{E} \right) \quad (118)$$

By substituting the two couple of stress and offset values (σ_1, d_1) and (σ_2, d_2) in Eq. (118) respectively, two equations in K and n are obtained:

$$\log d_1 = \log K + n \log \left(\frac{\sigma_1}{E} \right) \quad (119)$$

$$\log d_2 = \log K + n \log \left(\frac{\sigma_2}{E} \right) \quad (120)$$

and then subtracting the Eq. (120) with the Eq. (119) the solution for n may be deduced:

$$n = \frac{\log \left(\frac{d_2/d_1}{\sigma_2/\sigma_1} \right)}{\log \left(\frac{\sigma_2}{\sigma_1} \right)} \quad (121)$$

Thus from Eq. (117), K may be obtained:

$$K = \frac{d_2}{\left(\frac{\sigma_2}{E} \right)^n} \quad \text{or} \quad K = \frac{d_1}{\left(\frac{\sigma_1}{E} \right)^n} \quad (122)$$

Replacing the solution for K in Eq. (55), the stress-strain formula becomes:

$$\varepsilon = \frac{\sigma}{E} + d_2 \left(\frac{\sigma}{\sigma_2} \right)^n \quad \text{or} \quad \varepsilon = \frac{\sigma}{E} + d_1 \left(\frac{\sigma}{\sigma_1} \right)^n \quad (123)$$

where n is always obtained by Eq. (121).

A commonly used offset value is that corresponding to the yield stress, i.e. 0.002. In this manner, choosing the couple of values $(\sigma_y, 0.002)$, the expression of the stress-strain curve reduces to the simple formula:

$$\varepsilon = \frac{\sigma}{E} + 0.002 \left(\frac{\sigma}{\sigma_y} \right)^n \quad (124)$$

Moreover, introducing the “yield offset” as:

$$\alpha = 0.002 E/\sigma_y \quad (125)$$

the stress-strain curve finally assumes the well-known expression in Eq. (56) seen in Section 1.5:

$$\varepsilon = \frac{\sigma}{E} \left(1 + \alpha \left(\frac{\sigma}{\sigma_y} \right)^{n-1} \right)$$

where E and σ_y are the elastic modulus and the yield strength of the material, respectively, α is the yield offset defined in Eq. (125) and n is the hardening parameter defined in Eq. (121).